MODELLING THE DYNAMICS OF SOIL CHEMISTRY, GROUND VEGETATION COMPOSITION AND BIODIVERSITY CRITICAL LOADS AT FOREST SITES IN SWITZERLAND

Status Report[1]

EKG Geo-Science, Daniel Kurz, geo-science@bluewin.ch[2]

[1] The status report received only limited review. The contents of the status report as well as views and opinions expressed therein, do not necessarily reflect the views of the organizations ordering or supporting the work, and no official endorsement should be inferred.

[2] By order of the Federal Office for the Environment (FOEN), Switzerland
Contract Nos. 00.0052.PZ / P272-0595 (8T10/00.5100.PZ/0010 / P272-0595V), 00.5100.PZ / Q255-0237

Table of Contents

The author acknowledges contributions and support of B. Achermann and Dr. R. Meier (FOEN, Ittigen), Dr. M. Alveteg (Lund University), Dr. S. Belyazid (Stockholm University), Drs. L. Bonten, J. Mol-Dijkstra and G. J. Reinds (Wageningen Environmental Research), Drs. U-B. Brändli, M. Huber, L. Walthert and S. Zimmermann (WSL, Birmensdorf), Dr. S. Braun (IAP, Schönenbuch), Dr. T. Burger (Burger & Liechti GmbH, Ennetbaden), Dr. M. Posch (CCE, Bilthoven), Dr. J. Remund and B. Rihm (Meteotest, Bern) and Prof. H. Sverdrup (University of Iceland).

1 INTRODUCTION

As a consequence of switching to low sulphur fuels for power and heat production, improvements in energy efficiency, flue gas desulfurization in industrial facilities all partly imposed by international legislation (UNECE Convention on Long-range Transboundary Air Pollution (LRTAP), NECD) and economical structural changes in Eastern Europe, sulphur (S) emissions/depositions in Europe declined over the last decades. However, air pollution still is a problem in Europe due to (among others) far less decreasing emissions of nitrogen oxides (NO_x) and particularly ammonia (NH_3) resulting in total nitrogen (N) becoming the dominant air-borne pollutant (Amann et al. 2013; EMEP 2016). Consequently, the focus in effects-oriented research and policy shifted in the last decades from acidification to the various effects of persisting high atmospheric levels and loads of N. Additionally, there was growing interest in the links between effects of air pollution and climate change including mutual impact on biodiversity (ECE 2008). After some years of exploring this novel field of interest, biodiversity was finally adopted as endpoint for S and N critical loads calculations by the Task Force (TF) of the ICP Modelling & Mapping (M&M) and the Working Group on Effects (WGE) by agreeing on the metric for quantifying biodiversity damage (ECE 2015).
The first generation of dynamic bio-geochemical soil and surface water models used within the scope of the UNECE LARTAP Convention already considered N processes although via essentially mass balances, empirical and forcing functions. To keep up with the shift in focus, model developers amended their models by more detailed descriptions of carbon (C) and N dynamics also under the premise to provide input for downstream plant species diversity models. For example, the SAFE model (Alveteg 1998) was integrated into ForSAFE (Wallman et al. 2005; Belyazid 2006), to which ultimately Veg, a plant community composition simulation tool, was linked. More detailed C and N dynamics were implemented in the Very Simple Dynamic model (VSD, Posch & Reinds 2009), and the resulting VSD+ (Bonten et al. 2016) was coupled with the PROPS model predicting the probability of plant occurrence. A series of other model chains for terrestrial ecosystems were developed or further developed, of which MADOC-MultiMOVE (UK) and SMART2(-SUMO2)-MOVE/NTM3 (NL) were and are being used to assess biodiversity endpoints on national scales (i.a. Rowe et al. 2015). Over many years, the surface waters model MAGIC was tested with different concepts for improved N modelling and finally updated (Cosby et al. 2001; Oulehle et al. 2012). MAGIC was already earlier supplemented with GBMOVE (de Vries et al. 2010), the forerunner of MultiMOVE.

Some of the terrestrial dynamic bio-geochemical models – SAFE/ForSAFE and VSD/VSD+ – as well as their static equivalents – PROFILE and SMB – have been applied in Switzerland in research projects and in support of national and international effect-oriented work. Since the models were constantly tested, further developed and adapted to changing objectives, the results of earlier applications do not necessarily reflect the current state of model development. Additionally, in the wake of time also base data and model input data derivation have changed (Kurz & Posch 2015).

In 2015, the Coordination Centre for Effects (CCE) of the ICP M&M issued on behalf of the WGE a Call for Data 2015-17 encouraging the National Focal Centres (NFC) of the parties of the Convention to report (among other issues)

- S and N critical load (CL) functions accounting for the impact of S and N deposition on plant species diversity (bdiv CL).

In the sequel, the biodiversity models Veg and PROPS, earlier chained to ForSAFE, VSD and VSD+, underwent thorough revision regarding both databases as well as assessment of response functions. To enable the calculation of critical S and N loads, both models were linked

with the SMB and a series of subroutines, permitting to derive site-specific critical loads functions for the input plant communities. By order of the FOEN and in compliance with the Call for Data 2015-17, the revised model chains were also applied in Switzerland.

Consequently, this report documents

- recent work with VSD+ and PROPS including the comparison of the output with the results of the VSD-Veg chain,
- selected insights in the biodiversity critical loads calculations with both models PROPS and Veg and
- the outcome of the national biodiversity critical loads calculations in compliance with the Call for Data 2015-17 of the WGE and CCE.

2 METHODS AND MATERIALS

2.1 Models involved

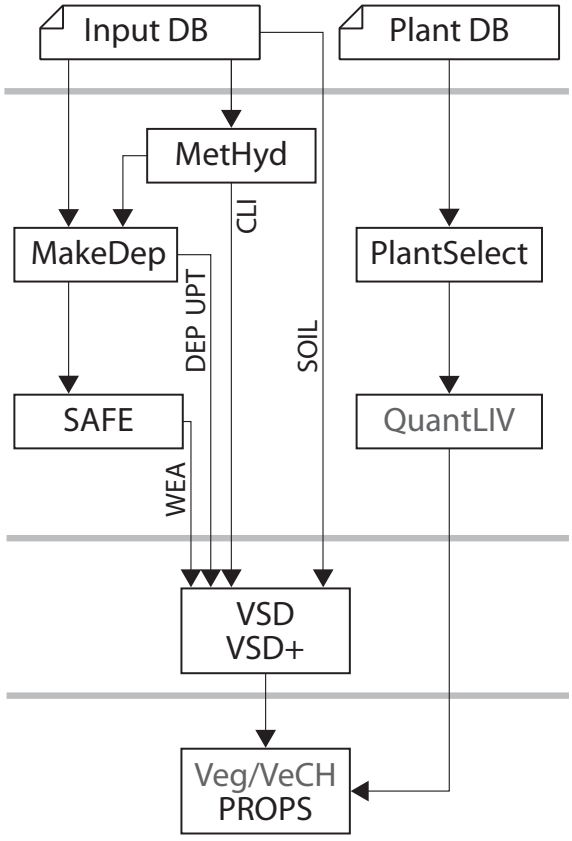

Figure 1 Model chain used to calculate critical loads of acidity and biodiversity critical loads with input from steady-state modelling.

Conventional critical loads of acidity were assessed by means of a variant of the Simple Mass Balance (SMB) model (Posch et al. 2015) also considering the extensions listed in the Mapping Manual (Chap. V.3.2.4; CLRTAP 2017). To allow weathering rates to be consistently calculated for conditions at critical load, the Sverdrup-Warfvinge Weathering (SWW) algorithm (e.g., Sverdrup and Warfvinge 1995) was linked to the SMB (acronym SWWSMB; version Mar 23, 2013). The set of equations implemented to calculate the weathering rates is compiled in Kurz & Posch (2015). By contrast, biodiversity critical load models still contain the "standard" SMB model and weathering fluxes were taken from either SAFE (average of a given period) or SWWSMB runs (Figure 1).

VSD (Posch & Reinds 2009) is the dynamic variant of the SMB model and has been used for modelling the impact of air pollutant deposition on natural and semi-natural ecosystems and for the calculation of target loads of airborne S and N on national and European scales. VSD relies on input fluxes of infiltration and runoff, atmospheric deposition, weathering and net uptake of ions by the vegetation, as well as net immobilization of N and denitrification (flux or factor). It models via mass balances, cation exchange and equilibria the concentration of major cat- and anions and via charge balance and forcing function hydrogen ion and aluminium concentrations in solution. Solute transport is described by assuming complete mixing of ions in solution in one homogenous soil compartment with fixed thickness, constant density and constant water content within the annual time step. Nitrification is assumed to be instantaneous and complete. Net N immobilisation depends on (1) a constant (acceptable and sustainable) long-term net immobilisation, implicitly assuming a proportional

amount of C to be immobilised and (2) a variable N immobilisation calculated as a fraction of the net N input and controlled by user-prescribed C/N ratios.

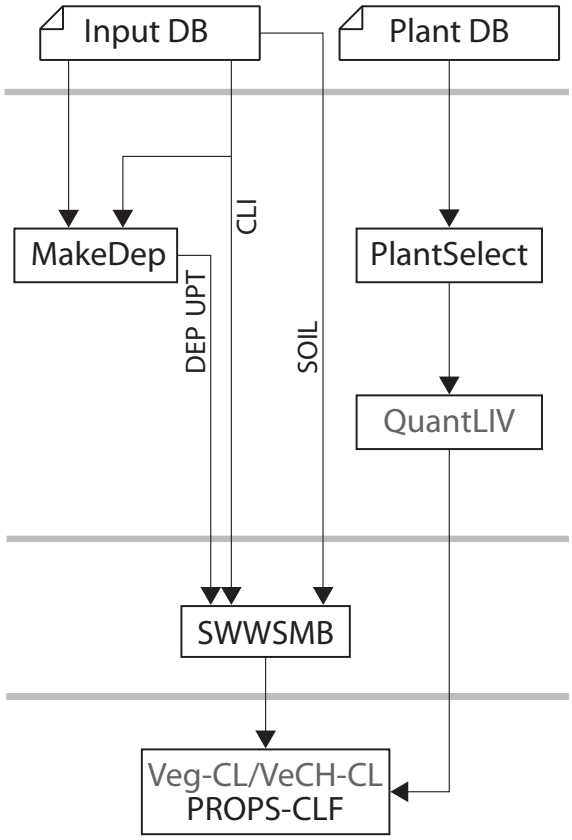

Figure 2 Model stacking required to obtain the dynamics of soil chemistry and ultimately of ground vegetation composition.

VSD+ (Bonten et al. 2016) contains the soil chemistry core of VSD but includes an explicit description of organic C and N turnover. Changes in the soil organic carbon content are calculated using RothC-26.3 (Coleman and Jenkinson 2014), which considers five soil organic pools: Decomposable Plant Material (DPM), Resistant Plant Material (RPM), Microbial Biomass (BIO), Humified Organic Matter (HUM) and Inert Organic Matter (IOM). The total amount of incoming plant material (Clf) is distributed over DPMin and RPMin according to a user-defined litter quality index (QIlf). Turnover of the first four pools is modelled as first-order process, which is modified by temperature, soil moisture and soil cover, as well as clay content in the case of BIO and HUM via correcting reference turnover rates. The IOM pool does not decompose. Input of N in VSD+ consists of deposition, litterfall, uptake and N fixation. Mineralisation and immobilisation of N are dependent on the turnover of the C pools, where the net mineralisation follows from changes in the sum of all organic N pools. In case the C turnover releases insufficient N for plant uptake, the transfer of N to HUM pool is reduced until sufficient N is available for uptake. To facilitate a more extensive calibration of VSD+, including uncertainties in observed soil solution chemistry, a procedure for Bayesian calibration was developed and implemented in VSD+Studio.

VSD was chained to Veg (Belyazid et al. 2011), and VSD+ was linked to PROPS. Veg is a plant community composition model, which has originally been developed as an add-on to the ForSAFE biogeochemical model (Sverdrup et al. 2007). Veg simulates the ground cover of a set of indicator plant species at a certain site and time in response to climatic (moisture, light and temperature) and geochemical conditions (nitrogen availability, base cation (Bc) availability and soil acidity). Veg requires expert information on plant-specific responses to the drivers listed above, which were compiled in a generic Veg parameter database incorporating the data from France, Sweden and Switzerland. To explore some of the peculiarities of standard Veg, the parameterisation of the model was altered for a test with Swiss forest plots. The alternative Veg model parameterisation (model acronym VeCH; Kurz 2016) involves only trapezoidal response functions for all drivers. This simplification allowed using Landolt's indicator tables (Landolt 2010) as primary data basis and expert knowledge regarding assignment of value ranges for indicator value classes.

The PROPS model assesses the occurrence probability of plant species as a function of soil chemical and climatic variables. A logistic regression technique was used to relate presence-absence data of plant species and driver data. Two databases were used to fit the probability

functions: The first database contained information on plant species occurrence for 16’000 relevés from the Netherlands, Austria, Ireland, Denmark and the United Kingdom, including measurements of at least one of the key soil parameters (pH, total soil N content (N_{tot}), soil C/N ratio (C/N) or nitrate concentration in the soil solution). The second database included only information on plant species occurrence in approximately 800’000 relevés in Europe (collected in the EU BioScore project, van Hinsberg et al. 2014). The values for the required soil parameters were estimated using the plant species composition and the probability curves fitted from the first database. A full description of the PROPS model including applications can be found in Reinds et al. (2012), Reinds et al. (2014), Rowe et al. (2015) and Reinds et al. (2015).

Originally, biodiversity models were used as end-of-pipe models in dynamic model chains and only recently Veg/VeCH and PROPS were linked to the SMB to also allow steady-state modelling (Section 3.4; Posch et al. 2014; Posch et al. 2015). The models Veg-/VeCH-CL and PROPS-CLF calculate critical S and N loads for a given habitat-specific plant community, using a fraction of the habitat suitability index (HSI; Section 2.2.8) as critical limit.

A stand-alone (single-site) variant of MetHyd (vs. Feb 20, 2017; M. Posch, CCE, pers. commun.; Posch and Reinds 2010; Bonten et al. 2016) was used to model climate and hydrological time-series data needed to run all downstream models, as well as rate modifying factors for mineralisation, nitrification and denitrification requested by VSD+. MetHyd calculates from input daily or monthly meteorological time-series and basic soil properties, daily evapotranspiration, soil moisture and percolation and from these the three rate modifying factors. Standard output covers annual averages of temperature, precipitation, percolation, soil water content, sun shine hours, photosynthetically active radiation and rate modifying factors.

To obtain other flux data required by dynamic and static soil chemistry models, we still used the standalone yield model MakeDep. MakeDep (Alveteg et al. 2002) is tailored for dynamic

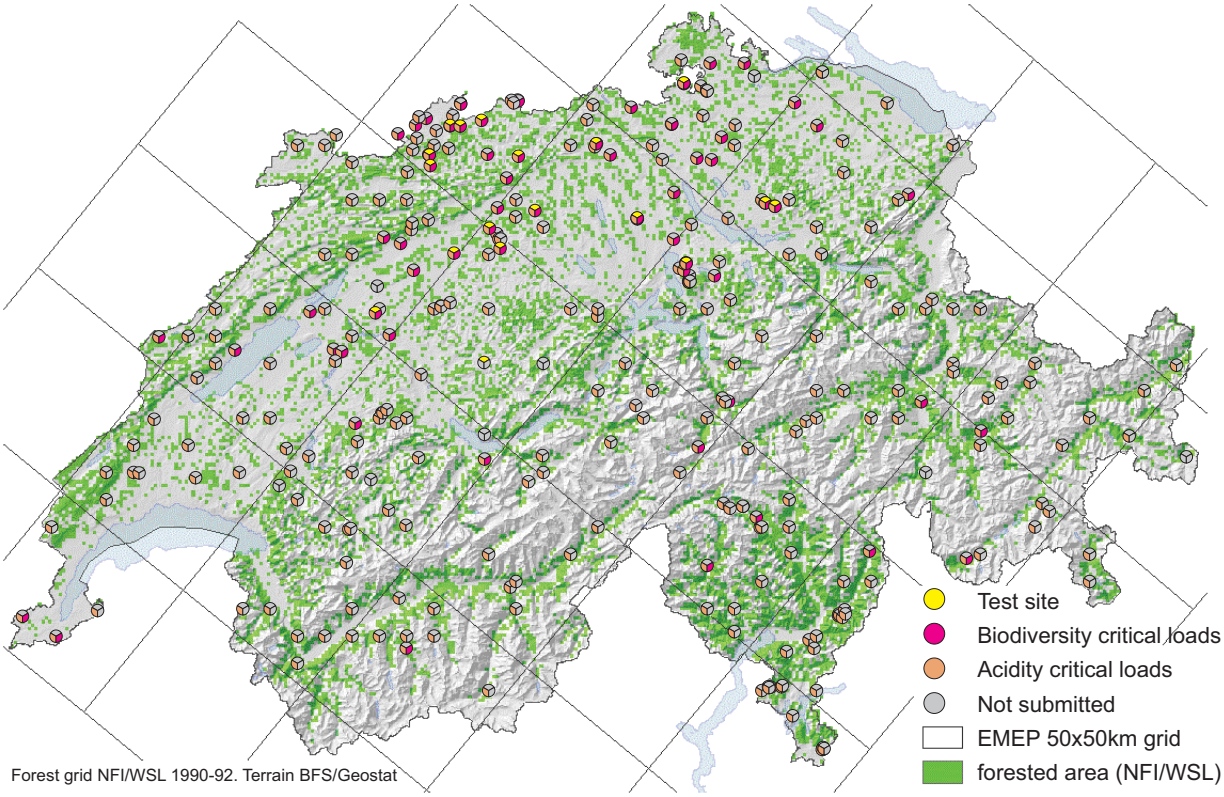

Figure 3 Map of the various forest plot categories.

(forest) soil acidification model applications and reconstructs historic and future deposition and nutrient uptake by the forest considering the mutual dependence of deposition, forest canopy growth/size and nutrient demand of the growing forest. MakeDep calibrates growth and deposition trends to current (growing) biomass and deposition and regards growth to be N limited. The basic set-up of the MakeDep model run is described in Kurz & Posch (2015; Section 2.3 and Appendix B).

2.2 Input

All model chains (Figure 1 and Figure 2) usually were operated with input data derived from a common input dataset, the resolution of which originally was tailored to the input requirements of the most complex biogeochemical model (ForSAFE). Consequently, current model chains needed specific input data modifications such as reduction in time-resolution from monthly to annual or combining soil layers in one layer the so-called rooting zone (of the over- or understorey vegetation). The list of input parameters used to run VSD and VSD+ is compiled in Table 1.

Model tests were performed on 22 forest monitoring sites of the intercantonal permanent forest observation programme operated by the Institute for Applied Plant Biology (IAP, Schönenbuch). For these sites also current soil solution chemistry and ground vegetation composition was provided. Biodiversity critical loads were calculated for 76 forest plots (including 20 of the 22 test sites), for which the "desired" plant community composition was available. The sites are part of the national database used for dynamic and acidity critical loads modelling. The total set covers 311 forest plots (Figure 3), of which 10 (including 2 test sites) were omitted from the final submission due to having negative acidity critical loads.

2.2.1 Climate

For the dynamic model runs we used site-specific meteorological and climate data provided by Meteotest (vs. 130525, B. Rihm, pers. commun., Jun 17, 2013; i.a. Remund et al. 2014), which included monthly values of mean air temperature, mean air temperature minima and maxima, minimum air temperature, number of frost days, precipitation sum, mean photosynthetic active radiation and relative sunshine duration for a time period between 1659 and 2100. Relevant output of MetHyd, which partly is annualized input, is plotted in Figure 4.

Considering the A1B climate scenario, the simulation resulted in a distinct increase of temperatures and an insignificant decrease of precipitation (Figure 4A and E). Both time-series exhibited substantial interannual variation but relative narrow range, the later being related to the limited spatial distribution of the selected sites. As a result of temperature dependent elevated actual evapotranspiration rates, both percolation and soil water contents moderately decreased in the second half of the simulation period. Soil hydraulic variables – water content at saturation (θ_s), at field capacity (θ_{fc} at pF2.5), at the onset of limited transpiration (θ_c at pF3.0) and at wilting point (θ_{wp} at pF4.2) – used to model annual moisture contents are estimated internally, using input soil properties and Wösten et al. (1999) to parameterise the van Genuchten (1980) equation. Since both temperature and soil moisture can be highly variable within a year, rate modifying factors required by the carbon and nitrogen routines in VSD+ were now calculated from daily rather than from annual mean input. Factors for mineralization (miR) and nitrification (nit) scatter around 1 and slightly increase towards the end of the simulation period (Figure 4F and G). No obvious trend was observed in the denitrification factor, which was always very low (Figure 4H).

Table 1 List of input parameters required to run VSD and VSD+. Abbreviations: (V/F): either a constant value or a file can be specified; {def}: default value in case of missing input.

Key word	Unit	Parameter description	Default	Model
SiteInfo	-	string with any info on the site (max 128 chars)		VSD, VSD+
period	a	starting and ending year of simulation		VSD, VSD+
parentCa	-	if >=0 simulate calcareous soil; value of parentCa (<=1) is fraction of Ca in limestone	{-1}	VSD, VSD+
thick	m	thickness of the soil compartment	(V)	VSD, VSD+
bulkdens	g cm^{-3}	bulk density of the soil	(V)	VSD, VSD+
Clay_ct	wt. %	amount of clay (particle size) in the fine-earth	(V)	VSD+
Excmod	-	cation exchange model option: 1: Gaines-Thomas; 2: Gapon	{1}	VSD, VSD+
CEC	meq kg^{-1}	cation exchange capacity of the soil	(V)	VSD, VSD+
bsat_0	-	initial base saturation; if missing (or <0) determined by model from steady state	{-1}	VSD, VSD+
lgKAlBC	-	log10 of selectivity constant for Al-Bc exchange; calibrated	{0}	VSD, VSD+
lgKHBC	-	log10 of selectivity constant for H-Bc exchange; calibrated	{2}	VSD, VSD+
lgKAlox	-	log10 of Al equilibrium constant ((mol/l)^(1-expAl))	(V/F)	VSD, VSD+
expAl	-	exponent in [Al] = KAlox·[H]^expAl (>0); 3: gibbsite equilibrium	{3}	VSD, VSD+
pCO2fac	-	CO_2 pressure in soil solution (multiple of pCO_2(atm) in air)	(V/F)	VSD, VSD+
RCOOmod	-	organic acid dissociation model option: 0: Oliver-type model; 1: mono-protic organic acid; <0: No organic acids simulated	{0}	VSD, VSD+
RCOOpars	-	1 or 3 parameters for (Oliver-type) mono-protic organics model: pK = par(21)+par(22)·pH-par(23)·pH^2; not read if RCOOmod<0		VSD, VSD+
cRCOO	mol m^{-3}	total concentration of organic acids (m·DOC); 0=no organic acids simulated	(V/F) {0}	VSD, VSD+
CNratmin	g g^{-1}	minimum C:N ratio in topsoil	{15}	VSD
CNratmax	g g^{-1}	maximum C:N ratio in topsoil	{40}	VSD
CNratseq	g g^{-1}	C:N ratio of material immobilised beyond Nim_acc	(V) {0}	VSD
Cpool_0	g m^{-2}	initial amount of C in topsoil (per unit area); calibrated	{0}	VSD, VSD+
CNrat_0	g g^{-1}	initial C:N ratio in topsoil; calibrated	{0}	VSD, VSD+
f_de	-	denitrification fraction (0<=f_de<=1)	{0}	VSD
Nim_acc	eq m^{-2} a^{-1}	'constant' (acceptable, minimum) N immobilized	(V/F) {0}	VSD
knit	-	nitrification rate constant	{4}	VSD+
kdenit	-	denitrification rate constant	{4}	VSD+
Nupeff	-	fraction of N deposition that is available for uptake	{0.92}	VSD+
QIlf	-	index of litter quality of litterfall	{0.25}	VSD+
cN_min	eq m^{-3}	minimum [N] in soil leachate	{0}	VSD
cCa_min	eq m^{-3}	minimum [Ca^{2+}] in soil leachate	{0.0001}	VSD
cMg_min	eq m^{-3}	minimum [Mg^{2+}] in soil leachate	{0.00001}	VSD
cK_min	eq m^{-3}	minimum [K^{+}] in soil leachate	{0.00001}	VSD
TempC	°C	average soil temperature	(V/F) {8}	VSD, VSD+
Precip	m a^{-1}	above canopy precipitation	(V/F)	VSD+
percol	m a^{-1}	percolation from the layer bottom (precipitation surplus)	(V/F)	VSD, VSD+
Theta	m3 m^{-3}	volumetric water content of the soil	(V/F)	VSD, VSD+
SO2_dep	eq m^{-2} a^{-1}	deposition of SO_x	(V/F) {0}	VSD, VSD+
Cl_dep	eq m^{-2} a^{-1}	deposition of Cl	(V/F) {0}	VSD, VSD+
NOx_dep	eq m^{-2} a^{-1}	deposition of NO_y	(V/F) {0}	VSD, VSD+
NH3_dep	eq m^{-2} a^{-1}	deposition of NH_x	(V/F) {0}	VSD, VSD+
Ca_dep	eq m^{-2} a^{-1}	deposition of Ca	(V/F) {0}	VSD, VSD+
Mg_dep	eq m^{-2} a^{-1}	deposition of Mg	(V/F) {0}	VSD, VSD+
K_dep	eq m^{-2} a^{-1}	deposition of K	(V/F) {0}	VSD, VSD+
Na_dep	eq m^{-2} a^{-1}	deposition of Na	(V/F) {0}	VSD, VSD+
Ca_we	eq m^{-3} a^{-1}	weathering rate for Ca	(V/F) {0}	VSD, VSD+
Mg_we	eq m^{-3} a^{-1}	weathering rate for Mg	(V/F) {0}	VSD, VSD+
K_we	eq m^{-3} a^{-1}	weathering rate for K	(V/F) {0}	VSD, VSD+
Na_we	eq m^{-3} a^{-1}	weathering rate for Na	(V/F) {0}	VSD, VSD+
Ca_upt	eq m^{-2} a^{-1}	net uptake of Ca	(V/F) {0}	VSD, VSD+
Mg_upt	eq m^{-2} a^{-1}	net uptake of Mg	(V/F) {0}	VSD, VSD+
K_upt	eq m^{-2} a^{-1}	net uptake of K	(V/F) {0}	VSD, VSD+
N_gupt	eq m^{-2} a^{-1}	net uptake of N	(V/F) {0}	VSD, VSD+
Clf	g m^{-2} a^{-1}	C flux due to litterfall (including harvest residue and fineroot turnover)	(V/F)	VSD+
Nlf	g m^{-2} a^{-1}	N flux due to litterfall (including harvest residue and fineroot turnover)	(V/F)	VSD+
Nfix	eq m^{-2} a^{-1}	N fixation from MakeDep (in periods with N_{gupt}>N_{dep}+N_{min})	(V/F)	VSD+
rf_miR	-	reduction factor for mineralization	(V/F)	VSD+
rf_nit	-	reduction factor for nitrification	(V/F)	VSD+
rf_denit	-	reduction factor for denitrification	(V/F)	VSD+
Observations:				
bsatobs	-	year and base saturation in that year (for -Exc calibration)	(V)	VSD, VSD+
CNobs	-	year, C pool (g m^{-2}) and C:N ratio (g g^{-1}) in that year (for -CN calibration)	(V)	VSD, VSD+
Cpoolobs	g m^{-2}	year and C pool in that year	(V)	VSD+
Npoolobs	g m^{-2}	year and N pool in that year	(V)	VSD+
CNratobs	g g^{-1}	year and C:N ratio in that year	(V)	VSD+
cXobs	eq m^{-3}	year, average annual concentration of X (e.g. SO_4^{2-}, Cl^{-}, pH, ...), standard deviation of concentration of X	(V/F)	VSD+

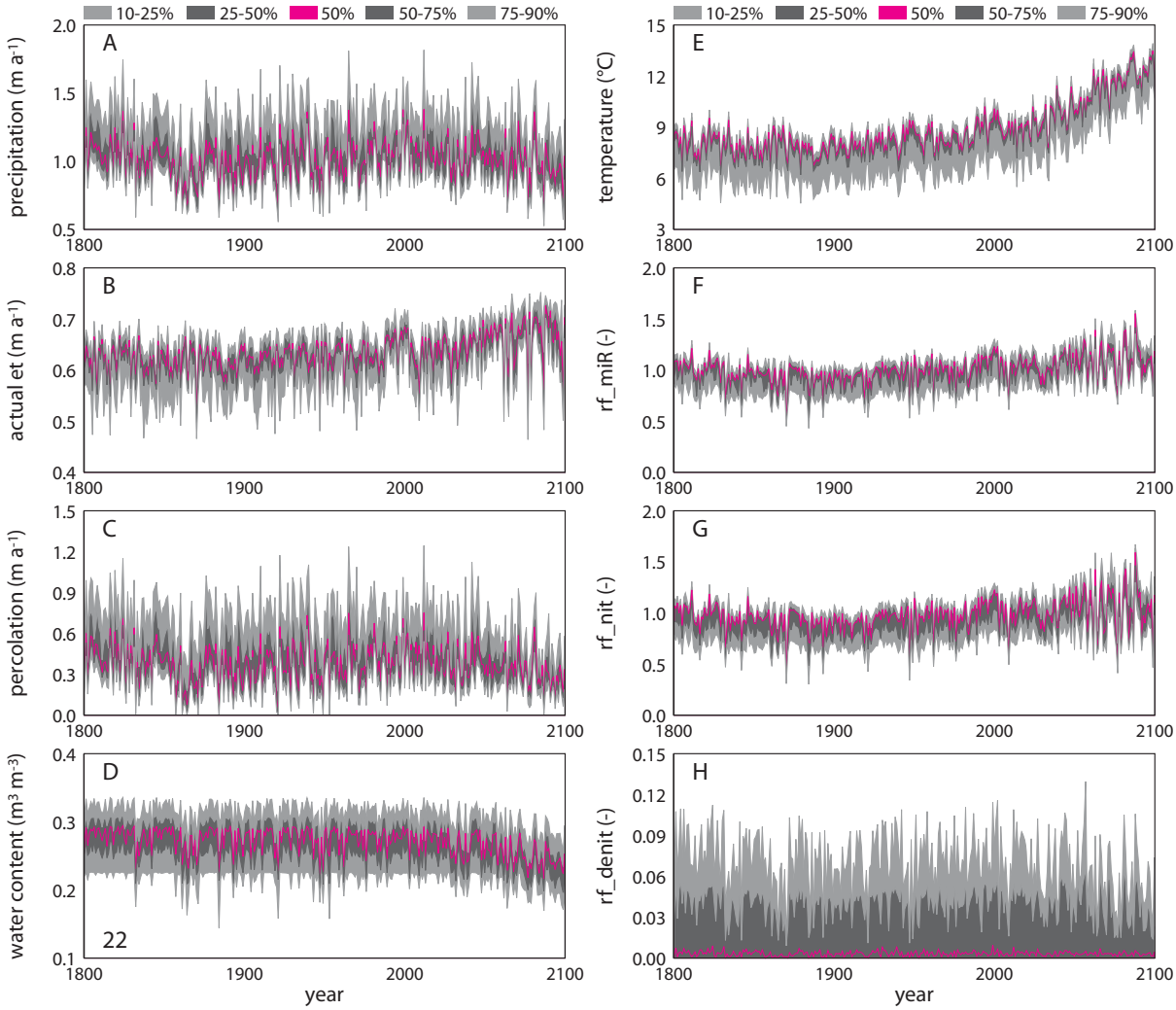

Figure 4 Trends and distribution of relevant climatic and hydrologic input to VSD/VSD+ as obtained from MetHyd. Abbreviations: et: evapotranspiration; rf: rate modifying factor for mineralisation in the RothC model (miR), nitrification (nit) and denitrification (denit).

2.2.2 Deposition

Deposition input for the dynamic models still was produced with MakeDep using model set-up and data as described in Kurz & Posch (2015; Appendix B). To allow reconstructing the site-specific deposition history as close as possible to “natural conditions”, we used site-specific episodic harvesting scenarios and enabled canopy scaling of dry deposition.

Figure 5 depicts the characteristic patterns of atmospheric deposition to forests in Switzerland with the peak of pollutant input in the 1980s and 90s and the subsequent substantial decrease as a result of air pollution control measures and structural changes in Eastern Europe. Regarding acidifying pollutants – oxidised S (SO_x), N (NO_y) and reduced N (NH_x), trends after 2020 were kept constant on levels set by the 1999 Gothenburg Protocol, and the variation in deposition input in the last third of the simulation period only is due to varying canopy owing to episodic harvesting. Base cation (Bc) and sodium (Na) deposition trends (Figure 5E and F) exhibit the same features resulting from the extrapolation of current BC (covering Ca, Mg, K and Na) loads by means of a single national BC trend (e.g., SAEFL 1998).

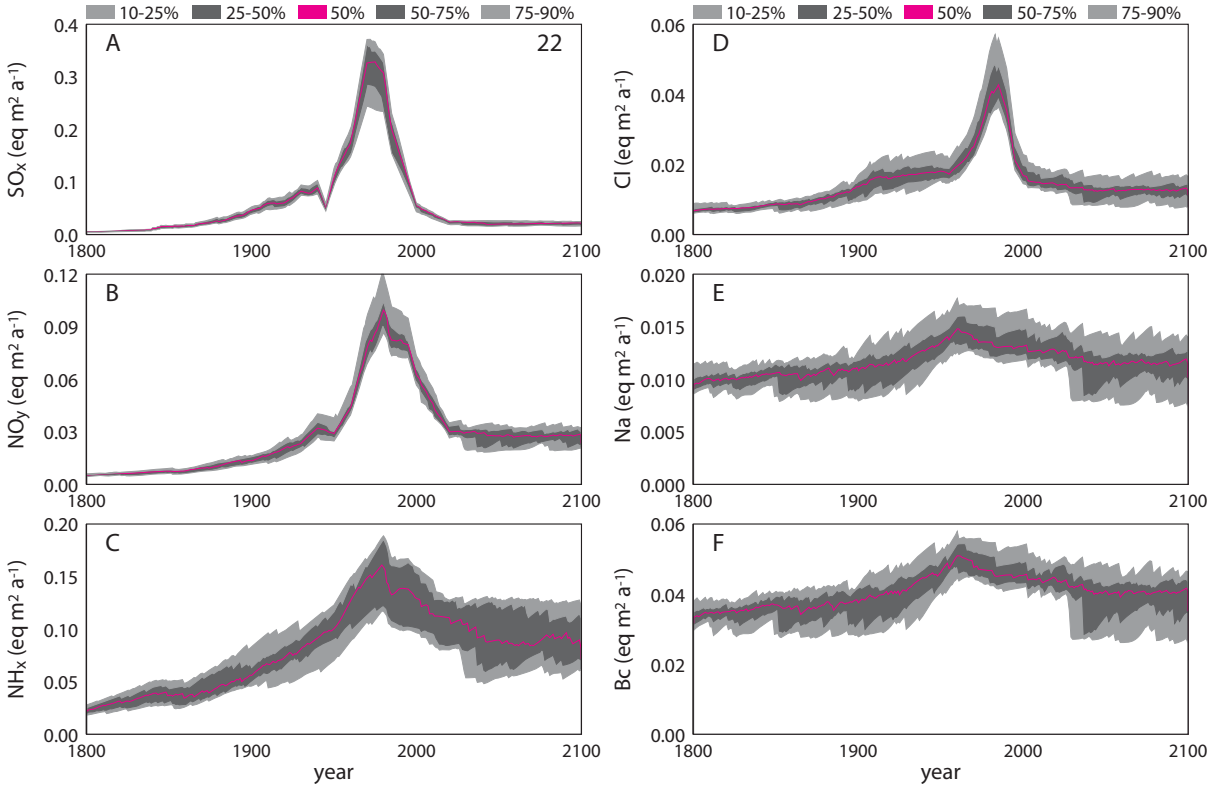

Figure 5 Trends and variation of atmospheric deposition at the selected 22 sites.

2.2.3 Nutrient fluxes

Simultaneously with deposition, fluxes of macronutrients, which are requested from all dynamic models, and C fluxes, required only by VSD+, were simulated by MakeDep. Regarding C, VSD+ requires only litterfall (LF) of C as input flux (key word <Clf> in Table 1), which was calculated from MakeDep's biomass output according to

$$(1) \qquad LF_C = \frac{1000}{2}\left(1.6\left(\left(m_c(t-1) - m_{H,c}\right)\left(f_{cd} + \frac{\left(1-f_{cd}\right)}{7}\right) + m_{h'c}\right) + m_{h'}\right)$$

where m_c is the stand's canopy mass (all m in kg m^{-2} a^{-1}) at the end of the previous time-step (t-1), f_{cd} the fraction of deciduous canopy with respect to the total canopy of the stand, m_H the amount of cut material and $m_{h'}$ the harvest residues. The term in the inner bracket is LF comprising (remaining) deciduous canopy falling every year, coniferous canopy of which 1/7th is replaced every year and leafage on the cut trees not removed ($m_{h'c}$). This LF was multiplied with 1.6 to account for the fine-root turnover. $m_{h'}$ was calculated from the amount of compartments on the cut trees ($m_{H,j}$) that are not removed from the stand according to

$$(2) \qquad m_{h'} = \sum_{j=1}^{3} m_{H,j}\left(1-f_j\right) \text{ and } m_{h'c} = m_{H,c}\left(1-f_c\right)$$

j standing for coarse roots, bark, branches, c for canopy and the term in the bracket is their fraction left in the stand. The multiplication by 1000 in eqn (1) is the unit change from kg to g m^{-2} a^{-1} and the division by 2 is to account for the assumption that only 50% of the biomass is C.

Regarding N, VSD+ requires LF and uptake (U), whereby both should also contain the share of the fine-root turnover. Since the N content of the biomass is variable, the N flux from har-

vest (h'_{N} - of woody compartments and $h'_{\mathrm{N},c}$ - of canopy litter left in the forest) in a given year was derived from the harvesting residues multiplied with the ratio of the pools (the amount of N bound (m_N in $\mathrm{mmol_c\ m^{-2}\ a^{-1}}$) in the biomass ($m$) with subscript j and c) of the previous year (t-1) according to

$$(3)\qquad h'_{\mathrm{N}} = \sum_{j=1}^{3} m_{H,j}\left(1-f_j\right)\left[\mathrm{N}\right]_j \qquad \text{where} \qquad \left[\mathrm{N}\right]_j = \frac{m_{N,j}(t-1)}{m_j(t-1)}$$
$$h'_{\mathrm{N},c} = m_{H,c}\left(1-f_c\right)\left[\mathrm{N}\right]_c \qquad\qquad \left[\mathrm{N}\right]_c = \frac{m_{N,c}(t-1)}{m_c(t-1)}$$

The requested LF_{N} (key word <Nlf>) now consists of the litterfall sensu stricto plus the N flux from harvest residues

$$(4)\qquad LF_{\mathrm{N}} = \frac{14}{1000}\left(1.6\left(\left(m_c(t-1)-m_{H,c}\right)\left(f_{cd}+\frac{\left(1-f_{cd}\right)}{7}\right)\left[\mathrm{N}\right]_c + h'_{\mathrm{N},c}\right) + h'_{\mathrm{N}}\right)$$

where 14/1000 transfers from $\mathrm{mmol_c\ m^{-2}\ a^{-1}}$ to the requested $\mathrm{g\ m^{-2}\ a^{-1}}$.

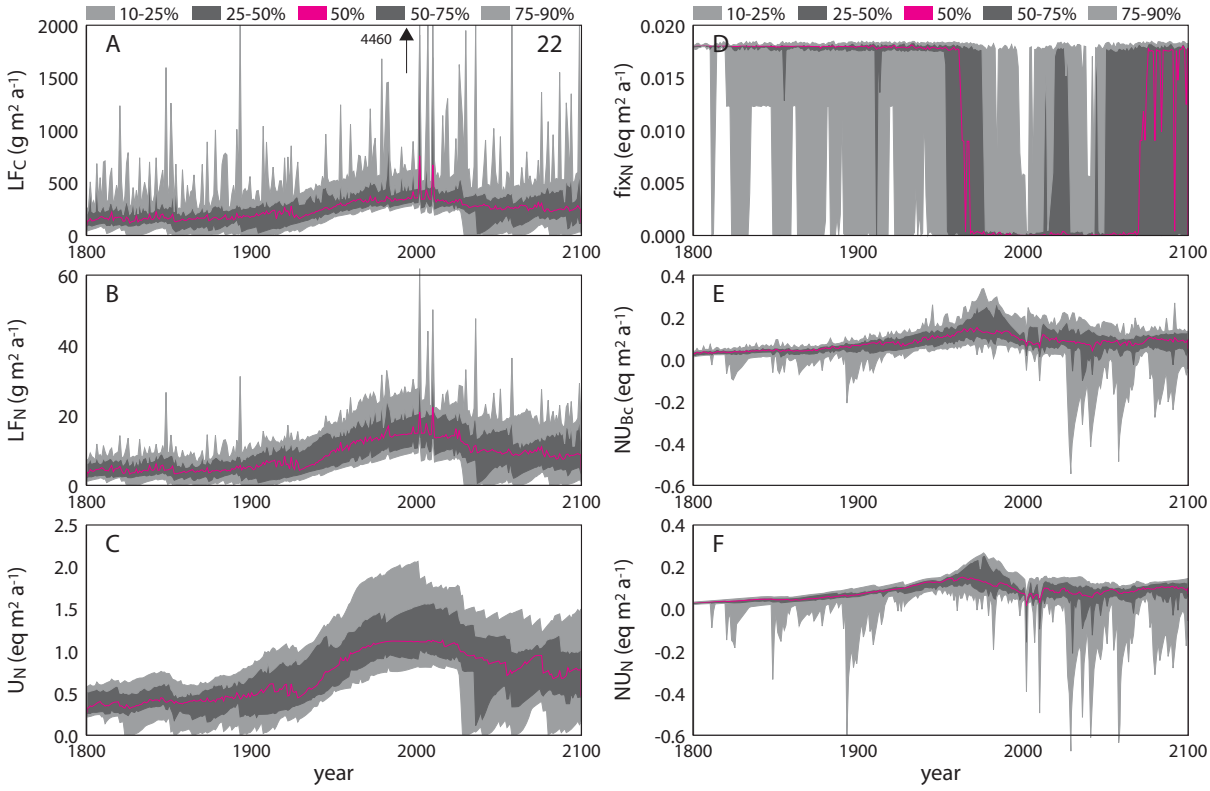

Figure 6 Trends of litterfall and uptake fluxes used as input to VSD+ and VSD. $\mathrm{LF_C}$ and $\mathrm{LF_N}$ are carbon and nitrogen flux due to litterfall, $\mathrm{U_N}$ is uptake of nitrogen, $\mathrm{NU_N}$ and $\mathrm{NU_{Bc}}$ are net-uptake of nitrogen and base cation and $\mathrm{fix_N}$ is fixation of nitrogen.

Uptake of N (U_{N}; key word <Ngupt>), also accounting for the fine-root turnover, was derived from MakeDep's net (growth) uptake of N (NU_{N}) and the litterfall sensu stricto using

$$(5)\qquad U_{\mathrm{N}} = \frac{1}{1000}\left(NU_{\mathrm{N}} + 1.6\left(m_c(t-1)-m_{H,c}\right)\left(f_{cd}+\frac{\left(1-f_{cd}\right)}{7}\right)\left[\mathrm{N}\right]_c\right)$$

where NU_{N} in MakeDep is

$$(6)\qquad NU_{\mathrm{N}} = H_{\mathrm{N}} + d\mathrm{N}_{\mathrm{tree}}dt^{-1}$$

with *H* standing for harvest and the differential term for the change of the N pool in the tree biomass within the given time step.

VSD+ also requires kind of net-uptake of individual base cations (*X* = Ca, Mg, K), which we derived from the base cation fluxes in MakeDep using

(7) $$NU_X = NU_X - NM_X$$

MakeDep allows to pool leaf and harvest litter on the forest floor, and to delay the mineralization. This was thought to not really be compatible with VSD+'s internal concept of C and N dynamics and suggested to alter the derivation of C and N input fluxes as described above. Bc input from vegetation, however, is interpreted as "standard" net flux as also being requested from VSD, and consequently input fluxes of Bc as well as of N for VSD, were calculated with the earlier agreed procedure (eq 7).

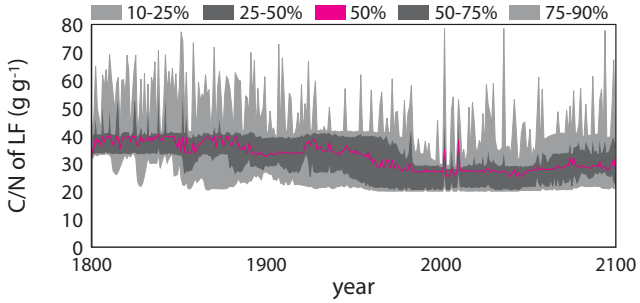

Figure 7 Trends of C/N ratio of litterfall.

Generally, standard fluxes (Figure 6A to C) were always positive while net fluxes (Figure 6E and F) were both positive and negative. Net uptake became negative, if uptake was smaller than the mineralisation input from the harvested residues on the forest floor. The trends exhibit that management was assumed to have been more intensive in the past (i.e. prior to 1900) and to be intensified again from current times onwards. Growth was limited in the past, which is revealed by lower LF in the past compared to current and future times. The reason for this limitation was lower N availability due to low deposition input, which is indicated by the compensating N fixation remaining mostly close to the maximum allowed value of 2.5 kg ha^{-1} a^{-1} (0.18 eq m^{-2} a^{-1} in Figure 6D) until the 1950s. The decrease in management pressure in the last century, also led to current higher forest growth rates. It has to be kept in mind that MakeDep only "sees the above ground" essentially using deposition (sensu stricto and fixation) and mineralisation (from harvest litter) in the N balance (in=out+accumulated) and does not account for the release of N from the N pool in the soil. While N is balanced that way, Bc uptake may be limited in the soil chemistry model, if the supply (from deposition, mineralisation, weathering and exchange) is lower than the demand. The trend of the C/N ratios (Figure 7) of litterfall also reproduced the increasing N supply in the course of time, the median C/N declining from roughly 40 to slightly below 30 in current times. Litterfall sensu stricto C/N ranged between 33 and 20 for deciduous and between 42 and 29 for coniferous leaf litter as a result of input leafage N content thresholds.

2.2.4 Weathering

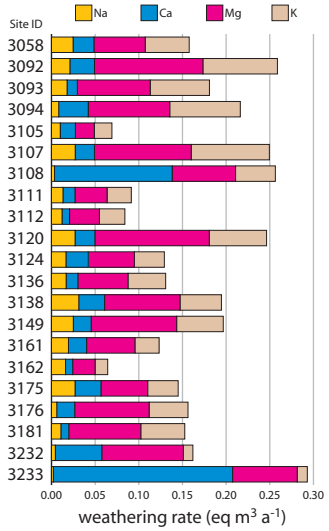

Figure 8 Range of current weathering rates.

Weathering fluxes were drawn from a single-layer SAFE model run for which the same input was used as with VSD and VSD+. While 80% of the modelled annual Mg, K and Na weathering rates fall within a reasonable narrow range (Figure 9B-D), the distribution of annual Ca weathering rates is skewed towards higher values (Figure 9A) due to calcareous soils in the population. Excluding soils containing >0.5% carbonate, current (2017) weathering rates were estimated to range from 21-312 for Na, 82-2053 for Ca, 217-1310 for Mg and 110-895 eq ha^{-1*} a^{-1} for K (*normalized layer thickness of 1 m). In non-calcareous soils, Mg and K weathering rates were generally higher than Ca and Na weathering rates (Figure 8). This most likely is a result of the redistribution of the surface areas (see Section 2.2.5) leading to a stronger weighting of sheet silicates (including clay minerals) and dark minerals to the account of feldspars. Weathering rates tended to somewhat increase in the course of time due to the temperature increase and despite of decreasing soil moisture.

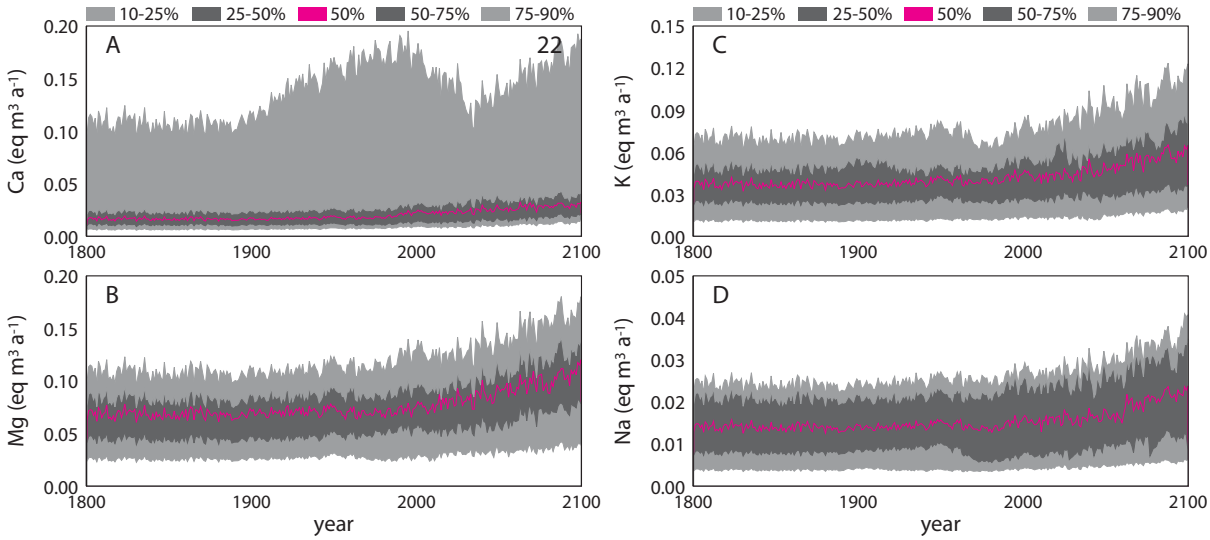

Figure 9 Trends and range of weathering rates obtained from a single-layer SAFE model run of the 22 sites.

2.2.5 Soil properties

Both VSD and VSD+ can be operated with limited soil input consisting of 11 variables (Table 1). More soil input is required to run the auxiliary models, MetHyd and SAFE, for the latter of which a series of parameters is used to calculate the weathering rates. These auxiliary parameters are listed in Kurz & Posch (2015) including transfer functions applied to derive soil input from soil raw data. Soil input was harmonized, i.e. irrespective of the type of soil chemistry model run (dynamic or static) the same procedure for deriving parameter values was used. Basically, this comprised averaging raw data for the (appropriate) rooting zone, converting raw data to soil bulk system and subsequently applying pedo-transfer functions.

Due to the tendency to overestimate sodium weathering, the assignment of the bulk weatherable surface to individual mineral species was modified already in the steady-state runs for the Call for Data in 2014-15 (Kurz & Posch 2015). There is a certain agreement that mineral con-

tents should be input as surface area fractions (Jönsson et al. 1995). Input as weight fractions would imply that e.g. clay minerals occur in equal amounts in the clay, silt and sand particle size fraction. There is enough analytical evidence (i.e. XRD analyses of clays) to reject this implication, and we reserved 90% of the clay particle size fraction for clay and secondary minerals such as aluminium and iron (hydr)oxides. How much of this occupancy target was realised, however, depended on the amount of clay and secondary minerals in the sample.

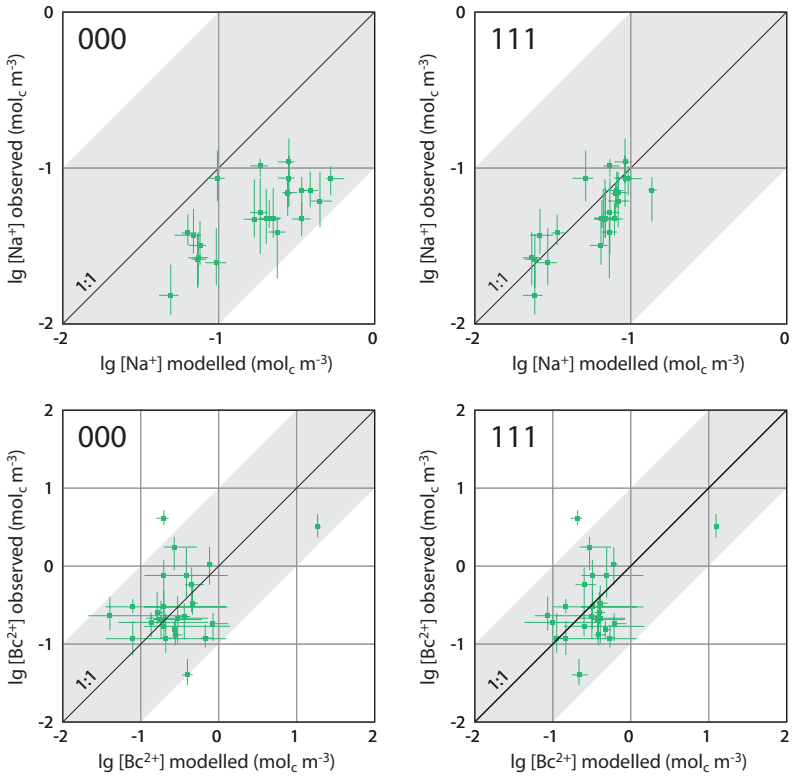

Figure 10 Impact of weatherable surface area modifications on the weathering rates and subsequently concentrations of base cations [Bc^{2+}] and sodium [Na^{+}] in the soil solution. 000: standard procedure, 111: full correction; Model: SAFE, single layer, median (dot) and spread of 10 to 90%ile (bar) of the period (ca. 1998-2008) given by the observations.

Although optical analyses of the sand fraction of Swedish and Swiss soils suggested a predominance of primary light minerals (quartz, K-feldspar, plagioclase, calcite, dolomite), we refrained from setting a general allocation target. To avoid unrealistically high sodium concentrations in the soil solution (Figure 10), we only considered feldspars to preferably occur in the sand particle size fraction. Finally, there were some concerns about samples with clay particle contents far above for what the 'standard' surface area assessment algorithm originally was built for (Nordic sandy soils). It was considered unlikely that all of the surface area of e.g. 50% clay is equally accessible for the percolating water and therefore for weathering processes (e.g., van der Salm 2001), and a function was used that, above a threshold (~20 wt. % clay particle size content), increasingly reduces the contribution of the clay particle size fraction to the bulk surface area.

2.2.6 Calibration

In both, VSD and VSD+ runs, the sites were essentially calibrated regarding the Gapon exchange coefficients (lgKAlBc, lgKHBc) and the initial pools of carbon and nitrogen in the topsoil (Cpool_0, CNrat_0). Parameter values and distribution types were set as compiled in Table 2. Reference values considered were present base saturation of the rooting zone (key word: bsatobs) and C and N pools (in g m^{-2}) of the first 0.30 m of the soils (key word: Cpoolobs, Npoolobs, CNratobs) including their assumed standard deviations. The number of calibration runs in VSD+ was set to the default 10'000. Calibration generally was started in 1800, however, for a few sites, no successful calibration was found within the set simulation period (1800 to 2100), and the start had to be shifted backward or forward: site 3120 to 1700, 3136 to 1500, 3161 to 1821 and 3162 to 1850. Forward shifting of the simulation start affected the analysis of regional output trends, the simulation period of which finally had to be

limited to 1850-2100.

Table 2 Parameters selected for calibration and setting of the their values.

		VSD+			VSD	
Parameter	Distribution	Mean	StdDev	Default	Minimum	Maximum
lgKAlBc	normal	0	1	0		-
lgKHBc	normal	2	1	2	-	-
Cpool_0	normal	10000	5000	-	-	-
CNrat_0	normal	30	20	-	-	-
CNrat	-	-	-	-	10	40

2.2.7 Plant input

Each plant exhibits a particular response to environmental drivers, the key values of its mathematical transformation were tabulated and integrated in the respective (ground-)vegetation models (Veg, VeCH, PROPS). Model users basically have to only provide the series of key species characterising the habitat of the considered sites independent of the type – dynamic or static (critical loads) – of planned model run. A subset (76) of the national dynamic modelling sites was categorised with regard to the prevailing forest type and a characteristic natural ground vegetation community was assigned to each forest type (S. Braun, IAP & T. Burger, Burger & Liechti GmbH, pers. commun., Feb 23, 2015). The plants in a community additionally were labelled according to their importance for the plant community: level 6 (determinant) to 1 (ubiquist). For the modelling, generally plants of level 6 to 3 were used and ubiquists were ignored.

2.2.8 Input for biodiversity critical loads modelling

Critical loads for biodiversity were assessed for a subset (76) of forest monitoring plots considered in the conventional acidity critical loads calculation using the PROPS-CLF model (www.wge-cce.org/Methods_Models/Available_Models) provided by the Coordination Centre for Effects. For internal consistency reasons, input for the Swiss PROPS-CLF runs was, unlike for dynamic model runs and biodiversity critical loads model tests, basically drawn from the acidity critical loads calculations with the SMB (Kurz & Posch 2015; Figure 1). In compliance with the decisions of the Task Force meeting of the ICP Modelling & Mapping in Rome (April 7–10, 2014), the Habitat Suitability Index (HSI) was used to quantify the response of the ground vegetation plant communities to varying S and N deposition:

$$HSI = \frac{1}{n}\sum_{j=1}^{n}\frac{p_j}{p_{j,max}}$$

where n is the number of species, p_j the occurrence probability of species j, and $p_{j,max}$ the maximum occurrence probability of species j. The model was set to make use of $p_{j,max}$ determined in the 2 dimensional (pH-N_{dep}) subspace, implying constant C/N, P and T as given by the site-specific input (see also Section 3.4.2). Modelling with PROPS-CLF requires specifying the bounding box of deposition, which was limited to 4000 eq ha^{-1} a^{-1} (equals 64 kg S and 56 kg N ha^{-1} a^{-1}). By common accord, a critical limit of $0.8 \cdot HSI_{max}$ was chosen to derive the critical load function in the N_{dep}-S_{dep} plane (Posch et al. 2015).

3 RESULTS

3.1 Calibration results

The 22 sites were successfully calibrated with both models VSD and VSD+. Successful in this context is a technical term and means that the model did not reject the found calibration result. A graphical analysis of modelled and observed parameter values (which were used for the calibration) exemplifies that modelled C pools, compared to the input, tended to be slightly underestimated particularly the higher C pools in VSD+ (Figure 11A). Modelled initial C pools differed substantially between the two models (Figure 11B), obviously reproducing the conceptual differences in the implemented C and N dynamics.

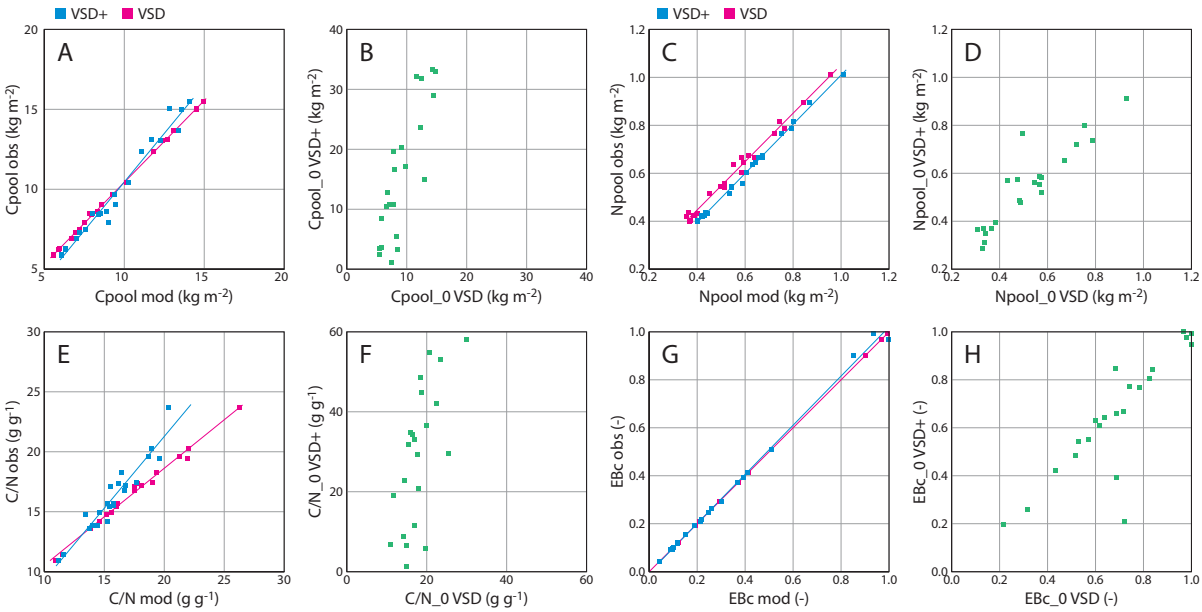

Figure 11 Comparison of calibrated entities with the input and scatter plot of initial pools, C/N and base saturation obtained from the two models.

Modelled and input N pools showed less scatter than found with the C pools (Figure 11C) and the observations were well reproduced by VSD+. VSD produced slightly and pretty systematically deviating N pools, on average ca. 8% lower values (intercept 44 g m^{-2}) than the observations. The calculated C/N ratio integrated the deviations in the two pools and consequently the regressions departed from the 1:1 line (Figure 11E). VSD+ returned a bit lower, VSD a bit higher C/N ratios than the input observations. Comparing the two model outputs revealed a much better correlation of initial N pools (Figure 11D) than found with C pools, but (logically) a similar pattern as with C pools was obtained with initial C/N ratios (Figure 11F). Current base saturation (Figure 11G) was mostly well reproduced with the exception of three samples with very high base saturation, which VSD+ had some difficulties to calibrate.

3.2 Trends in soil chemistry

3.2.1 Solid phase chemistry trends

As a consequence of the current model settings and input, VSD+ C pools decreased, partly substantially, at 16 sites and increased at 6 sites. The regional trend (Figure 12, left column) therefore showed a wide spread of C pools between 2.7 and 25.6 (min/max) in the early simulation period which fell to 6 to 13.8 in 2000 and to 5.7 to 18.7 kg C m^{-2} by the end of the modelling period.

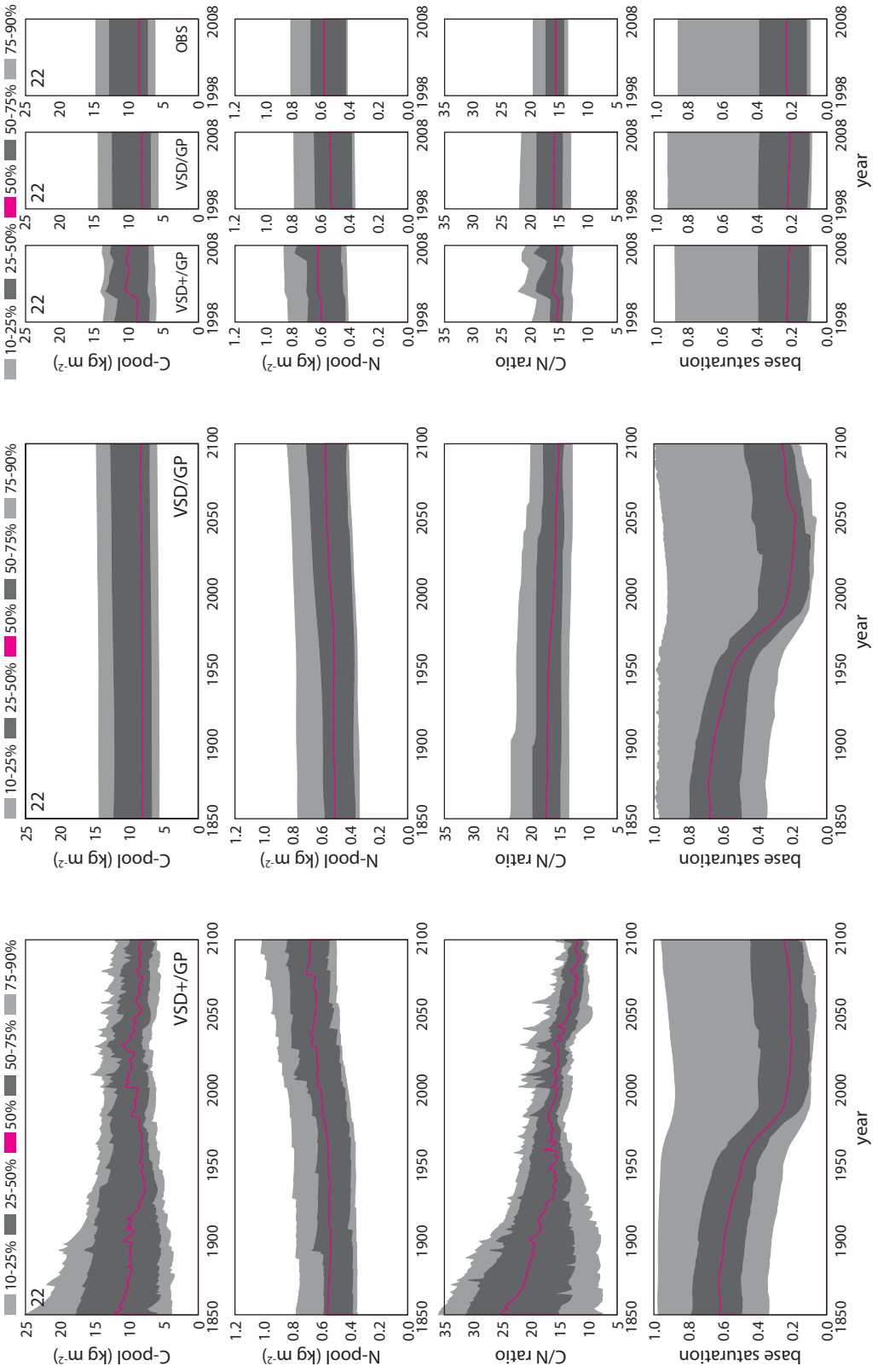

Figure 12 Regional trends of soil solid phase chemical parameters. VSD+ runs were calibrated from different years onwards, VSD from 1800 onwards. As deposition scenario beyond 2020, Gothenburg Protocol (GP) was used. Small numbers in the top left corner of the plots refer to the number of sites considered in the plot.

N pools modelled by VSD+ increased at 19 sites and showed no trend at 3 sites. The range of found N pools was largely similar throughout the simulation period spanning from 291 to 975 in 1850, from 397 to 1010 and finally from 490 to 1307 g N m^{-2} by 2100. C/N integrated the

trends of C and N pools and declined at 16 sites over time, while it remained indifferent or inclined at 6 sites. C/N ranged from 5.9 to 43.7 at the start of the simulation period narrowed to 10.9 to 20.3 in 2000 and ended with 8.6 to 14.9 in 2100. A decline in forest soil C/N was not unexpected given the excess N input in the recent decades, but VSD+ indicated that this change could also be driven by a loss in the C pools.

VSD results showed neither the variability nor the pronounced trends of VSD+'s C and N pools. Within the modelling period, C pools consistently increased by between 1 and 7%, N pools by between 3 and 36%, and the spread of minimum and maximum value was always roughly the same, i.e. that of the calibration input. The reason of this "non-performance" of the C-N processes implemented in VSD is not yet understood. As a result of the pools' trends, C/N slightly decreased by on average 10% and the median C/N fell from 17.4 in 1850 to 15.1 in 2100.

Compared to observations (Figure 12, small plots to the right of the figure), VSD+ moderately overestimated C and slightly overestimated N pools under the regional perspective. It has to be kept in mind that observations refer to specific varied years extended to the time window prior to running the statistics, and do not reflect the dynamics of the system.

Regional base saturation revealed the expected pattern with considerably lower values in the wake of the peak of acidification and rising values as the result of increasingly reduced acidifying input. Generally both models indicated that deposition reductions in compliance with the Gothenburg Protocol would only lead to limited recovery of regional base saturation until 2100. The regional pattern of base saturation returned by the two models was surprisingly comparable in terms of trend as well as spread of values. The median base saturation declined from 0.68 (VSD) and 0.62 (VSD+) in 1850 to 0.23 (both models) in 2000 and increased to 0.26 (VSD) and 0.25 (VSD+) towards the end of the simulation period. Range and median of modelled base saturation compared also reasonably well with observed base saturation (Figure 12, small plots to the right of the figure).

3.2.2 Soil solution chemistry trends

Regional trend patterns of soil solution chemistry (Figure 13) generally showed features, which had to be expected from the run and input settings such as lower sulphate concentrations ($[SO_4^{2-}]$) in the second half of the modelling period, increasing sodium concentrations ($[Na^+]$) as a result of increased weathering due to higher temperatures, decreasing hydrogen ion and aluminium concentrations ($[H^+]$, $[Al^{3+}]$) as well as molar Al/Bc ratios as function of decreasing acidification pressure. Regardless of model used, trend patterns of ions only influenced by hydrology and weathering (chloride (Cl^-), SO_4^{2-}, Na^+) didn't differ. From a regional perspective (right most plots), both models returned slightly higher $[Cl^-]$ and $[Na^+]$, slightly lower $[SO_4^{2-}]$ and less variation than the observations (monthly values plotted) and somewhat failed to reproduce the observed decreasing trends of $[Cl^-]$ and $[Na^+]$. Base cation concentrations ($[Bc^{2+}]$) peaked during the peak of acidification and subsequently decreased in the second half of the simulation to ranges below those of pre-acidification times. VSD+ returned a larger span of 80% of $[Bc^{2+}]$ than VSD and little lower values for the 10, 25 and 50 percentiles. VSD+ $[Bc^{2+}]$ were also lower than VSD and observed $[Bc^{2+}]$ during the observation period and both models again didn't catch the weak decreasing trend of observed $[Bc^{2+}]$. While all other ions revealed at least comparable trends independent of the model used, nitrate concentrations ($[NO_3^-]$) trends differed substantially. VSD+ $[NO_3^-]$ were relatively stable the median ranging from 4.5 to 53 $\mu mol_c\ L^{-1}$ and the range of 80% of values fell within 3 orders of magnitude (3 to 2800 $\mu mol_c\ L^{-1}$).

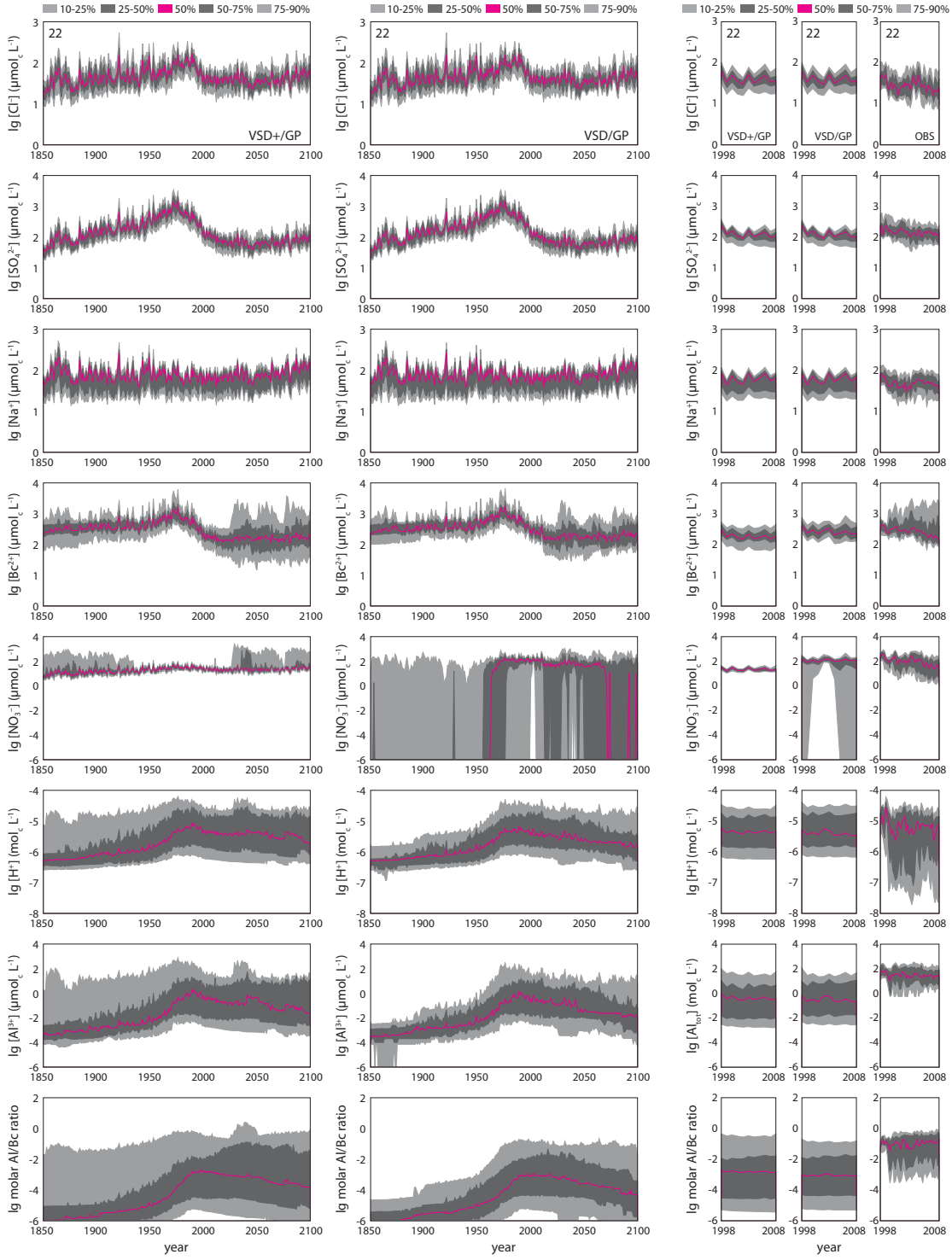

Figure 13 Regional trends of solution chemistry.

VSD modelled very low [NO_3^-] (≤ 1E-06 µmol$_c$ L^{-1}) before 1950 for the majority of the sites and a subsequent steep increase as a result of increasing N deposition. The median plateaued at 80 to 180 µmol$_c$ L^{-1} between 1971 and 2011 before falling to lower values again towards the end of the simulation period. The range of 80% of values fell within almost 9 orders of magnitude. [NO_3^-] during the observation period was a bit underestimated by VSD+ and a bit overestimated by VSD, and the observed decreasing trend was not modelled. The models returned comparable regional trend patterns for [H^+], [Al^{3+}] and molar Al/Bc with distinctly increasing values in the wake of acidification and slowly declining tendency as a result of reduced acidification pressure. Generally, the spread of related percentiles (e.g. 10 and 90) of

VSD+ was larger in the pre- and partly also in the post-acidification period compared to VSD results. Both models tended to underestimate all three parameters in comparison to observations.

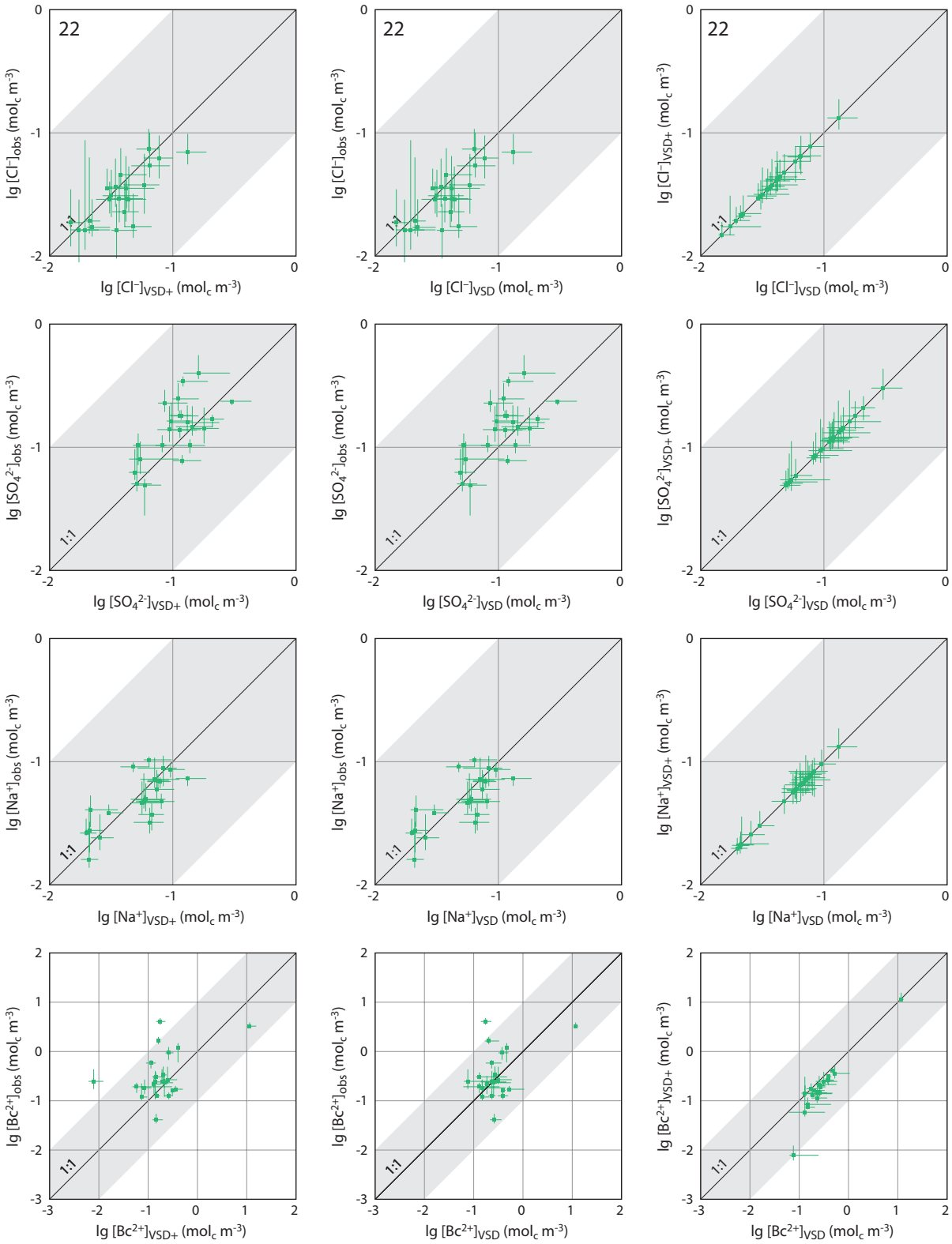

Figure 14 Solution chemistry obtained from VSD+ and VSD compared with monitoring data and plotted against one another. Log-log scale, median (dot) and 10th and 90th percentile (line) of site-specific observation period (maximum 1998 to 2008), values limited to 1E-07 mol$_c$ m^{-3}. Gray shaded area covers ±1 order of magnitude.

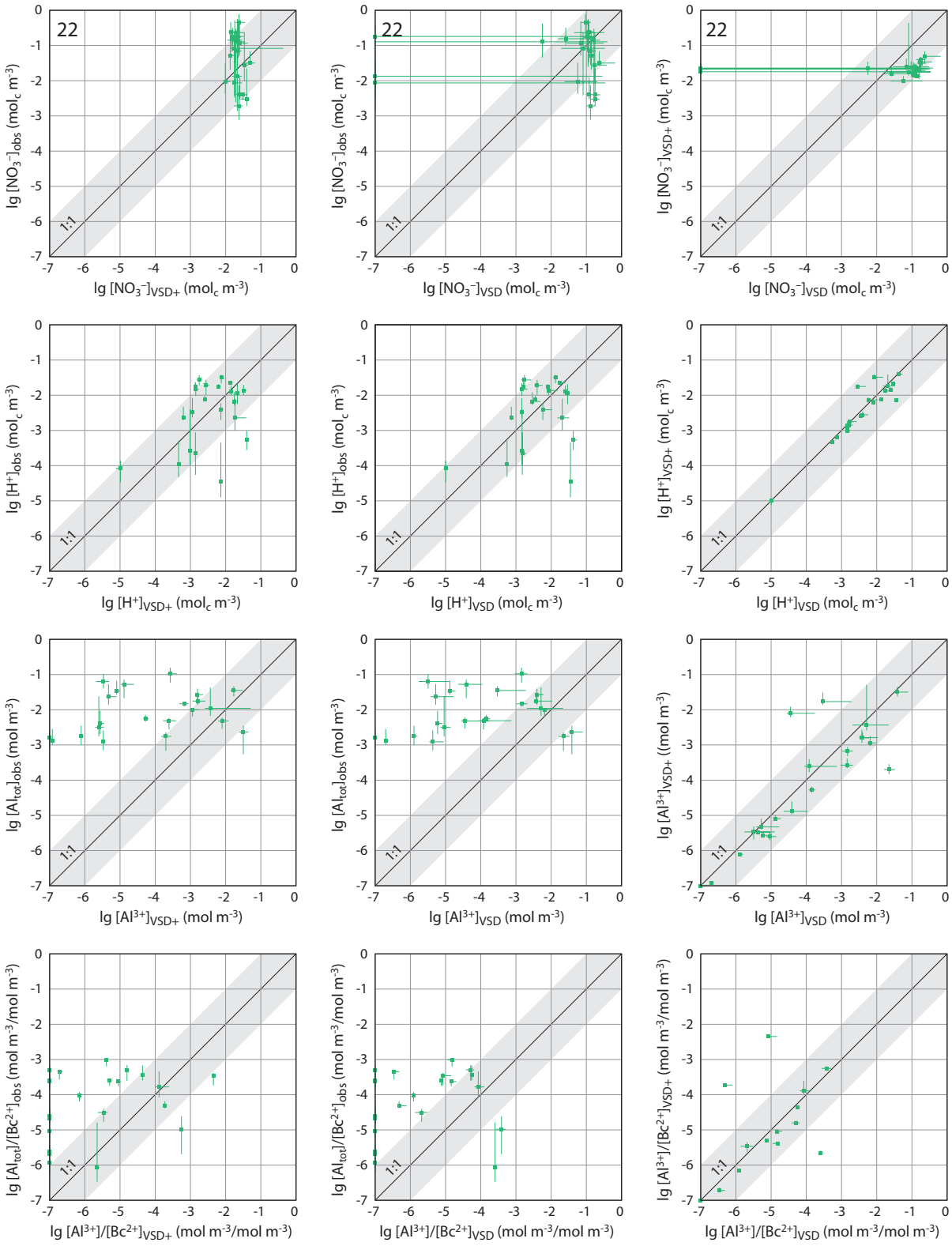

Figure 15 Continued from previous page.

3.2.3 Simulated versus observed chemistry

The soil solution chemistry returned from VSD+ and VSD is plotted in Figure 14 and Figure 15 against the monitoring data provided by the IAP. The graphs depict median and 10th and 90th percentile as “error bars” of both annual model data and annual average of monthly to bi-weekly measurements from the appropriate soil depth for the given monitoring period, which

varies from site to site (maximum time span from 1998 to 2008).

Deviation of modelled and observed conservative ion, such as [Cl^-] and [SO_4^{2-}] was less than ±1 order of magnitude (grey shaded area in the plots) irrespective of model used. The scatter of model results only (right most column) reveals that both models predicted practically the same values. Modelled [Cl^-] tended to often be a little overestimated, while [SO_4^{2-}] at some sites was lower than the measurements. Observed and predicted sodium concentrations ([Na^+]) fell well within ±1 order of magnitude and overestimation regarding observations by the models generally was smaller than with chloride.

[Bc^{2+}] and [NO_3^-], both influenced by biological processes, showed larger scatter and patterns tended to be stretched along the y-axis. [Bc^{2+}] appeared to have partly been underestimated by VSD+, and generally VSD+ produced lower values than VSD. Modelled [NO_3^-] of VSD+ scattered within a relatively limited range and showed no correlation with observations on regional scale. With exceptions, VSD+ produced lower [NO_3^-] than VSD. The pattern of VSD median [NO_3^-] plotted against measurements was comparable with that resulting from VSD+ although the range of medians was larger and particularly the spread of 90% of the values was dramatically extended at certain sites.

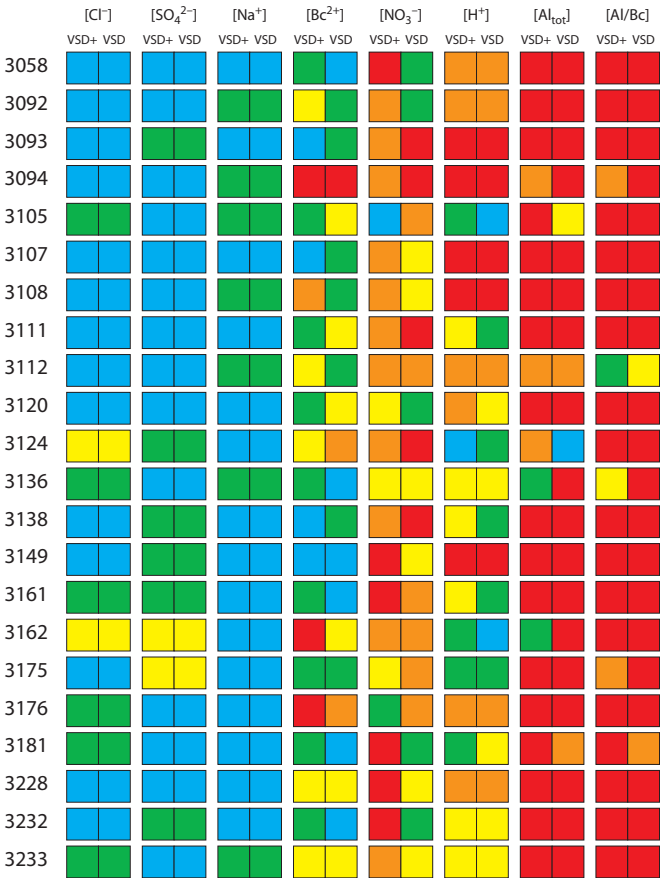

Figure 16 Pattern of Czekanowski index of average annual observed and modelled ion concentrations in the soil solution (monitoring period 1998-2008). CzI classes: ≤1: blue, < 0.8: green, <0.6: yellow <0.4: orange, <0.2: red.

The models tended to return [H^+] within the same order of magnitude and comparable patterns if plotted against observations. Considering the differences in [Bc^{2+}] and [NO_3^-], a convergence of modelled [H^+] with measurements could not be expected. Modelled and measured [H^+] roughly were of the same order of magnitude although the pattern was stretched along the y-axis, and some outliers were also observed. The same holds for modelled aluminium and aluminium to base cation ratio both showing a much larger range of (i.e. often much lower) values than the measurements. It has to be kept in mind that modelled aluminium only covers Al^{3+}, while measured aluminium usually covers all aluminium species caught with the used type of analysis (Al_{tot}).

The comparison of time series of predictions and observations (within the same period) by means of a displacement measure (Czekanowski Index (CzI); Posch et al. 2010; Figure 16) confirmed the general situation i.e., acceptable convergence of modelled and measured [Cl^-], [SO_4^{2-}], [Na^+] and partly [Bc^{2+}], a weak match of [NO_3^-] and [H^+] and an almost complete mismatch of [Al] and Al/Bc ratio.

3.3 Evolution of the ground vegetation composition

The VSD+ model run was used to model vegetation composition in terms of probabilities of occurrence of plant species with PROPS, which is linked to VSD+ via the user interface. The database of PROPS currently contains 4053 plant species. The selected 22 sites were classified into 16 forest types comprising a total of 160 characteristic species (importance level 6 to 3 only considered; Appendix I). 5 of the 160 species were only parameterised as genus and Lathyrus linifolius was missing in the PROPS database.

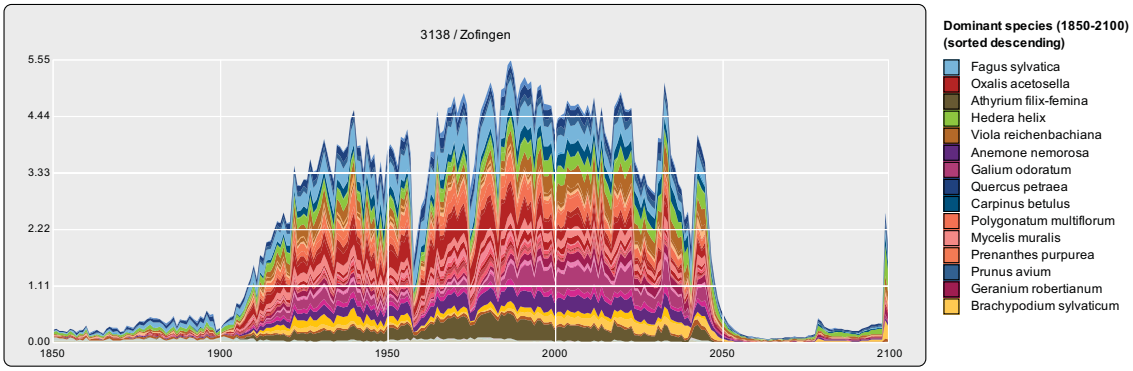

Figure 17 Plot of cumulative plant occurrence probabilities calculated with PROPS on the basis of a VSD+ run.

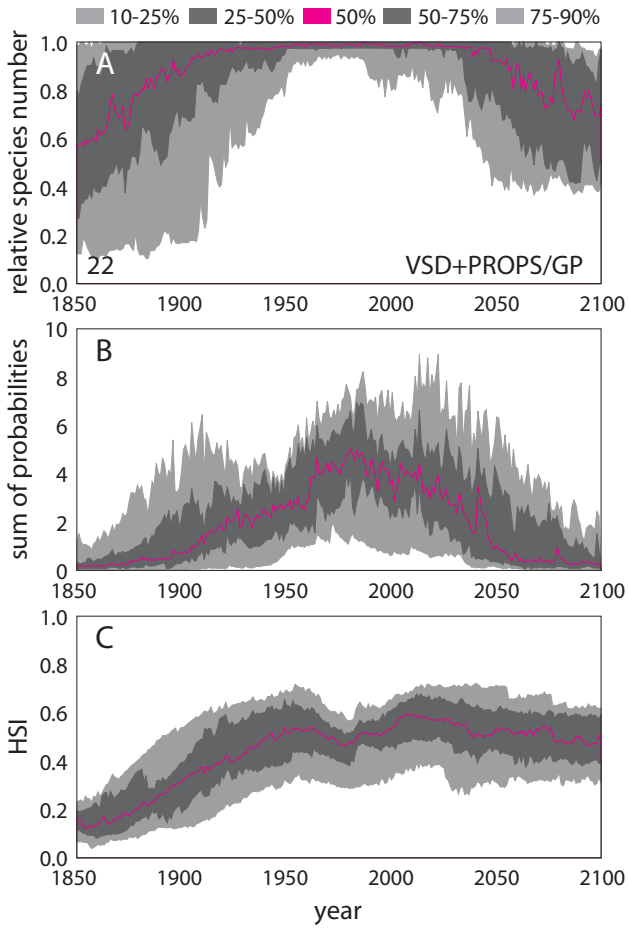

Figure 18 Regional trends of ground vegetation occurrence probabilities. A: site-specific percentage of species with occurrence probability ≥0.00001; B: distribution of site-specific cumulative occurrence probabilities; C: habitat suitability index.

PROPS returned probabilities of occurrence of every plant in the selection between 0 and 1 for every year within the simulation period (Figure 17; Appendix II). Often the occurrence probabilities of plants were fairly low, 83% of returned values being <0.1. The probability was limited to 1E-05 therefore the output tables contained also plants with zero probability of occurrence in particular years. Figure 17 and Figure 18 reveal that primarily in early and late stages of the simulation very low including zero probabilities of occurrence were modelled. The median of the percentage of species with occurrence probability ≥1E-05 over all sites plateaued between 1946 and 2034 with values >98% and fell to 57% in 1850 and 70% in 2100, respectively (Figure 18A). There was a reasonably short period between 1953 and 1988 during which the majority of sites, i.e. 90%, had a percentage of species of ≥90% with occurrence probability above 1E-05. The sample site Zofingen (Figure 17), e.g., has 40 characteristic plant species and the maximum annual sum of returned probabilities was 5.5 being roughly 14% of the potential annual maximum of 40. Figure 18B displays the regional pattern of site-specific sums of

probabilities of occurrence with a median maximum in 1981 and peaks between 2010 and 2020 not exceeding 9 (90%tile) despite of sites with up to 78 species in their habitat. The maximum site-specific sum of probabilities of occurrence was 1.67 at the start and 2.98 at the end of the simulation. The habitat suitability index (HSI) gives more weight to the low occurrence probabilities and started with values between 0.01 and 0.27 (Figure 18C). It steadily increased to a first peak in the 1950's and then temporally decreased in the period when the majority of the plants at the majority of the sites had occurrence probabilities above 1E-05. After a second peak between 2010 and 2020 the regional pattern levelled out towards the end of the simulation period. The trends imply that conditions were most favourable for the selected plant communities in the 2010's, particularly unfavourable in the early years and less favourable towards the end of the simulation.

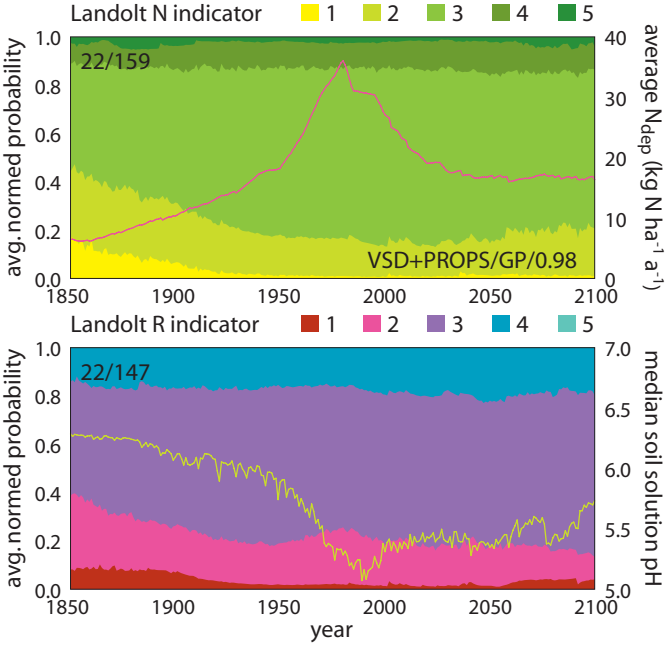

Figure 19 Regional average Landolt N and R indicator group probability trends calculated from normalised PROPS plant occurrence probabilities (N: 159, R: 147 species classified) at 22 sites. Lines in the plots represent average N deposition and median soil solution pH trends.

The previous indices are merely statistical figures and do not contain significant quality information. To analyze the changes in the ground vegetation composition with respect to acidity and N related trophic state of the forests, the selected species were classified using Landolt's R and N indicators (Landolt, 2010). Both indicators have 5 classes whereby N1 and 2 are being addressed as oligothrophic, 3 as mesotrophic and 4 and 5 as eutrophic. R1 and 2 represent acidic, 3 neutral and 4 and 5 increasingly basic substrata. As mentioned earlier, the number of species considered in the current PROPS runs was limited to 160. The majority of selected species fell into N classes 3 (87, 54%), 2 (36), and 4 (28), 6 species fell into N class 1, 2 into N class 5 and 1 species had no classification. R classes contained 9 (1), 30 (2), 57 (3) 50 (4) and 1 (5), and 13 species were rated insensitive to soil pH. Since relative shifts among the classes were of interest, modelled plant occurrence probabilities at each site (Appendix II) were added up group-wise and then normalized to 1[3]. The regional trends, which were attained by averaging the site patterns, are plotted in Figure 19. Regarding N, group 2 and 3 dominated the patterns covering between 72 and 85% of the normalized occurrence probability. The share of oligotrophic plants (group 1 and 2) decreased from 44 at the start of the simulation to 13% by the year 2001, and subsequently recovered to 21% towards the end of the simulation. The pattern matches pretty well the average N deposition trend, which peaked in 1980 and levelled out in the second half of the simulation period at twice as high loads as in the past. The share of oligotrophic plants decreased essentially to the favour of group 3 plants, and eutrophic plants apparently did not profit from the higher N deposition. The regional R group trends compared pretty well with the regional N group pattern and did not correlate with the median soil solution pH. This most

[3] $p_{LN} = \sum_{i=1}^{n} p_{i,LN} \Big/ \sum_{i=1}^{a} p_i$
where p_i is the probability of occurrence of species i (in a given year), n is the number of species in the particular Landolt indicator (subscript LN) group (1 to 5) and a is the number of all species considered on the site.

likely is due to 26 of 42 species in N1 and N2 class fell also in R1 and R2 class.

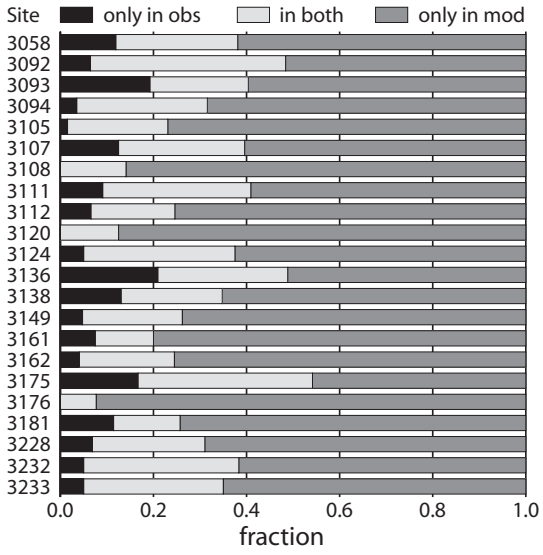

Figure 20 Distribution of observed and modelled plant species among these two datasets.

A comparison of PROPS output with observations or Veg/VeCH model results seemed at current state not really meaningful, and was consequently omitted. Regarding the former, we found a substantial difference in species composition of observed and modelled plant communities. As mentioned earlier, the selected 22 sites covered 16 different forest types (Appendix I, Table 4). Each of the forest types was characterised by between 36 and 82 plant species (31 to 78 species, if species down to significance level 3 were considered) and the overall total of plant species considered was 175 (160 with significance level down to 3; Appendix I, Table 5). 6 of the desired species were not listed in the PROPS database, for 5 of which, however, generic data was available. In the original Veg parameter table, 11 (of the 160) desired species were missing while the VeCH parameterisation contained all of the species. The number of typical species mostly was substantially, i.e. on average 3.7 times, higher than the number of species observed. The number of common species ranged from 4 to 26 and was on average only 24% of the total population (Figure 20). Many of the sites currently have plants occurring that are not part of the site-specific "desired" or "typical" plant community. This number ranged from 0 to 10 or from 0 to 21% of the total population. Additionally, PROPS returned occurrence probabilities unlike Veg/VeCH and observations providing coverage fractions. Statistical approaches to "bring the two worlds together" are only recently being explored (W. Wamelink, WUR, pers. commun., Apr 6, 2017) and not yet consolidated.

3.4 Biodiversity critical loads

3.4.1 Derivation of critical loads with the Veg and PROPS models

Veg calculates the growth strength (*S*) of a species (*j*) as the product of the plant's growth strengths in response to the individual drivers (*i*)

$$S_j = \prod_{i=1}^{n} S_{j,i} \quad (8)$$

where *i* (in the current critical loads calculations) refers to temperature (T in °C), water saturation[4] (θ_s in $m^3\ m^{-3}$), soil solution nitrate concentration ([N] in mg N L^{-1}) and pH. For critical loads calculations we have, compared to the original Veg, excluded the drivers palatability (missing data) and competition (for light and nutrients) as well as light at ground level[5],

[4] Water saturation (θ_s) is calculated from soil water content (Θ), water content at wilting point (Θ_{wp}) and total pore volume of the soil (*TPV*, all in $m^3\ m^{-3}$) according to:
$\theta_s = (\Theta - \Theta_{wp}) / (TPV - \Theta_{wp})$

[5] Competition for nutrients originally was related to the rooting depth of the plant and became irrelevant when Veg was linked to single soil layer models. Competition for light could be ignored, as it depends only on plant height, which in turn currently is an independent though plant-specific default value not affecting the HSI calculation. Light at ground level (referring to the filtering of light by the overstorey canopy) was not considered, because it is difficult to assess, essentially forest management dependent, often inhibiting plant growth and not a driver in PROPS.

which essentially is dependent on forest management. The parameters required to derive plant response to individual drivers are compiled in a parameter table of which two versions were used:

- original Veg model parameterisation (model acronym Veg-CL; vs 2013-11-04, Braun pers. commun.) covering trapezoidal response functions for environmental drivers and logistic functions for chemical drivers – data basis: expert knowledge;
- revised Veg model parameterisation (model acronym VeCH-CL; Kurz, 2016) covering trapezoidal response functions for all drivers – data basis Landolt (2010) and expert knowledge regarding assignment of value ranges for indicator value classes.

To get N and S critical loads, the response of each species of a plant community initially was determined in the [N]-pH plane (orthogonal grid, 100 bins) keeping the climate drivers (temperature and water saturation of the soil) constant (average of a selected period). In a second step, the response of the plant community was obtained by

- normalising each plant strength matrix with the maximum strength in the matrix
- summing up all normalised plant matrices and
- dividing the resulting matrix by the number of plants considered.

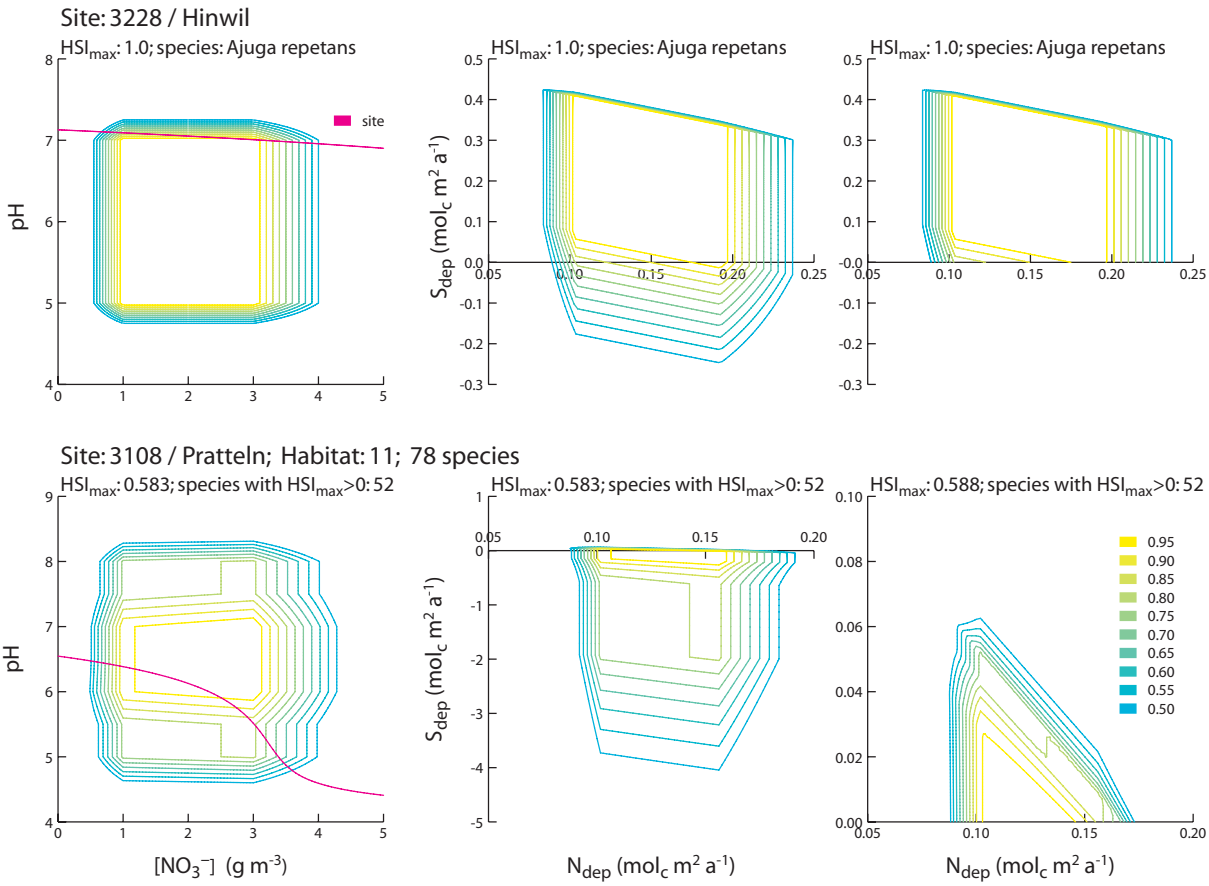

Figure 21 Top row: Single species response in the [N]-pH plane (left), transfer of isolines of fractions of HSI_{max} into the N_{dep}-S_{dep} plane by means of the SMB model (middle) and response of the plant with deposition restricted to positive values (Q1 of the deposition plane; right graph), respectively (VeCH-CL, T: 8.58 °C, θ: 0.501 m^3 m^{-3}). Bottom row: Same series of graphs for the desired ground vegetation plant community in Pratteln. Note the decrease of HSI_{max} as a result of 26 species having HSI_{max}=0 due to incompatible environmental conditions (VeCH-CL, T: 9.31 °C, θ: 0.448 m^3 m^{-3}).

The procedure complies with the calculation of the habitat suitability index (HSI), which was declared by the Task Force of the ICP Modelling & Mapping (Rome, 7–10 April) as the index to be used for common European biodiversity modelling:

(9) $$HSI = \frac{1}{n}\sum_{j=1}^{n}\frac{p_j}{p_{j,max}}$$

where n is the number of species, p_j the occurrence probability (strength, …) of species j, and $p_{j,max}$ the maximum occurrence probability (strength, …) of species j.

Part of the [N]-pH pairs used to model the plant community response may be unachievable by the soil solution of a given site simply due to limited capacity of the site to buffer acidity (Figure 21). As a consequence, to cover the full plant response in the [N]-pH plane often would have required negative S deposition, which in turn means that this sub-space could not be affected by N and S emission/deposition measures. This was considered nonsensical and therefore [N] and pH was limited to a range obtained from reasonable and positive (Q1) N and S deposition input. The transfer from N and S deposition values into respective [N] and pH (and vice-versa) was done by means of the Simple Mass Balance Model (SMB).

Either way of determining the plant community response in the needed Q1 of deposition should produce comparable isolines, if HSI_{max} of the unlimited response is found in Q1. In many cases, however, plant community response and deposition Q1 were somewhat displaced leading to often remarkably deviating HSI_{max} for the restricted deposition field (Table 3).

While the topology of the plant response in the [N]-pH plane obtained from VeCH-CL often resembled an irregular pyramid, Veg-CL produced smoother topologies that were not closed at high pH. The reason for this is found in the parameterisation of the pH response, which is, unlike the [N] response, a “single-branch” logistic function (Figure 22).

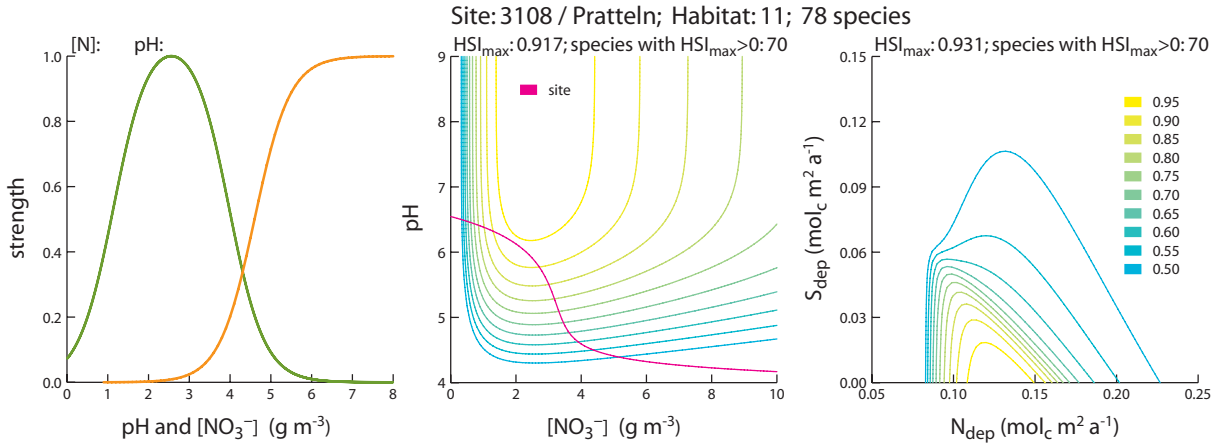

Figure 22 Plant community response patterns in the [N]-pH and N_{dep}-S_{dep} planes obtained from Veg-CL (Site: Pratteln, T: 9.31 °C, θ: 0.448 m^3 m^{-3}). Left graph shows the logistic response functions of a single species regarding [N] and pH, which led to the characteristic patterns in the [N]-pH plane.

Critical loads were finally derived from the isolines of fractions of HSI_{max} in the N_{dep}-S_{dep} plane by determining a polygon with maximal two nodes, at CLN_{min}-CLS_{max} and CLN_{max}-CLS_{min}, which approximated the isoline (Figure 23). The maximum S_{dep} value found in the isoline was assigned to CLS_{max}, and the maximum N_{dep} value associated with max(S_{dep}) (if there was more than one) was assigned to CLN_{min}. The second node was found by searching max(N_{dep}) in the isoline, which was allocated to CLN_{max}. The maximum S_{dep} value associated with max(N_{dep}) (if there was more than one) was taken as CLS_{min}. The curve segment finally was connected with the axis by setting a point at CLS_{max} with N_{dep}=0 and at CLN_{max} with S_{dep}=0. Dependent on the shape of the isoline, the number of nodes could also be <2, if, e.g., max(S_{dep}) associated with CLN_{max} was zero (Figure 23 middle graph). In this case, the simpli-

fied approach often produced a function that did not well match with the underlying isoline and obviously a polygon with more nodes or other geometry could be taken into account.

The PROPS model assesses the occurrence probability of plant species (p) as a function of soil chemical and climatic variables using

(10) $$p = \frac{1}{1 + \exp(-z)}$$

where z is a quadratic polynomial

(11) $$z = a_0 + \sum_{i=1}^{n} a_i \cdot x_i + \sum_{i=1}^{n} \sum_{j=1}^{n} a_{i,j} \cdot x_i \cdot x_j$$

The number of (normalised/log-transformed) variables x_i is five including soil solution pH, soil C:N, N deposition, annual average precipitation and air temperature.

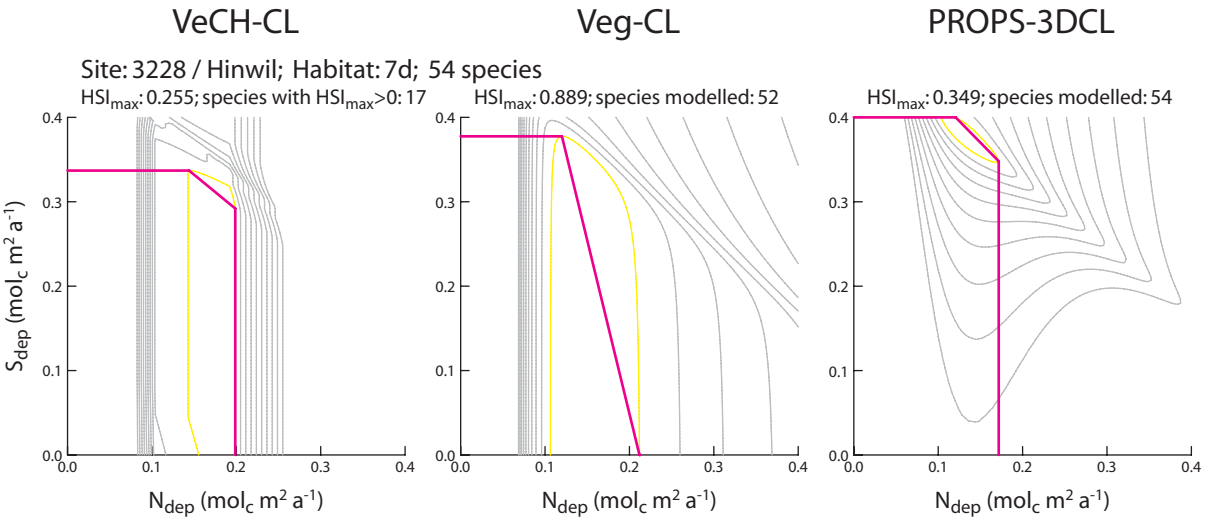

Figure 23 Fit of N-S critical load function on the underlying isoline (0.95·HSI_{max}). Notice the limits of the simplified fit (middle graph), which result from the demand: maximal two nodes and only one non-axis-parallel curve segment. At least, the critical load function is within the domain embraced by the isoline and therefore complies with the precautionary principle.

To allow the use of the model in the assessment of S and N critical loads, PROPS was linked with the SMB model. Details on the calculation of critical loads and the use of PROPS-CLF on the European scale are described in Posch et al. (2014) and Posch et al., (2015). On request of the NFCs (CCE WS Dessau, April 2016), the CCE also provided a single-site, stand-alone version of PROPS-CLF (www.wge-cce.org/Methods_Models/Available_Models).

Since the procedure to calculate S and N critical loads with Veg-/VeCH-CL was harmonised with the methodology in PROPS-CLF, the description above basically also holds for PROPS-CLF. However, PROPS-CLF, unlike Veg/VeCH-CL, uses $p_{j,max}$ from the entire allowed (variable limits given by the spread in the measurements) 2 (pH-N_{dep}), 3 (pH-N_{dep}-C/N) and 5 (pH-N_{dep}-C/N-T-P) dimensional (sub-)space to normalise the plants' response in Q1 of deposition. In case 5, the overall probability maximum of the 5-dimensional PROPS probability function is taken, in case 3, the user-supplied P and T values (i.e. for a given 'climate') are used, in case 2 also the C/N ratio is fixed at the given C/N and the maximum is computed in the pH-N_{dep} subspace only. Using $p_{j,max}$ or $S_{j,max}$ – in the case of Veg-/VeCH-CL – from the entire allowed subspace reduces the dependence of HSI_{max} on the size of the deposition space, which indeed can be considered as advantageous.

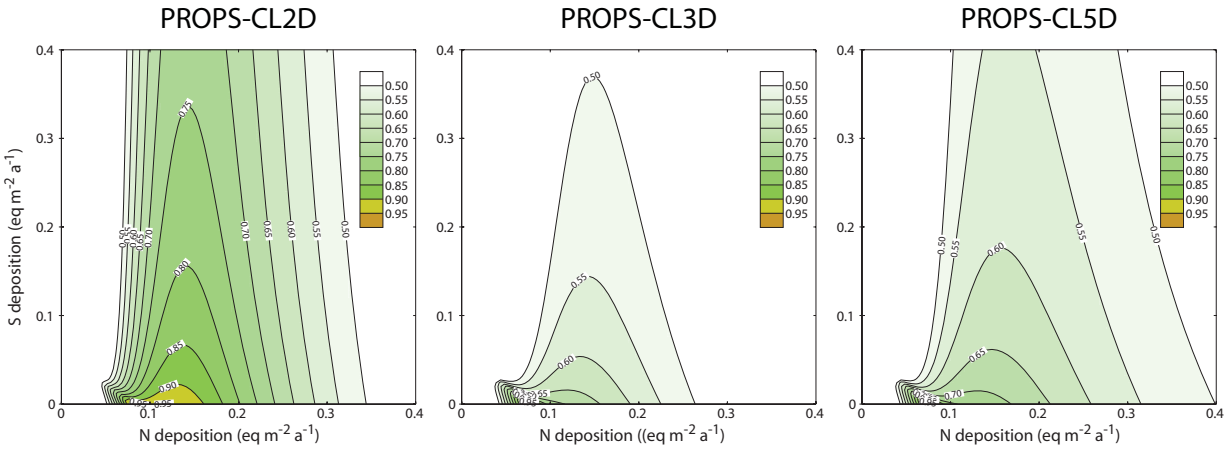

Figure 24 Changes in the topology of the plant community response in the deposition plane as result of computing $p_{j,max}$ in 2 (pH-N_{dep}), 3 (pH-N_{dep}-C/N) and 5 (pH-N_{dep}-C/N-T-P) dimensions (sample site 3105; C/N: 13.59, T: 9.97 °C, P: 0.854 m if fixed).

Posch et al., (2015) also describe an alternative geometrical derivation of the critical load function in the N_{dep}-S_{dep} plane. Defining S_{dep} of HSI_{max} as S_{min}, CLN_{max} is found by proceeding along increasing N deposition (keeping S_{dep} fixed) until the pre-defined fraction of HSI_{max} is reached. CLS_{max} is found by assigning N_{dep} of HSI_{max} to CLN_{min} and proceeding along increasing S deposition (keeping N_{dep} fixed) until again the pre-defined fraction of HSI_{max} is reached. This method avoids computing isolines, which can, in large-scale applications be quite CPU-time-consuming.

3.4.2 Some HSI issues

Generally, HSI (2-dimensional matrix) of a given plant community (as well as its maximum) is dependent on the reference system within which it is calculated. Reference system refers here to type (deposition or chemical variables) and number of fixed and variable variables used to determine the plant response. As mentioned earlier PROPS-CLF allows to model plant-specific maximum probabilities ($p_{j,max}$) in the 2, 3 and 5 dimensional space, and HSI_{max} decreases systematically with increasing dimension (Table 3). The dimensionality also affects the topology of the response (Figure 24) and thereby (since derived from isolines of the response topology) the critical loads.

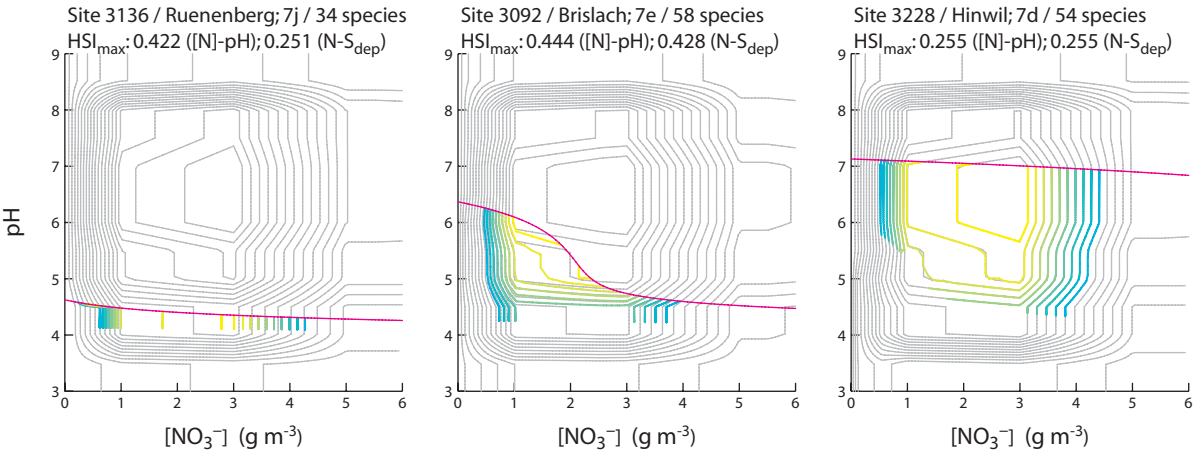

Figure 25 Response patterns obtained from VeCH-CL (light at ground level as driver excluded) using both [N]-pH (isolines in grey, 0.95 to 0.05·HSI_{max}) and S_{dep}-N_{dep} (isolines (recalculated into [N]-pH by means of the SMB) coloured; 0.95 to 0.50·HSI_{max}) as reference system. Note the decreasing displacement of the isolines (from left to right) as a result of decreasing differences in HSI_{max}.

A simplified approach, exploiting isolated driver responses, was used earlier with VeCH (Kurz, 2016), to visualize the ecological niche of the plant communities. It was found that maximum HSI of the response to water saturation, light at ground level and [N] was always below 1, illustrating the heterogeneity of the individual plants in the considered communities regarding response to the respective drivers and also the particularities of the response function (trapezoid). In static calculations with fixed climate variables, this led to a significant amount of species with strength matrices (e.g. [N]-pH) containing only zeros, and consequently (since $S_{j,max}$=0) normalized matrices with only zeros. Still they counted in the calculation of the average community HSI matrix and lowered HSI_{max}. This phenomenon was primarily found with VeCH-CL and partly also with Veg-CL results (Table 3) and was one of the reasons to exclude light at ground level as driver.

Table 3 Variability of PROPS-CLF, VeCH-CL and Veg-CL HSI_{max} of plant communities as a result of dimensionality of $p_{j,max}$ and choice of reference system - (unrestricted) [N]-pH or (restricted) N_{dep}-S_{dep} plane) using site-specific average climate (1980-2010) and observed C/N ratio. Abbreviations: d: number of desired species; m: number of species with HSI_{max}>0; L+: including light at ground level as driver; L-: excluding light at ground level as driver.

			PROPS-CLF			VeCH-CL									VEG-CL	
			N_{dep}-S_{dep}			[N]-pH				N_{dep}-S_{dep}					[N]-pH	N_{dep}-S_{dep}
SiteID	d	m	HSI_{max} 2D	HSI_{max} 3D	HSI_{max} 5D	m	HSI_{max} L+	m	HSI_{max} L-	m	HSI_{max} L+	m	HSI_{max} L-	m	HSI_{max} L-	HSI_{max} L-
3058	37	37	0.695	0.618	0.381	25	0.539	27	0.582	25	0.367	27	0.394	36	0.893	0.897
3092	58	58	0.639	0.07	0.042	28	0.413	30	0.444	28	0.394	30	0.428	54	0.915	0.937
3093	42	42	0.666	0.407	0.259	15	0.3	29	0.536	15	0.228	29	0.374	41	0.887	0.895
3094	55	55	0.6	0.176	0.107	30	0.446	34	0.503	30	0.435	34	0.484	51	0.905	0.922
3105	64	64	0.555	0.221	0.126	20	0.284	37	0.464	20	0.276	37	0.463	59	0.866	0.900
3107	42	42	0.684	0.508	0.301	15	0.3	29	0.536	15	0.228	29	0.4	41	0.887	0.895
3108	78	78	0.682	0.053	0.033	32	0.369	52	0.583	32	0.373	52	0.588	70	0.913	0.931
3111	40	40	0.769	0.537	0.314	19	0.365	24	0.448	19	0.356	24	0.421	38	0.864	0.897
3112	57	57	0.663	0.49	0.325	26	0.297	32	0.352	26	0.188	32	0.217	56	0.883	0.895
3120	40	40	0.739	0.217	0.135	22	0.44	28	0.548	22	0.432	28	0.515	39	0.889	0.928
3124	38	38	0.532	0.445	0.212	15	0.263	23	0.37	15	0.262	23	0.39	35	0.783	0.789
3136	34	34	0.571	0.213	0.134	8	0.194	17	0.422	8	0.135	17	0.251	31	0.912	0.911
3138	40	40	0.668	0.574	0.329	24	0.394	25	0.394	24	0.369	25	0.369	39	0.883	0.915
3149	40	40	0.732	0.47	0.29	16	0.34	28	0.548	16	0.319	28	0.488	39	0.889	0.905
3161	37	37	0.678	0.154	0.107	5	0.108	17	0.365	5	0.108	17	0.336	36	0.893	0.874
3162	47	47	0.669	0.593	0.354	13	0.213	31	0.463	13	0.17	31	0.305	45	0.893	0.907
3175	40	40	0.549	0.424	0.279	15	0.239	29	0.43	15	0.232	29	0.416	37	0.833	0.846
3176	52	52	0.637	0.511	0.354	12	0.188	26	0.413	12	0.163	26	0.328	49	0.921	0.923
3181	31	31	0.627	0.202	0.14	7	0.167	11	0.283	7	0.148	11	0.225	30	0.905	0.889
3228	54	54	0.643	0.349	0.225	9	0.141	17	0.255	9	0.141	17	0.255	52	0.888	0.889
3232	57	57	0.647	0.558	0.378	24	0.307	24	0.307	24	0.301	24	0.301	56	0.883	0.854
3233	57	57	0.619	0.363	0.254	24	0.307	24	0.307	24	0.302	24	0.302	56	0.883	0.854

Determining plant community response in the restrictive Q1 of deposition may also affect the HSI pattern (Figure 25) and HSI_{max}. If HSI_{max} of the unconfined system was not within Q1, then often remarkably deviating (lower) HSI_{max} were found with the restrictive deposition field (Table 3).

3.4.3 Biodiversity critical loads in compliance with the Call for Data 2015/17

The 22 sites used for dynamic modelling were initially also used to explore the static models. In rare cases, all models and model configurations returned comparable topologies of the plant community response in the N_{dep}-S_{dep} plane (Figure 26). In many cases, however, there were substantial discrepancies, which resulted in differing (biodiversity) critical loads functions (mostly) irrespective of the critical limit applied. This was not unexpected having in mind the diverse concepts, databases and plant response parameterisations. In practice, all independently determined critical load functions of a site – acidity, nutrient N, biodiversity – will be merged into a single site-specific critical load function, and hence the model dependent variation in biodiversity critical loads may not necessarily become an issue.

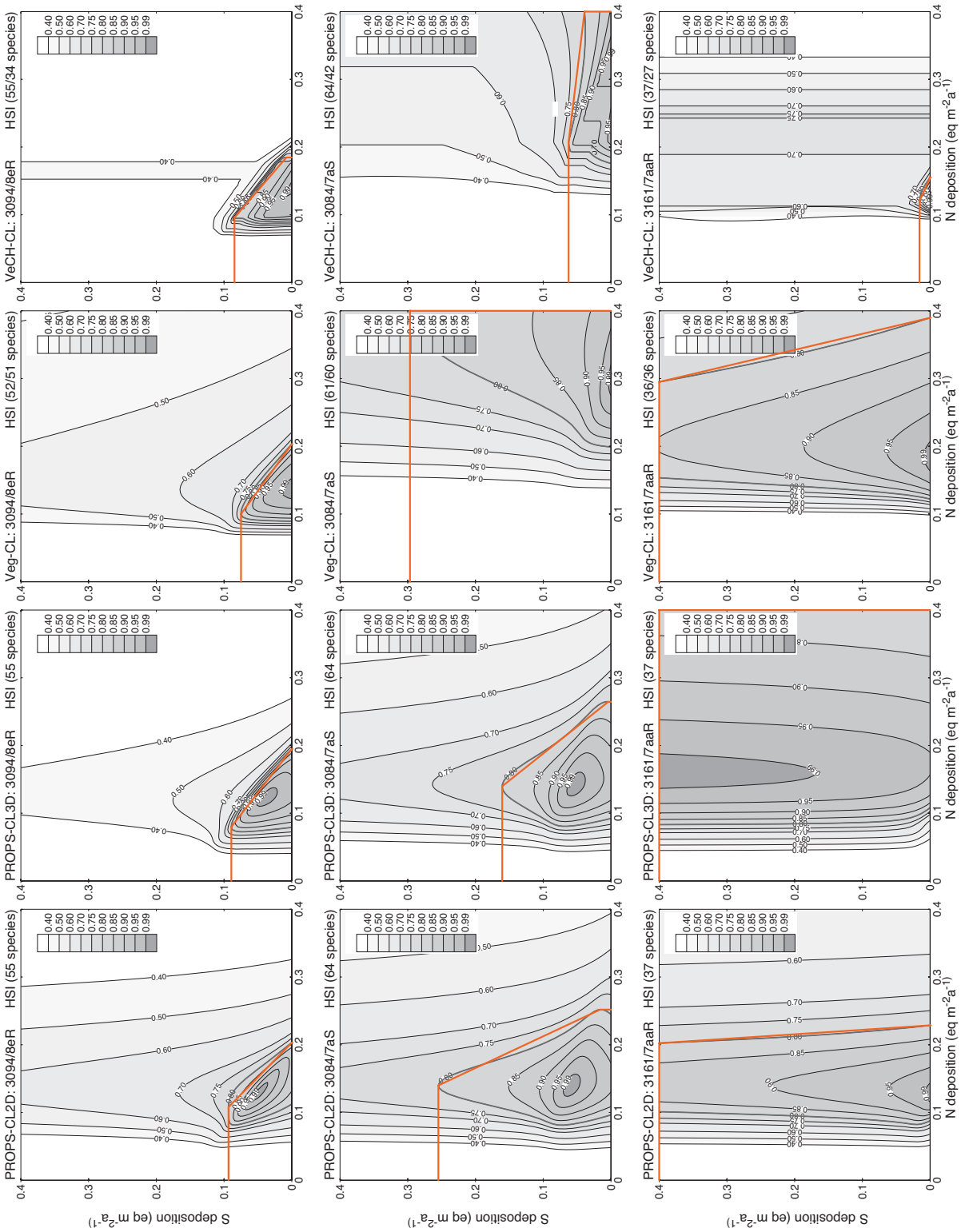

Figure 26 Similarities (top line of plots – rare case) and differences in topologies of desired plant communities of sample sites in the N_{dep}-S_{dep} plane dependent on choice of model or model configuration. Red line is critical load function for a critical limit of $0.8 \cdot HSI_{max}$.

Figure 27 summarizes the potential impact of biodiversity critical loads obtained from different vegetation models on combined (bdivCL, aciCL, nutCL) N and S critical load functions. All plant communities at selected 22 forest sites appeared comparably insensitive to sulphur (acidity) deposition irrespective of the vegetation model used to assess the biodiversity critical load. For a systematic lowering (median $CLS_{max}/CL_{max}(S) < 1$) of $CL_{max}(S)$ (conventional

acidity critical load), VeCH-CL required a protection level ≥80% (critical limit ≥0.8·HSI_{max}) and PROPS-CLF required a protection level ≥90% (Figure 27, left column of graphs).

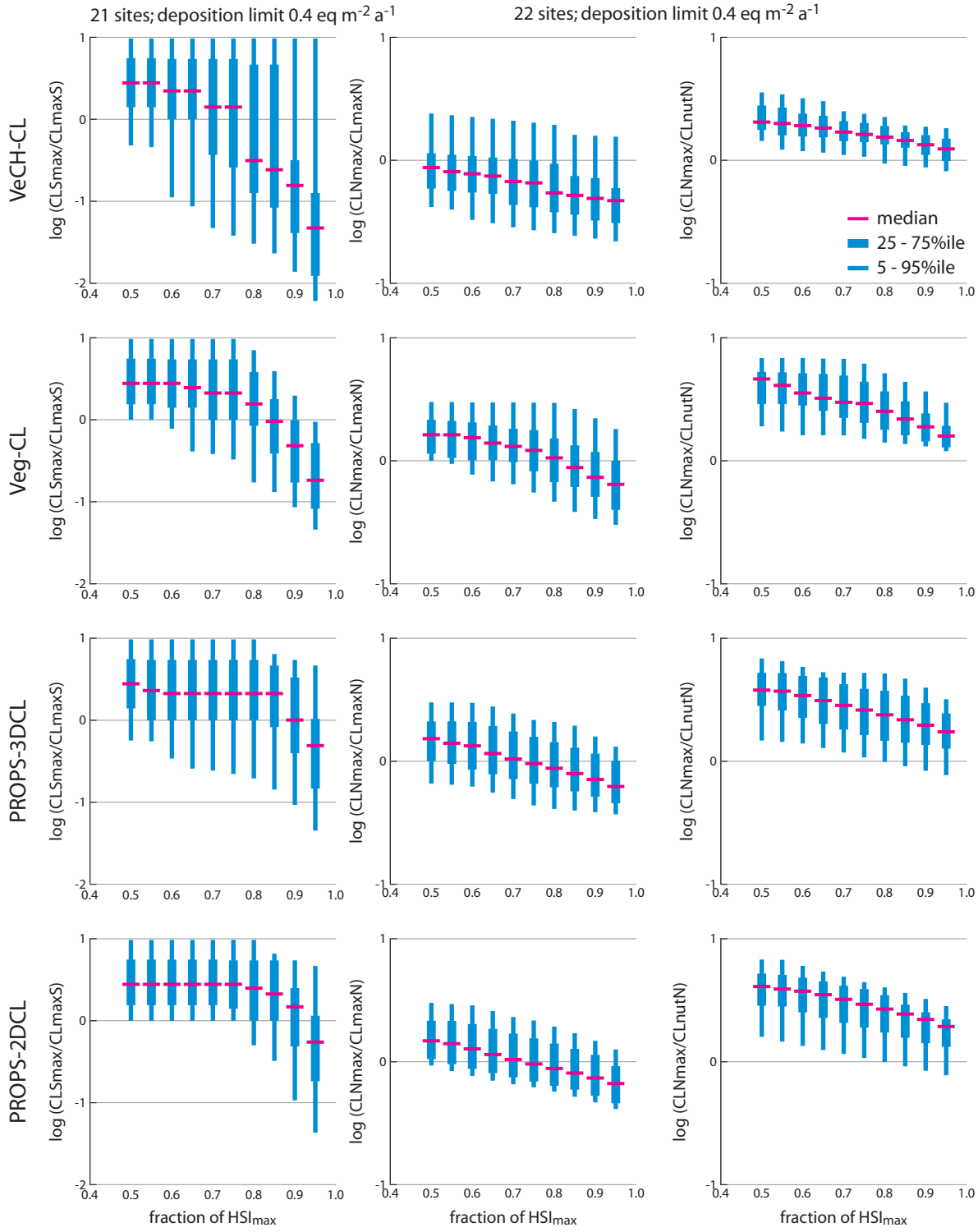

Figure 27 Distribution of ratios of biodiversity and conventional critical loads at 22 sites. CLS_{max} and CLN_{max} are biodiversity $CL_{max}(S)$, $CL_{max}(N)$ and $CL_{nut}(N)$ are conventional critical loads.

The given plant communities tended to curtail $CL_{max}(N)$. The most sensitive parameterisation regarding N deposition response apparently was implemented in VeCH-CL. VeCH CLN_{max} were mostly lower than conventional $CL_{max}(N)$ and already with a protection level of 70%, 75% of the sites had CLN_{max} lower to substantially lower than $CL_{max}(N)$. With the PROPS parameterisation, the given plant communities are less sensitive regarding N deposition and

the median ratio starts to fall below unity at a protection level of about 75%.

Whether there will be a systematic change in the combined critical load function primarily depends on the question whether $CL_{nut}(N)$ will be kept or replaced by CLN_{max}. CLN_{max} was mostly higher than $CL_{nut}(N)$ irrespective of vegetation model and protection level used implying that the leaching criterion used to assess $CL_{nut}(N)$ for forests is more restrictive than biodiversity critical loads.

To comply with the Call for Data 2015-17, biodiversity critical loads calculations were extended to all forest sites for which the plant community composition was available (76). Section 2.2.8 describes model setting and input derivation. Basically, the result confirmed the findings of the tests with the restricted set of sites. Biodiversity (Figure 28A) compared to acidity (Figure 28B) critical loads for forests appeared to mostly be less restricting regarding S deposition, but tended to often curtail N deposition between 2000 and 2500 eq ha^{-1} a^{-1}. The impact on the combined conventional critical load function considering also nutrient N critical loads ($CL_{nut}(N)$; Figure 28C), however, was marginal, since the leaching criterion used in Switzerland to assess $CL_{nut}(N)$ limited N deposition mostly to <1500 eq ha^{-1} a^{-1}.

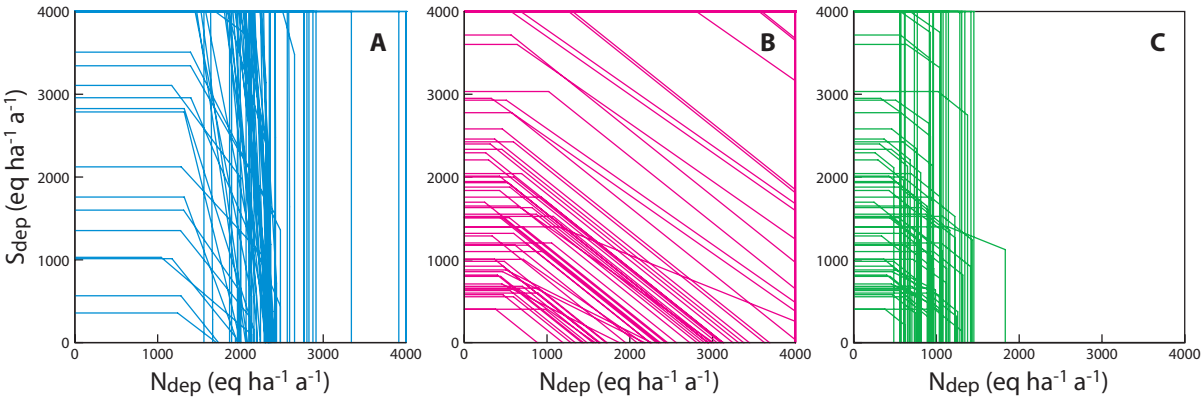

Figure 28 Plots of PROPS-CLF biodiversity (A) conventional acidity (B) and combined acidity and nutrient N (C) critical loads functions for 76 forest plots in Switzerland in compliance with the Call for Data 2015-17.

4 SUMMARY AND CONCLUSIONS

In 2015, the WGE of the UNECE LRTAP Convention issued a Call for Data 2015-17 inviting the parties of the Convention to amend classical with biodiversity critical loads. Up to that point in time there has already been a series of dynamic geochemical-biodiversity model chains in use and a prototype of a static model based on PROPS was being tested. As a result of this extended model testing, the Dutch vegetation model PROPS was reworked during the first year of the Call, and the Swiss NFC (ICP M&M) decided to use the extra time for a revision of the parameter table of the Swedish ground vegetation simulation model Veg on the basis of the indicator value system of Landolt, with the intention to improve the internal consistency of the parameterization. Drivers were limited to three climate (temperature, water saturation, light at ground level) and two chemical drivers (pH, and concentration of nitrate in soil solution) as well as competition, and plant response functions were simplified. The revised version of Veg (called VeCH) was linked to VSD and applied to 22 forest sites. The model chain predicted reasonably coherent behaviour of the vegetation composition with increasing and decreasing nitrate as well as hydrogen ion concentration in the soil solution. On the other hand, VeCH was, as earlier Veg versions, unable to reproduce current observed plant compositions on the site level.

Upon availability of the revised VSD+PROPS model chain, the 22 sites were again simulated with VSD+ and VSD using utmost harmonized input. The two dynamic soil chemistry models returned different range and trend of C pools and C/N ratios on regional scale but comparable base saturation patterns. The behaviour of VSD regarding the solid chemistry was rather unexpected and has to be regarded as provisional.

Both models returned comparable regional soil solution chemistry trends and patterns for the conservative ions Cl^- and SO_4^{2-} as well as for Na^+ and Bc^{2+}, the latter two being additionally influenced by weathering and nutrient cycling. VSD+ modelled relative stable [NO_3^-] with a relative limited spread of about 3 orders of magnitude (80% of values) unlike VSD, which returned very low [NO_3^-] ($\leq$ 1E-06 $\mu mol_c\ L^{-1}$) before 1950 for the majority of the sites and a subsequent steep increase as a result of increasing N deposition. As a consequence, moderate discrepancies were also found in the regional [H^+], [Al^{3+}] and molar Al/Bc trends simulated by the two models.

Simulated and observed [Cl^-] and [SO_4^{2-}] and [Na^+] usually matched acceptably well irrespective of the soil chemistry model used, the CzI being $\geq$0.8 at two- thirds of the sites. Slightly larger discrepancies were found with [Bc^{2+}], although the majority of the sites still having values within the same order of magnitude. [NO_3^-] from both models tended to weakly match the observations as did [H^+], and [Al^{3+}] and molar Al/Bc mostly deviated strongly from the observations. The modelled aluminium concentration is dependent on the [H^+], which in turn is dependent on the mass balance of cat- and anion of which [NO_3^-] particularly remained difficult to model. Additionally, modelled [Al^{3+}] was compared with [Al_{tot}] which may cover several aluminium species.

Earlier versions of the PROPS model considered [NO_3^-] in the soil solution as driver which – having the difficulties in [NO_3^-] modelling in mind – entailed regional Landolt index patterns that were not very conclusive. Besides extending the database, the revision of the PROPS model involved also a change in drivers considered, from solution [NO_3^-] to N deposition and C/N ratio. This measure improved the relation between the trophic state of the system surrogated by N deposition and the plant composition in that the probability of occurrence of oligotrophic plants decreased with increasing N deposition. The patterns of Landolt R indicator class probability of occurrence in relation to pH evolution were less conclusive, and at quite some sites resembled the N indicator patterns. We interpreted this as result of a combination of the partial correlation of the two Landolt indicators (e.g. site 3162, with 62% of the species having equal R and N class), and the dominance of the response to N deposition changes over the response to pH change particularly with the given range of the latter of mostly circa 1 pH unit. Regarding the relevance of discrepancies between modelled and monitored solution chemistry, it cannot be ruled out, although PROPS became less susceptible to solution ion concentrations with the change in drivers, that at certain sites the floristic composition would change, if modelled pH would be closer to the observations.

The current plant selection, exhibited a feature, the relevance of which was not yet further investigated. In general, the plants' probability of occurrence was very low prior to 1900 and decreased again after 2050. Optimal conditions for the probability of occurrence of the selected plants obviously prevailed roughly between 1950 and 2030. Regarding the past, this may be considered as irrelevant, concerning the future, however, it should be understood why plant occurrence probability declined. Among the drivers considered, primarily the temperature shifted in this period obviously towards a range that was suboptimal for the growth of currently used plant associations. Although regional HSI (due to the implicit normalisation) stayed relatively constant throughout the second half of the simulation period, the relevance

of critical loads based on maladjusted plant associations should be questioned.

To explore the potential of the static model outcome, biodiversity critical loads were calculated following the procedure outlined by the CCE for the same sample sites using VeCH-CL, Veg-CL and PROPS-CLF. Since plant response to varying drivers often differed substantially among the three models, resulting critical loads functions only rarely compared. Generally, VeCH-CL returned for a given protection level lower S and N critical loads than Veg- and PROPS-CLF. Irrespective of the model, only protection levels above 80% of HSI_{max} led to a systematic lowering of $CL_{max}(S)$. CLN_{max} from VeCH-CL was mostly lower than $CL_{max}(N)$ while Veg- and PROPS-CLF CLN_{max} were less restrictive (protection levels 70% of HSI_{max} and higher required to get a systematic reduction of $CL_{max}(N)$). Irrespective of the protection level applied, all models predict higher CLN_{max} than $CL_{nut}(N)$, which was calculated in Switzerland by an obviously very restrictive leaching criterion.

To comply with the Call for Data 2015-17 of the WGE/CCE, the Swiss NFC finally decided to use the PROPS-CLF model in the 2D mode with S and N depositions confined to 4000 eq ha^{-1} a^{-1} and $0.8 \cdot HSI_{max}$ as critical limit. Biodiversity critical loads functions were calculated for 76 sites, for which forest type and characteristic flora were available. The results of the extended forest plot population basically confirmed the general picture already seen with the test sites that was $CL_{max}(N)$ often being curbed by CLN_{max}, which in turn was cut back by $CL_{nut}(N)$ limiting the critical N deposition to the selected forests to mostly <1500 eq ha^{-1} a^{-1}. It has to be kept in mind that, for technical reasons (consistency in the tables sent to the CCE), input for the last biodiversity critical loads calculation was drawn from the input of the acidity critical load run

There are some issues remaining that could further be tackled:

- The currently considered 76 sites roughly cover 25% of the sites used for acidity critical loads calculations and dynamic modelling and are not homogenously distributed over the forested area of Switzerland. The subsample may therefore not fully represent the variability of (forest) biodiversity critical loads. Basic input for the whole set of forest plots is available and only the missing phytosociological classification of the forests including the list of typical/desired plant species impede the extended application of the model.
- In case a spatial extension of the biodiversity critical loads modelling is considered, the reason for declining plant occurrence probabilities after 2030 – a period of growing significance – should initially be clarified. The outcome of this analysis may impact the procedure of selecting adequate desired/typical plant species.
- The critical limit – $0.8 \cdot HSI_{max}$ – was merely set by common accord. It is not very evident how plant compositions change, if HSI_{crit} is lowered to a fraction of HSI_{max}, in this particular case to $0.8 \cdot HSI_{max}$. This should be further investigated to substantiate the currently used HSI_{crit}.
- Critical N loads to forests in Switzerland appear to essentially be limited by either the nutrient or the empirical N critical load, which both aim at protecting to a certain degree similar elements of the ecosystem as the biodiversity critical load. Given the circumstance of systematic differences in the three critical loads, conceptual views, critical load derivation and background data should be further explored and discussed, to ensure the reliability of the predictions.

5 REFERENCES:

Alveteg M, 1998. *Dynamics of Forest Soil Chemistry.* PhD thesis, Department of Chemical Engineering II, Lund University, Lund, Sweden.

Alveteg M, Kurz D, Becker R, 2002. Incorporating nutrient content elasticity in the MakeDep model. Sustainable Forestry in Temperate Regions – Proceedings from a SUFOR International Workshop, April 7–9, 2002, Lund, Sweden. *Reports in Ecology and Environmental Engineering* 1:2002: 52–67.

Amann M, Klimont Z, Wagner F, 2013. Regional and global emissions of air pollutants: Recent trends and future scenarios. *Annual Review of Environment and Resources* 38: 31-55.

Belyazid S, Kurz D, Posch M, 2011. *Revising model application and parameterization for simulating ground vegetation changes.* Workshop Report to the attention of the Swiss Federal Office for the Environment (FOEN), the Swedish Environmental Protection Agency (SNV) and the Coordination Centre for Effects (CCE).

Belyazid, S, 2006. *Dynamic Modeling of Biogeochemical Processes in Forest Ecosystems.* PhD thesis, Department of Chemical Engineering II, Lund University, Lund, Sweden.

Bonten LTC, Reinds GJ, Posch M, 2016. A model to calculate effects of atmospheric deposition on soil acidification, eutrophication and carbon sequestration. Environmental Modelling & Software 79: 75-84.

CLRTAP, 2017. Manual on Methodologies and Criteria for Modelling and Mapping Critical Loads and Levels and Air Pollution Effects, Risks and Trends. UNECE Convention on Long-range Transboundary Air Pollution; www.icpmapping.org/Latest-update_Mapping_Manual

Coleman K, Jenkinson DS, 2014. *RothC - A model for the turnover of carbon in soil. Model Description and Users Guide.* Rothamsted Research, Harpenden, UK; https://www.rothamsted.ac.uk/sites/default/files/RothC_guide_DOS.pdf

Cosby BJ, Ferrier RC, Jenkins A, Wright RF, 2001. Modelling the effects of acid deposition: Refinements, adjustments and inclusion of nitrogen dynamics in the MAGIC model. *Hydrology and Earth System Sciences* 5: 499-517.

De Vries W, Wamelink GWW, van Dobben H, Kros J, Reinds GJ, Mol-Dijkstra JP, Smart SM, Evans CD, Rowe EC, Belyazid S, Sverdrup HU, van Hinsberg A, Posch M, Hettelingh J-P, Spranger T, Bobbink R, 2010. Use of dynamic soil-vegetation models to assess impacts of nitrogen deposition on plant species composition and to estimate critical loads: An overview. *Ecological Applications* 20: 60-79.

ECE, 2008. Report of the Executive Body on its twenty-fifth session held in Geneva from 10 to 13 December 2007. United Nations, Economic Commission for Europe, Executive Body for the Convention on Long-range Transboundary Air Pollution, Geneva, ECE/EB.AIR/91, prg. 31; www.unece.org/fileadmin/DAM/env/documents/2007/eb/EB/ece.eb.air.91.e.pdf

ECE, 2015. Report of the Executive Body on its thirty-third session held in Geneva from 8 to 11 December 2014. United Nations, Economic Commission for Europe, Executive Body for the Convention on Long-range Transboundary Air Pollution, Geneva, ECE/EB.Air/127; www.unece.org/fileadmin/DAM/env/documents/2014/AIR/EB/ECE_EB.AIR_127_ENG.pdf

EMEP, 2016. *Air pollution trends in the EMEP regions between 1990 and 2012.* EMEP/CCC-Report 1/2016 NILU, Kjeller, Norway; www.unece.org/fileadmin/DAM/env/documents/2016/AIR/Publications/Air_pollution_trends_in_the *EME*-Pregion.pdf

Jönsson C, Warfvinge P, Sverdrup H, 1995. Application of the SAFE model to the Solling spruce site. *Ecological Modelling* 83: 85–96

Kurz D, Posch M, 2015. *Revising critical loads of acidity for forests in Switzerland for the Call for Data 2014/15.* Interim Report, EKG Geo-Science, Bern.

Kurz, D, 2016. *Revising the Veg model with regard to its potential use in calculating critical loads of acidity and nitrogen for forests in Switzerland (Call for Data 2015/17).* Interim Report, EKG Geo-Science, Bern.

Landolt E, 2010. Flora indicativa. Ökologische Zeigerwerte und biologische Kennzeichen zur Flora der Schweiz und der Alpen. Haupt Verlag, Bern, 1. Auflage 2010, ISBN: 978-3-258-07461-0.

Oulehle F, Cosby BJ, Wright RF, Hruska J, Kopacek J, Kram P, Evans CD, Moldan F, 2012. Modelling soil nitrogen: the MAGIC model with nitrogen retention linked to carbon turnover using decomposer dynamics. *Environmental Pollution* 165: 158-166.

Posch M, Belyazid S, Kurz D, Reinds GJ, 2010. The VSD-Veg model: progress and prospects. In: J Slootweg, M Posch, J-P Hettelingh (eds), *Progress in Modelling of Critical Thresholds and Dynamic Modelling, including Impacts on Vegetation in Europe. CCE Status Report 2010*. Report 680359001/2011, National Institute for Public Health and the Environment (RIVM), Bilthoven, NL: 49–54; www.wge-cce.org

Posch M, de Vries W, Sverdrup HU, 2015. Mass balance models to derive critical loads of nitrogen and acidity for terrestrial and aquatic ecosystems. In: W de Vries, J-P Hettelingh, M Posch (eds), *Critical Loads and Dynamic Risk Assessments: Nitrogen, Acidity and Metals in Terrestrial and Aquatic Ecosystems.* Springer, Dordrecht, Netherlands: 171-205; DOI: 10.1007/978-94-017-9508-1_6

Posch M, Hettelingh J-P, Slootweg J, Reinds GJ, 2014. Deriving critical loads based on plant diversity targets. In: J Slootweg, M Posch, J-P Hettelingh, L Mathijssen (eds), *Modelling and mapping the impacts of atmospheric deposition on plant species diversity in Europe: CCE Status Report 2014.* Coordination Centre for Effects, Bilthoven, Netherlands, ISBN 978-90-6960-276-9: 41-46; www.wge-cce.org

Posch M, Hettelingh JP, Slootweg J, Reinds GJ, 2015. Critical loads for plant species diversity. In: J Slootweg , M Posch, J-P Hettelingh (eds), *Modelling and mapping the impacts of atmospheric deposition of nitrogen and sulphur: CCE Status Report 2015.* Coordination Centre for Effects, Bilthoven, Netherlands, ISBN: 978-90-6960-283-7: 45-54; www.wge-cce.org

Posch M, Reinds GJ, 2009. A very simple dynamic soil acidification model for scenario analyses and target load calculations. *Environmental Modelling & Software* 24: 329-340.

Posch M, Reinds GJ, 2010. *MetHyd – A Meteo-Hydrological Pre-processor – Description and User Manual.* Coordination Centre for Effects, Bilthoven, Alterra, Wageningen.

Reinds GJ, Bonten L, Mol-Dijkstra JP, Wamelink GWW, Goedhart P, 2012. Combined effects of air pollution and climate change on species diversity in Europe: First assessments with VSD+ linked to vegetation models. In: M Posch, J Slootweg, J-P Hettelingh (eds), *Modelling and mapping of atmospherically-induced ecosystem impacts in Europe: CCE Status Report 2012.* Coordination Centre for Effects, Bilthoven, Netherlands, ISBN 978-90-6960-262-2: 49–61; www.wge-cce.org

Reinds GJ, Mol-Dijkstra J, Bonten L, Wamelink W, De Vries W, Posch M, 2014. VSD+PROPS: Recent developments. In: J Slootweg, M Posch, J-P Hettelingh, L Mathijssen (eds), *Modelling and mapping the impacts of atmospheric deposition on plant species diversity in Europe: CCE Status Report 2014.* Coordination Centre for Effects, Bilthoven, Netherlands, ISBN 978-90-6960-276-9: 47-53; www.wge-cce.org

Reinds GJ, Mol-Dijkstra JP, Bonten L, Wamelink GWW, Hennekens S, Goedhart P, Posch M, 2015. PRObability of Plant Species (PROPS) model: Latest developments. In: J Slootweg , M Posch, J-P Hettelingh (eds), *Modelling and mapping the impacts of atmospheric deposition of nitrogen and sulphur: CCE Status Report 2015.* Coordination Centre for Effects, Bilthoven, Netherlands, ISBN: 978-90-6960-283-7: 55-62; www.wge-cce.org

Remund J, Rihm B, Huguenin-Landl B. 2014. Klimadaten für die Waldmodellierung für das 20. und 21. Jahrhundert. Meteotest, Bern.

Rowe EC, Wamelink GWW, Smart SM, Butler A, Henrys PA, van Dobben HF, Reinds GJ, Evans CD, Kros J, De Vries W, 2015. Field survey based models for exploring nitrogen and acidity effects on plant species diversity and assessing long-term critical loads. In: W de Vries, J-P Hettelingh, M Posch (eds), *Critical Loads and Dynamic Risk Assessments: Nitrogen, Acidity and Metals in Terrestrial and Aquatic Ecosystems.* Springer, Dordrecht, Netherlands: 297-326.

SAEFL (ed), 1998. *Acidification of Swiss forest soils – Development of a regional dynamic assessment.* Swiss Agency for the Environment, Forests and Landscape (SAEFL), Bern, *Environmental Documentation Air/Forest* 89.

Sverdrup H, Warfvinge P, 1995. Estimating field weathering rates using laboratory kinetics. In: AF White, SL Brantley (eds), *Chemical Weathering of Silicate Minerals.* Mineralogical Society of America, *Reviews in Mineralogy* 31: 485-541.

Sverdrup S, Belyazid S, Nihlgård B, Ericson L, 2007. Modelling change in ground vegetation response to acid and nitrogen pollution, climate change and forest management in Sweden 1500–2100 A.D. *Water, Air and Soil Pollution Focus* 7: 163-179

Van der Salm C, 2001. Assessment of the regional variation in weathering rates of loess and clay soils in The Netherlands. *Water, Air and Soil Pollution* 131: 217–243

Van Genuchten MT, 1980. A closed-form equation for predicting the hydraulic conductivity of unsaturated soils. *Soil Science Society of America Journal* 44: 892-898.

Van Hinsberg A, Hendriks M, Hennekens SM, Sierdsema H, van Swaay C, Rondinini C, Santini L, Delbaere B, Knol OM, Wiertz J, 2014. *BioScore 2.0 – A tool to assess the impacts of European Community policies on Europe's biodiversity.* First Draft, Dec. 2014.

Wallman P, Svensson MGE, Sverdrup H, Belyazid S, 2005. ForSAFE – an integrated process-oriented forest model for long-term sustainability assessments. *Forest Ecology and Management* 207 (1-2): 19-36.

Wösten JHM, Lilly A, Nemes A, Le Bas C, 1999. Development and use of a database of hydraulic properties of European soils. *Geoderma* 90: 169-185.

6 APPENDIX I

Table 4 List of sites used for model tests.

No	Site No	Site name	Main tree type	Altitude	Forest type
1	3138	Zofingen	Buche/Fichte	534	6
2	3175	Rafz	Fichte	536	7*
3	3093	Brislach	Fichte	421	7aa
4	3107	Aeschi	Buche/Fichte	506	7aa
5	3111	Olsberg	Buche	381	7aaB
6	3120	Aarwangen	Buche	475	7aaB
7	3149	Habsburg	Buche	430	7aaB
8	3058	Frienisberg	Buche/Fichte	730	7aaR
9	3161	Muri	Fichte	482	7aaR
10	3105	Muttenz	Buche	360	7aS
11	3228	Hinwil	Fichte	646	7d
12	3162	Muri	Buche	491	7dR
13	3092	Brislach	Buche	416	7e
14	3136	Ruenenberg	Buche	586	7j
15	3124	Busswil	Fichte	596	8*
16	3181	Zugerberg	Fichte	904	8aaR
17	3112	Aeschau	Buche/Fichte	950	8d
18	3232	Bachtel	Fichte	1046	8d
19	3233	Bachtel	Buche	1041	8d
20	3094	Breitenbach	Buche	457	8eR
21	3108	Pratteln	Buche	416	11
22	3176	Zugerberg	Buche/Fichte	979	18aaR

Table 5 List of plant species typifying the forest habitat types of the considered sites. Numbers in the list express the importance of the species in the characterisation of the plant community.

No in Table 2	1	2	3,4	5,6,7	8,9	10	11	12	13	14	15	16	17,18,19	20	21	22
Forest type	6	7*	7aa	7aaB	7aaR	7aS	7d	7dR	7e	7j	8*	8aaR	8d	8eR	11	18aaR
Plant species	Importance															
Atrichum undulatum			1			3			3	1			3			
Dicranum scoparium	3	5					3	3			5		3			2
Eurhynchium praelongum						1										
Eurhynchium striatulum		3	1													
Eurhynchium striatum		3	1													
Hylocomium splendens	3	5					3	3			5		3			2
Hypnum cupressiforme		3														
Plagiochila asplenioides													1			
Plagiomnium undulatum						4									5	
Pleurozium schreberi		1														
Pleuridium subulatum										1						
Polytrichum formosum	3	5	1	1	1		3	3			5		3			2
Rhytidiadelphus loreus	3	5					3	3			5		3			2
Scleropodium purum		3														
Thuidium tamariscinum		5				1					3					
Athyrium distentifolium											3	3	4	3		3
Athyrium filix-femina	5	4	3	3	3	5	5	5	5	1	4	3	5	5	3	3
Blechnum spicant		4									4					
Dryopteris affinis													3			
Dryopteris carthusiana	2	5	2	2	2	2	2	2			5	5	5			5
Dryopteris dilatata	2	5	2	2	2	2	2	2			5	5	5			5
Dryopteris filix-mas			1	1	1	5	6	6	5	2		1	3	5	5	3
Gymnocarpium dryopteris											3	3	4	3		3
Oreopteris limbosperma													3			
Polystichum aculeatum											3	3	4			3
Pteridium aquilinum	3	5	3	3				3								
Avenella flexuosa		3									3					
Brachypodium sylvaticum	5		3	3	3	5	5	5	6	5		3	5	6	5	3
Bromus benekenii										2					5	
Bromus ramosus										2					5	
Carex brizoides	1		3	6	1											
Carex digitata	6		3	3	3	5	5	5	5	5		3	6	5	5	3
Carex flacca									6	3				6	3	
Carex pendula						4									5	
Carex pilosa				3												
Carex pilulifera	2	5									5		2			
Carex remota						4									5	
Carex sylvatica				1	1	5	6	6	5	2			3	5	5	3
Deschampsia cespitosa				1		5			3					3	5	3
Festuca altissima												2	2	3		3
Festuca gigantea				2		4									5	
Hordelymus europaeus												2	2	3		3
Milium effusum			1		1	5	6	6	5	2			3	5	5	3
Poa nemoralis				3					3							
Poa trivialis										3						
Aconitum lycoctonum																2
Actaea spicata														3		3
Adenostyles alliariae																3

No in Table 2	1	2	3,4	5,6,7	8,9	10	11	12	13	14	15	16	17,18,19	20	21	22
Forest type	6	7*	7aa	7aaB	7aaR	7aS	7d	7dR	7e	7j	8*	8aaR	8d	8eR	11	18aaR
Plant species	Importance															
Adenostyles glabra																2
Aegopodium podagraria						4									5	
Ajuga reptans					1	5	6	6	5	2			3	5	5	3
Allium ursinum															6	
Anemone nemorosa	6		3	3	3	5	5	5	5	5		3	6	5	5	3
Angelica sylvestris						4									5	
Anthriscus nitida																3
Aquilegia vulgaris									6	3				6	3	
Arum maculatum															5	
Aruncus dioicus											3	3	4	3		3
Asarum europaeum										2					5	
Cardamine heptaphylla																2
Cardamine pentaphyllos																2
Chaerophyllum hirsutum																2
Chaerophyllum villarsii																2
Circaea alpina																3
Circaea lutetiana			1		1	4									5	
Corydalis cava															3	
Epilobium montanum	5		3	3	3	5	5	5	5	5		3	5	5	5	3
Euphorbia amygdaloides									6	3				6	3	
Euphorbia dulcis										2					5	
Fragaria vesca					3	3			3	3				3		
Galeopsis tetrahit		1	3	3	3	3	3								3	
Galium mollugo						3										
Galium odoratum	5		3	3	3	5	5	5	5	5		3	5	5	5	3
Galium rotundifolium	3	5	3	3	3	3	2	2			5	3	3			5
Galium sylvaticum	5	3	5	5	5	5	5	5	5	5					5	
Geranium robertianum	5	4	3	3	3	5	5	5	5		4	3	5	5	3	3
Geum urbanum						5			3					3	5	3
Glechoma hederacea															6	
Helleborus foetidus										2					5	
Hepatica nobilis									1						5	
Homogyne alpina											3					
Impatiens noli-tangere				3		4									5	
Impatiens parviflora		1	3	3	3	3	3						3			
Juncus effusus						3										
Lamium montanum						5	6	6	5	2			3	5	5	3
Lathyrus linifolius	6	2					4	4	2		2		6	2		2
Lathyrus vernus										2					5	
Leucojum vernum															3	
Lilium martagon										2					5	
Luzula luzuloides	6	2					4	4	2		2		6	2		3
Luzula multiflora		4									4					
Luzula nivea	6	2					4	4	2		2		6	2		2
Luzula pilosa	5	3	3	3	3	2	3	3	3	1	3	3	5	3	2	3
Luzula sylvatica	6	2					4	4	2		2		6	2		2
Lysimachia nemorum	5	4	3	3	3	5	5	5	5		4	3	5	5	3	3
Maianthemum bifolium	5	3	3	3	3	2	3	3	3	2	3	3	5	3	2	3
Melampyrum pratense		3									3					
Melampyrum sylvaticum											3					
Melica nutans									6	3				6	3	
Melica uniflora									1							
Mercurialis perennis										2					5	
Moehringia trinervia	5	3	3	3	3	2	3	3	3		3	3	5	3	2	3
Mycelis muralis	5	3	3	3	3	2	3	3	3		3	3	5	3	2	3
Neottia nidus-avis										2					5	
Oxalis acetosella	5	4	3	3	3	5	5	5	5	2	4	3	5	5	3	3
Paris quadrifolia						5			3					3	5	3
Petasites albus												2	2	3		3
Phyteuma spicatum	5		3	3	3	5	5	5	5	5		3	5	5	5	3
Polygonatum multiflorum	6		3	3	3	5	5	5	5	5		3	6	5	5	3
Polygonatum verticillatum												2	2	3		3
Potentilla sterilis									3							
Prenanthes purpurea	5	4	3	3	3	5	5	5	5		4	3	5	5	3	3
Primula elatior						5			3					3	5	3
Pulmonaria obscura															5	
Ranunculus auricomus						4									5	
Ranunculus ficaria						4									5	
Ranunculus lanuginosus																2
Ranunculus nemorosus						3										
Ranunculus repens						1										
Sanicula europaea						5	6	6	5	2			3	5	5	3
Scrophularia nodosa						3							3			
Stachys sylvatica						4									5	
Stellaria nemorum																2
Tamus communis										2					5	
Teucrium scorodonia	6	2					4	4	2		2		6	2		2
Valeriana montana																3
Veronica chamaedrys									3							
Veronica officinalis	6	2					4	4	2				6	2		2
Veronica urticifolia	5	4	3	3	3	5	5	5	5		4	3	5	5	3	3
Vicia sepium							3									
Viola biflora																3
Viola reichenbachiana	6		3	3	3	5	5	5	5	5		3	6	5	5	3
Calluna vulgaris		1														

No in Table 2	1	2	3,4	5,6,7	8,9	10	11	12	13	14	15	16	17,18,19	20	21	22
Forest type	6	7*	7aa	7aaB	7aaR	7aS	7d	7dR	7e	7j	8*	8aaR	8d	8eR	11	18aaR
Plant species	Importance															
Clematis vitalba										2					5	
Cornus sanguinea									6					6	3	
Corylus avellana			3	3		3										
Crataegus laevigata									3						3	
Daphne laureola										2					5	
Daphne mezereum										3					5	
Euonymus europaeus							1								3	
Frangula alnus											3					
Hedera helix	3	1	5	3	3	3	3	3	3	5					3	
Ilex aquifolium				2					3	3		3			3	
Ligustrum vulgare									6	3				6	3	
Lonicera alpigena														3		3
Lonicera nigra											3	3	4			3
Lonicera periclymenum						1										
Lonicera xylosteum			3			3							3			
Rosa arvensis									6	3				6	3	
Rosa pendulina														3		3
Rubus fruticosus	3	5	5	5	6	3	3	6	3	3	3	6	3	6		6
Rubus idaeus		3	3	3	3	3				3			3			
Sambucus nigra			3		3	3							3			
Sambucus racemosa		1	3			3										
Vaccinium myrtillus	3	5					3	3			5		3			2
Vaccinium vitis-idaea											3					
Viburnum lantana									6	3				6	3	
Viburnum opulus						3				3				3		
Abies alba			3	3	3	3	3	3	3	3	5	3	3			5
Acer campestre									6					6	3	
Acer platanoides						3	3									
Acer pseudoplatanus		1	5	5	5	3	3	3	3	3			3	3	3	
Betula pendula						3	3									
Carpinus betulus	5	3	5	5	5	5	5	5	5	5					5	
Castanea sativa	5	3	5	5	5	5	5	5	5	5					5	
Fagus sylvatica	5	5	5	5	5	5	5	5	5	5	5	5	5	5	5	5
Fraxinus excelsior			3	3	3	5	3		3	5			3	3	5	
Juglans regia			3				3			3						
Picea abies		5									5					
Pinus sylvestris		3				1			3		3					
Prunus avium	5	3	5	5	5	5	5	5	5	5					5	
Quercus petraea	5	3	5	5	5	5	5	5	5	5					5	
Quercus robur	5	3	5	5	5	5	5	5	5	5				1	5	
Sorbus aucuparia		3	3		3		3					3	3			
Ulmus glabra									3							

7 APPENDIX II

Plots of cumulative plant occurrence probability time-series obtained from VSD+PROPS:

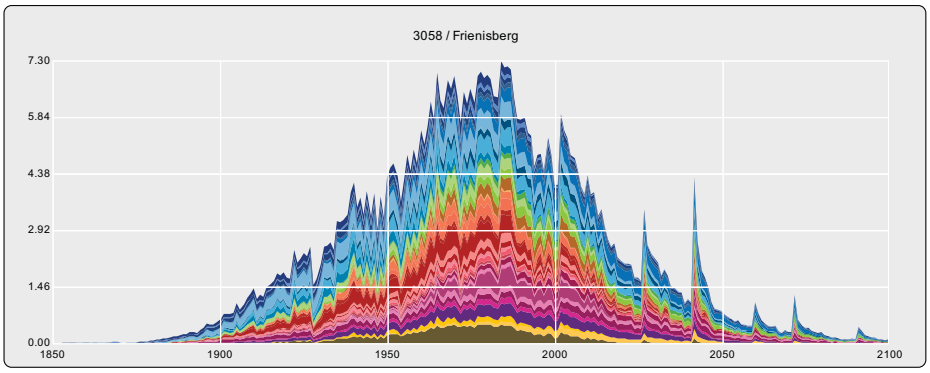

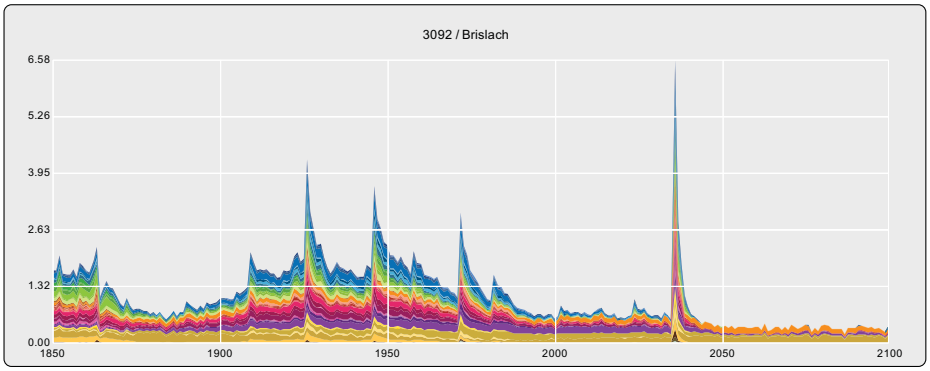

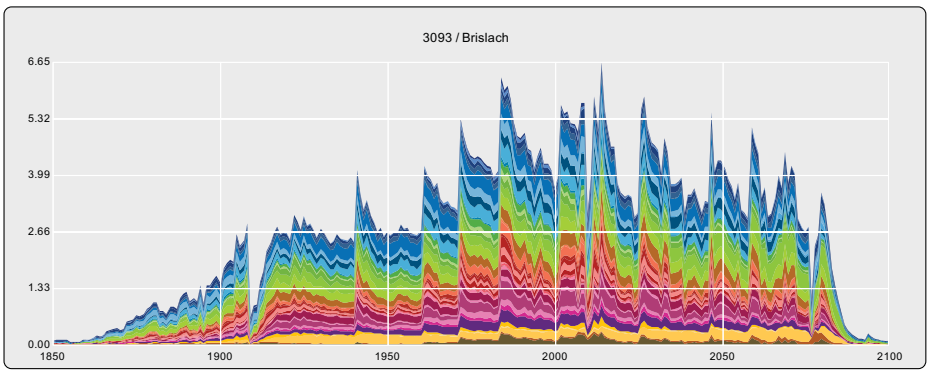

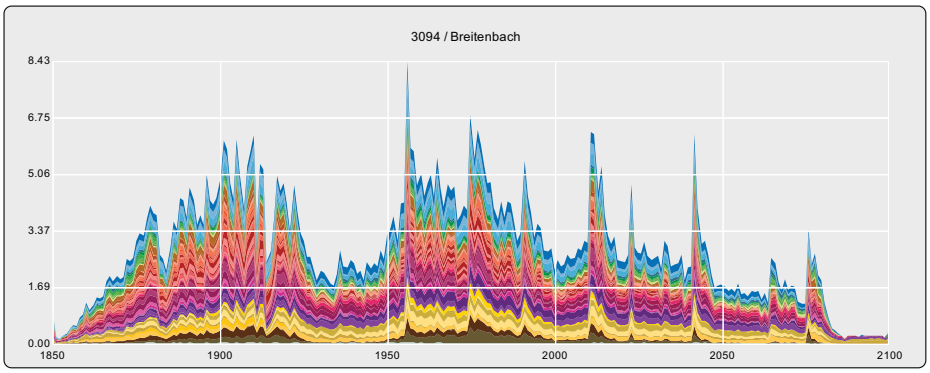

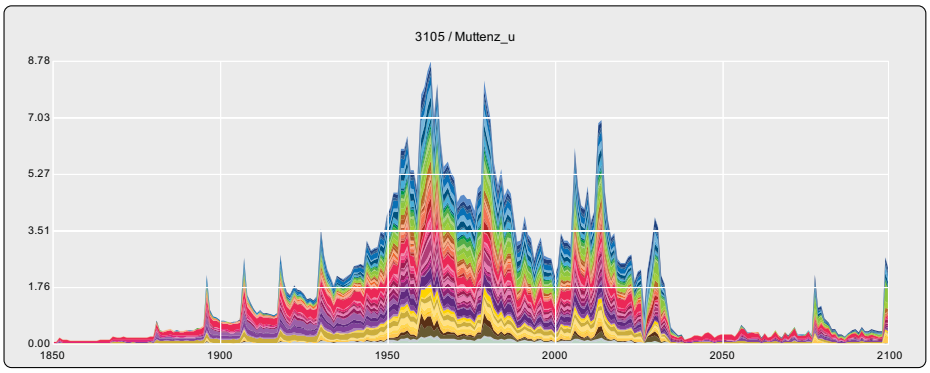

Dominant species (1850-2100) (sorted descending)

- Juncus effusus
- Deschampsia cespitosa
- Fraxinus excelsior
- Hedera helix
- Anemone nemorosa
- Ajuga reptans
- Corylus avellana
- Carpinus betulus
- Angelica sylvestris
- Quercus petraea
- Acer pseudoplatanus
- Fagus sylvatica
- Sambucus nigra
- Fragaria vesca
- Carex sylvatica

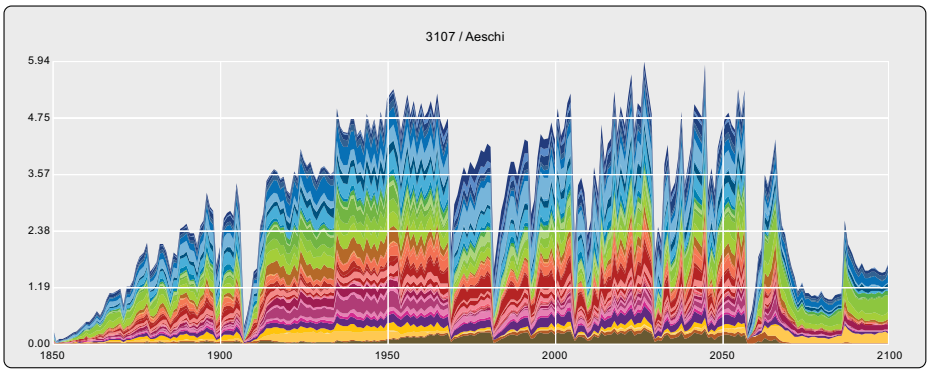

Dominant species (1850-2100) (sorted descending)

- Fagus sylvatica
- Acer pseudoplatanus
- Corylus avellana
- Hedera helix
- Fraxinus excelsior
- Quercus petraea
- Oxalis acetosella
- Carpinus betulus
- Anemone nemorosa
- Viola reichenbachiana
- Polygonatum multiflorum
- Athyrium filix-femina
- Sorbus aucuparia
- Prunus avium
- Brachypodium sylvaticum

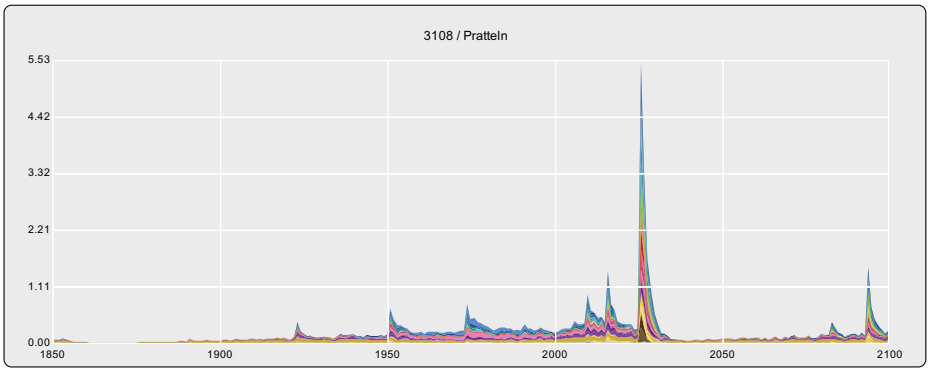

Dominant species (1850-2100) (sorted descending)

- Deschampsia cespitosa
- Galeopsis tetrahit
- Ajuga reptans
- Quercus robur
- Quercus petraea
- Anemone nemorosa
- Fraxinus excelsior
- Hedera helix
- Carex flacca
- Plagiomnium undulatum
- Carpinus betulus
- Acer pseudoplatanus
- Fagus sylvatica
- Angelica sylvestris
- Prunus avium

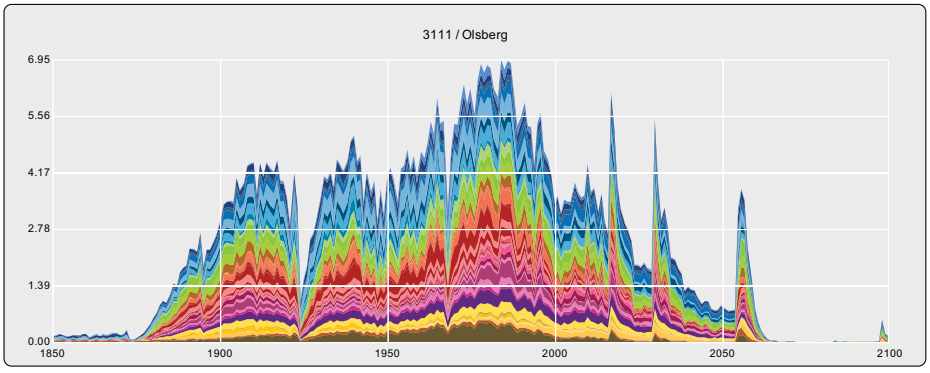

Dominant species (1850-2100) (sorted descending)

- Fagus sylvatica
- Corylus avellana
- Acer pseudoplatanus
- Hedera helix
- Fraxinus excelsior
- Anemone nemorosa
- Oxalis acetosella
- Quercus petraea
- Carpinus betulus
- Athyrium filix-femina
- Viola reichenbachiana
- Polygonatum multiflorum
- Poa nemoralis
- Rubus idaeus
- Galium odoratum

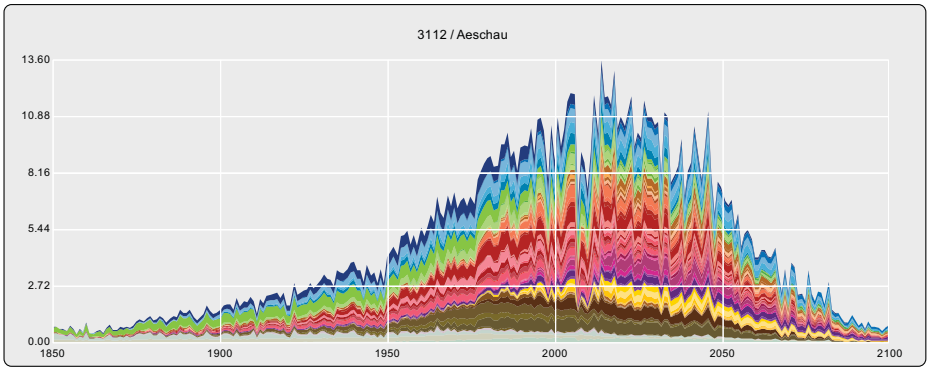

Dominant species (1850-2100) (sorted descending)

- Vaccinium myrtillus
- Fagus sylvatica
- Sorbus aucuparia
- Oxalis acetosella
- Acer pseudoplatanus
- Athyrium filix-femina
- Rubus idaeus
- Abies alba
- Dryopteris dilatata
- Luzula luzuloides
- Dryopteris filix-mas
- Dicranum scoparium aggr.
- Anemone nemorosa
- Hylocomium splendens
- Prenanthes purpurea

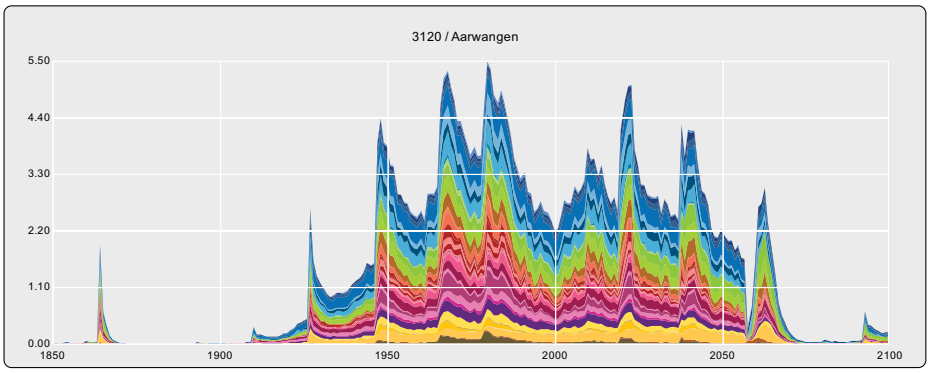

Dominant species (1850-2100) (sorted descending)

- Fraxinus excelsior
- Acer pseudoplatanus
- Corylus avellana
- Hedera helix
- Brachypodium sylvaticum
- Geranium robertianum
- Viola reichenbachiana
- Carpinus betulus
- Anemone nemorosa
- Fagus sylvatica
- Prunus avium
- Polygonatum multiflorum
- Galium odoratum
- Poa nemoralis
- Galeopsis tetrahit

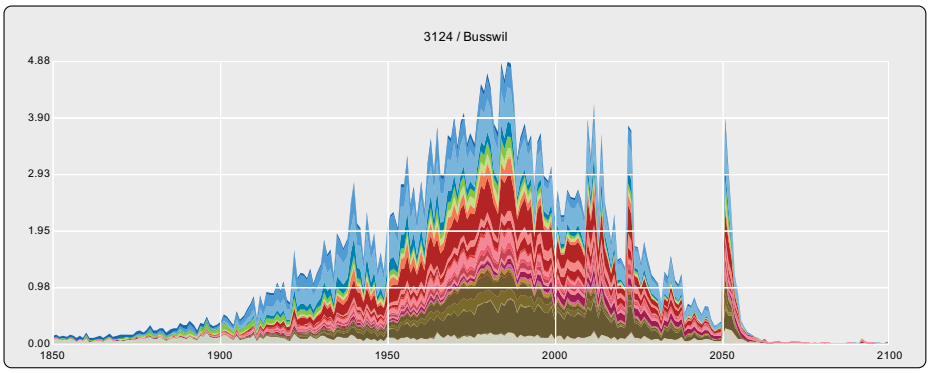

Dominant species (1850-2100) (sorted descending)

- Fagus sylvatica
- Oxalis acetosella
- Athyrium filix-femina
- Picea abies
- Abies alba
- Dryopteris dilatata
- Moehringia trinervia
- Vaccinium myrtillus
- Prenanthes purpurea
- Mycelis muralis
- Dryopteris carthusiana
- Dicranum scoparium aggr.
- Maianthemum bifolium
- Pinus sylvestris
- Geranium robertianum

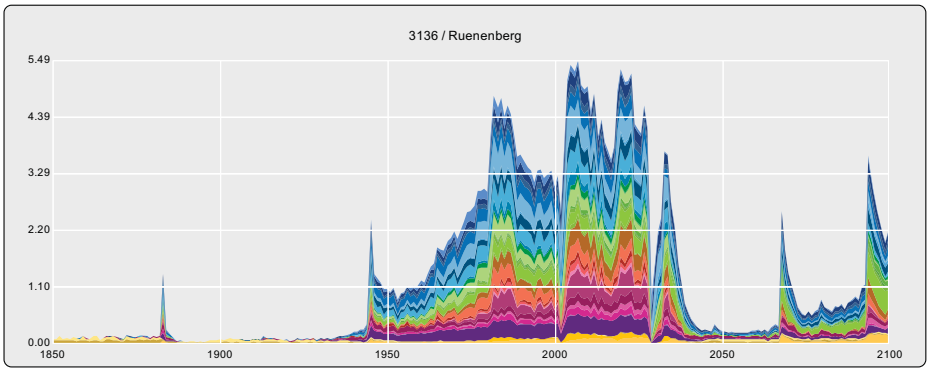

Dominant species (1850-2100) (sorted descending)

- Fagus sylvatica
- Anemone nemorosa
- Acer pseudoplatanus
- Fraxinus excelsior
- Hedera helix
- Quercus petraea
- Carpinus betulus
- Viola reichenbachiana
- Rubus idaeus
- Polygonatum multiflorum
- Galium odoratum
- Fragaria vesca
- Prunus avium
- Quercus robur
- Brachypodium sylvaticum

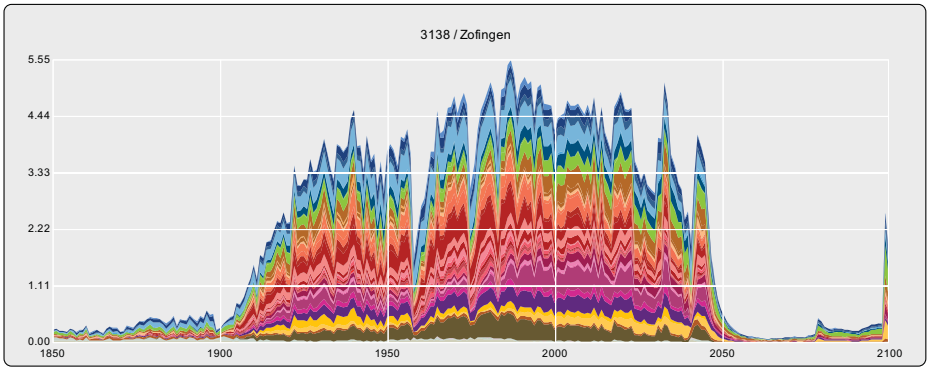

Dominant species (1850-2100) (sorted descending)

- Fagus sylvatica
- Oxalis acetosella
- Athyrium filix-femina
- Hedera helix
- Viola reichenbachiana
- Anemone nemorosa
- Galium odoratum
- Quercus petraea
- Carpinus betulus
- Polygonatum multiflorum
- Mycelis muralis
- Prenanthes purpurea
- Prunus avium
- Geranium robertianum
- Brachypodium sylvaticum

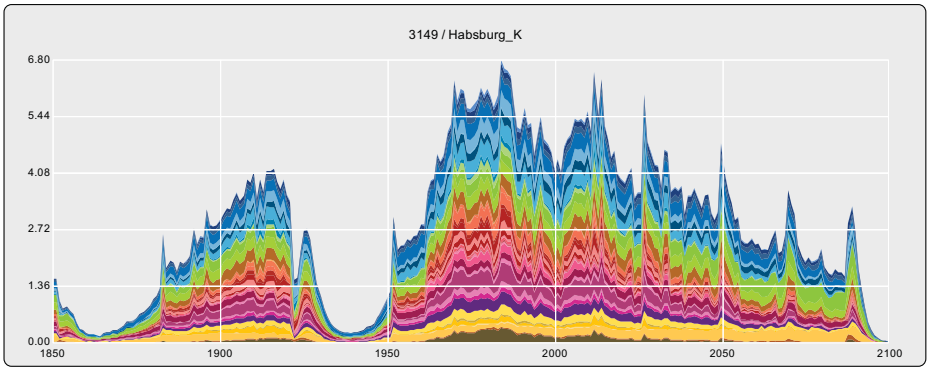

Dominant species (1850-2100) (sorted descending)

- Fraxinus excelsior
- Hedera helix
- Corylus avellana
- Acer pseudoplatanus
- Viola reichenbachiana
- Brachypodium sylvaticum
- Galium odoratum
- Geranium robertianum
- Fagus sylvatica
- Carpinus betulus
- Anemone nemorosa
- Prunus avium
- Poa nemoralis
- Polygonatum multiflorum
- Quercus petraea

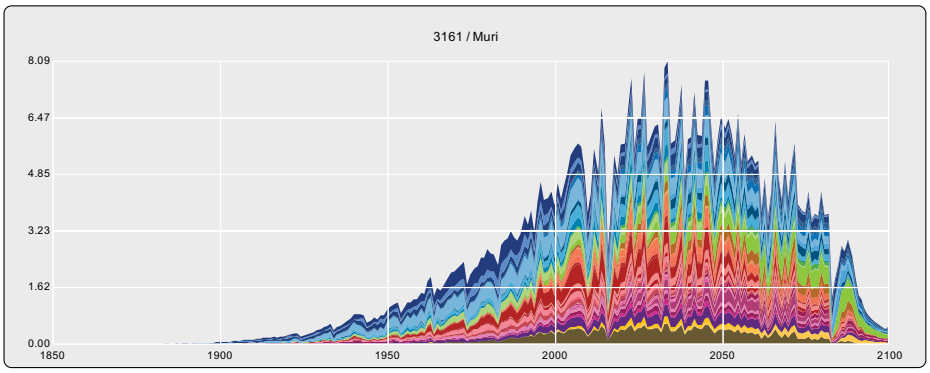

Dominant species (1850-2100)
(sorted descending)

- Fagus sylvatica
- Sorbus aucuparia
- Oxalis acetosella
- Quercus petraea
- Hedera helix
- Athyrium filix-femina
- Acer pseudoplatanus
- Anemone nemorosa
- Rubus idaeus
- Carpinus betulus
- Viola reichenbachiana
- Polygonatum multiflorum
- Fraxinus excelsior
- Quercus robur
- Abies alba

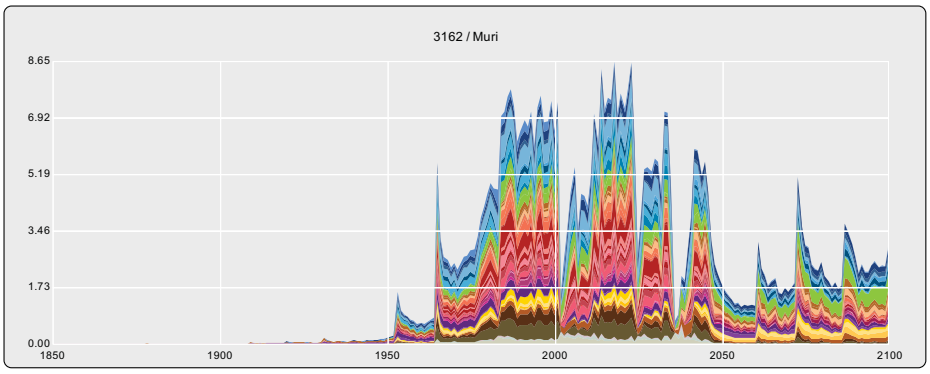

Dominant species (1850-2100)
(sorted descending)

- Fagus sylvatica
- Hedera helix
- Oxalis acetosella
- Quercus petraea
- Athyrium filix-femina
- Acer pseudoplatanus
- Anemone nemorosa
- Vaccinium myrtillus
- Teucrium scorodonia
- Dryopteris filix-mas
- Carpinus betulus
- Pteridium aquilinum
- Polygonatum multiflorum
- Quercus robur
- Luzula luzuloides

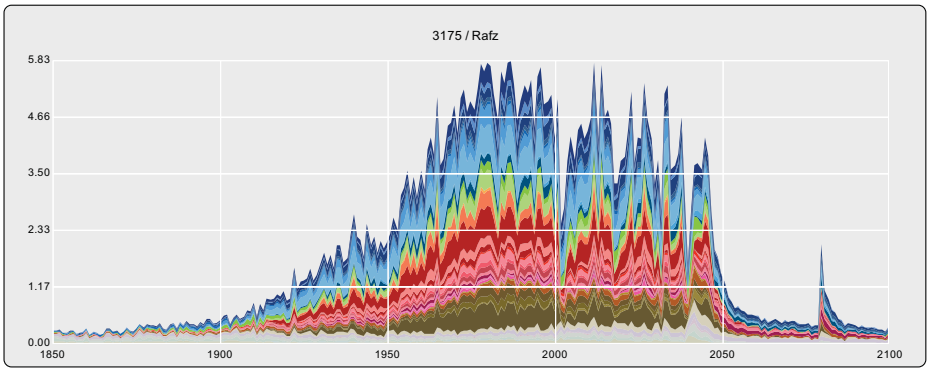

Dominant species (1850-2100)
(sorted descending)

- Fagus sylvatica
- Oxalis acetosella
- Athyrium filix-femina
- Quercus petraea
- Picea abies
- Sorbus aucuparia
- Rubus idaeus
- Prenanthes purpurea
- Carpinus betulus
- Vaccinium myrtillus
- Scleropodium purum
- Mycelis muralis
- Pteridium aquilinum
- Thuidium tamariscinum
- Hypnum cupressiforme aggr.

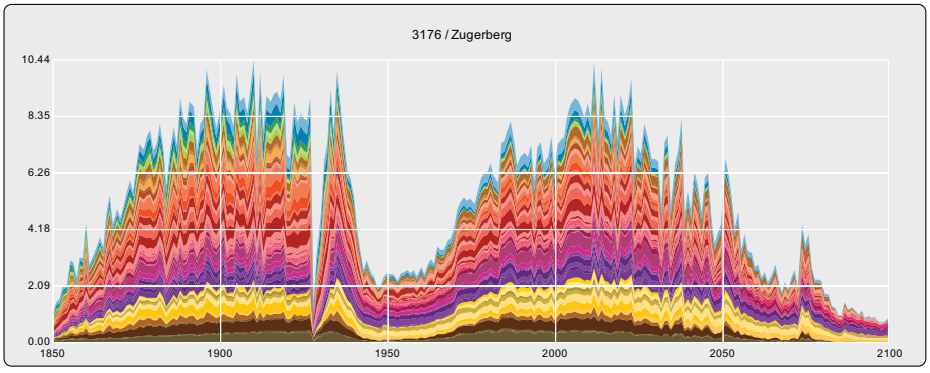

Dominant species (1850-2100)
(sorted descending)

- Fagus sylvatica
- Galium odoratum
- Dryopteris filix-mas
- Oxalis acetosella
- Viola reichenbachiana
- Athyrium filix-femina
- Paris quadrifolia
- Carex sylvatica
- Phyteuma spicatum
- Abies alba
- Prenanthes purpurea
- Ajuga reptans
- Anemone nemorosa
- Carex digitata
- Primula elatior

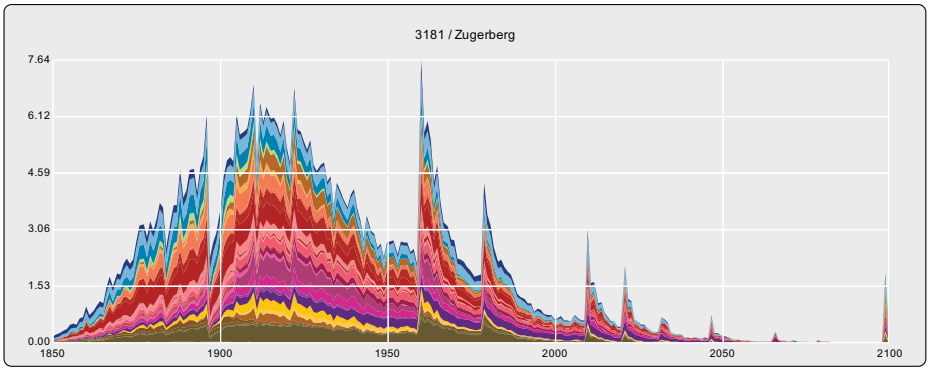

Dominant species (1850-2100)
(sorted descending)

- Oxalis acetosella
- Fagus sylvatica
- Athyrium filix-femina
- Anemone nemorosa
- Abies alba
- Phyteuma spicatum
- Galium odoratum
- Viola reichenbachiana
- Prenanthes purpurea
- Epilobium montanum
- Lysimachia nemorum
- Sorbus aucuparia
- Mycelis muralis
- Geranium robertianum
- Carex digitata

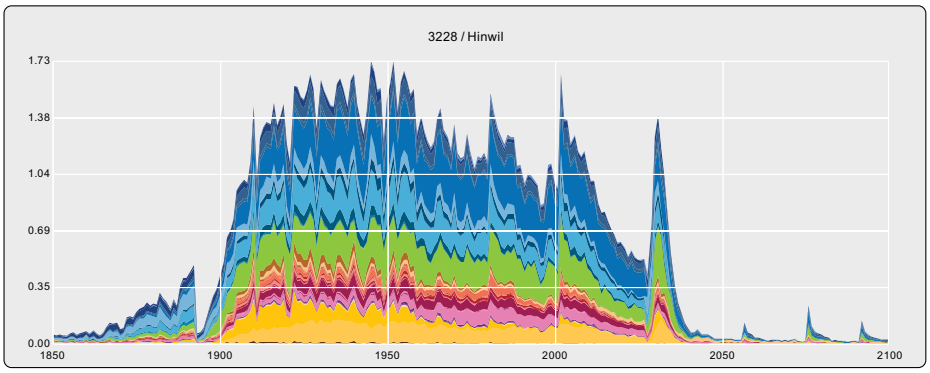

Dominant species (1850-2100) (sorted descending)

- Fraxinus excelsior
- Hedera helix
- Acer pseudoplatanus
- Brachypodium sylvaticum
- Prunus avium
- Fagus sylvatica
- Carex digitata
- Galeopsis tetrahit
- Geranium robertianum
- Quercus petraea
- Acer platanoides
- Carpinus betulus
- Juglans regia
- Polygonatum multiflorum
- Viola reichenbachiana

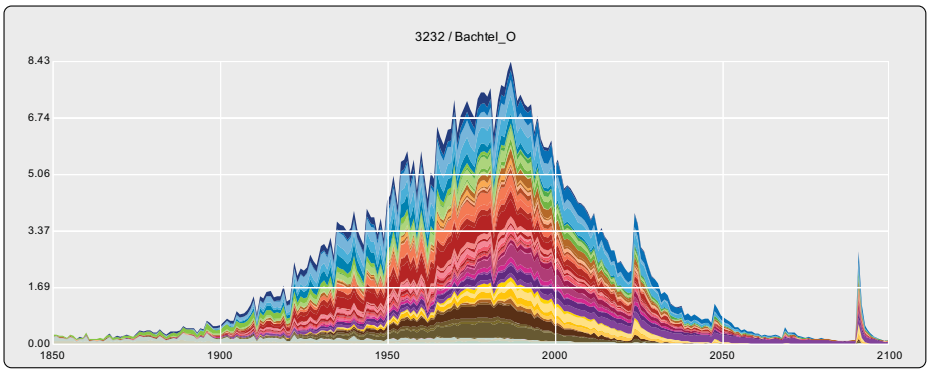

Dominant species (1850-2100) (sorted descending)

- Acer pseudoplatanus
- Fagus sylvatica
- Oxalis acetosella
- Fraxinus excelsior
- Ajuga reptans
- Sorbus aucuparia
- Abies alba
- Rubus idaeus
- Athyrium filix-femina
- Phyteuma spicatum
- Dryopteris filix-mas
- Prenanthes purpurea
- Anemone nemorosa
- Vaccinium myrtillus
- Carex sylvatica

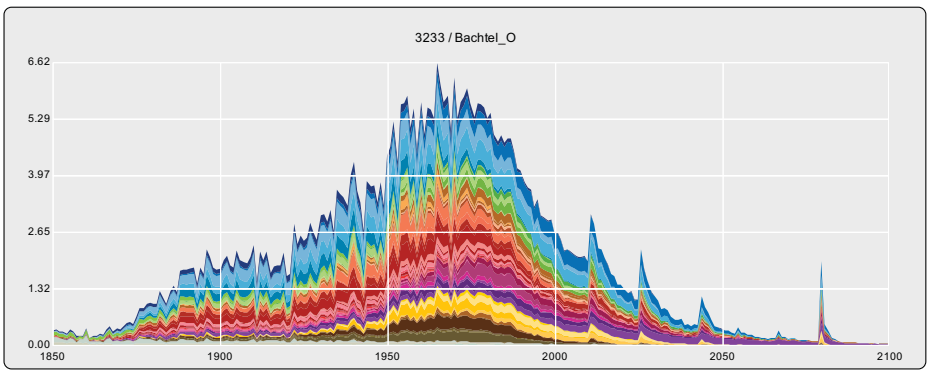

Dominant species (1850-2100) (sorted descending)

- Acer pseudoplatanus
- Fagus sylvatica
- Fraxinus excelsior
- Oxalis acetosella
- Abies alba
- Ajuga reptans
- Phyteuma spicatum
- Prenanthes purpurea
- Sorbus aucuparia
- Rubus idaeus
- Dryopteris filix-mas
- Anemone nemorosa
- Athyrium filix-femina
- Carex digitata
- Viola reichenbachiana

Normalized plant occurrence probability time-series after grouping the plants into Landolt indicator N and R classes. Small numbers in the top of the plots are site number and number of plant species considered. Red and yellow lines are N deposition and pH of the soil solution, respectively.

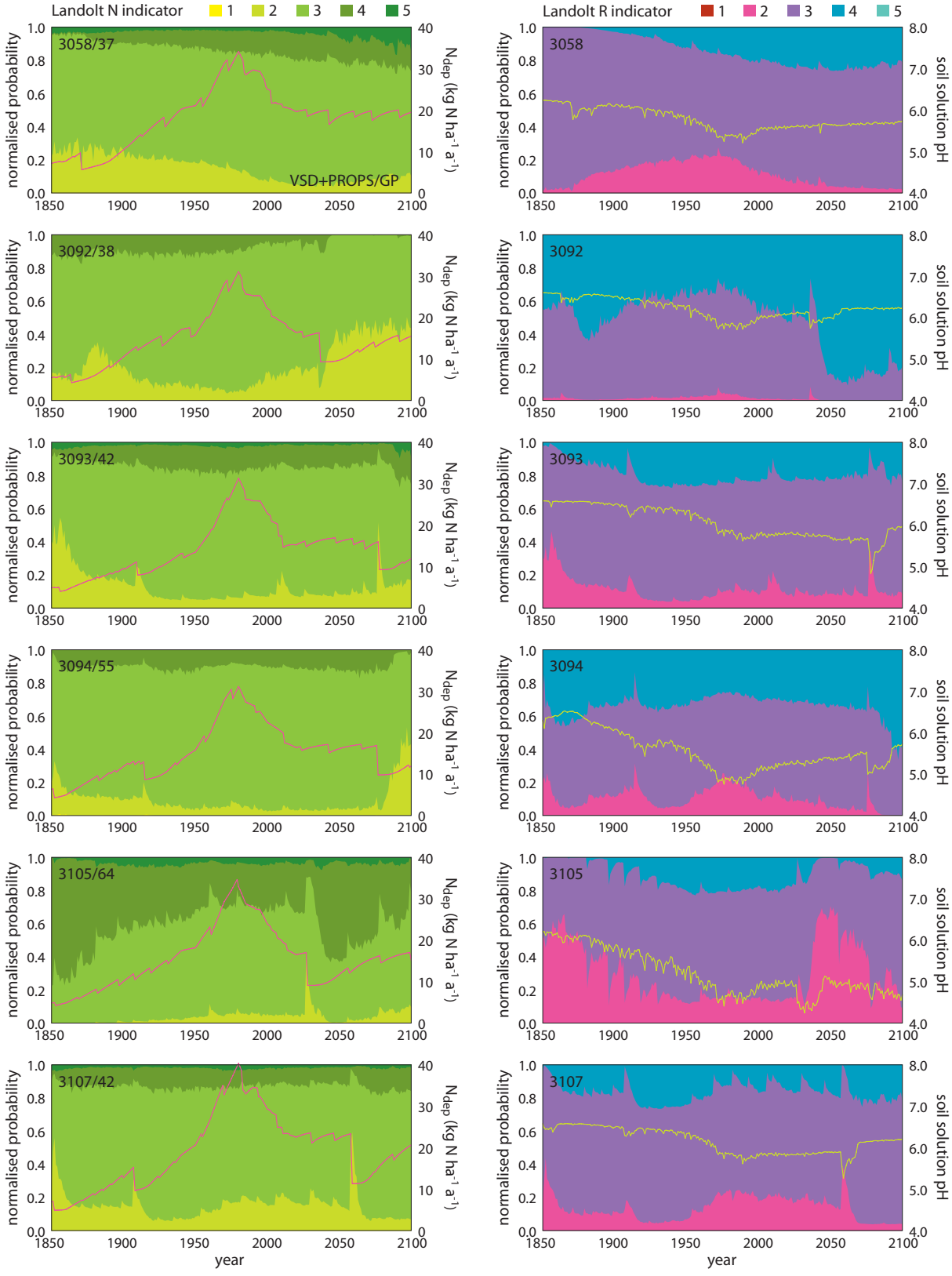

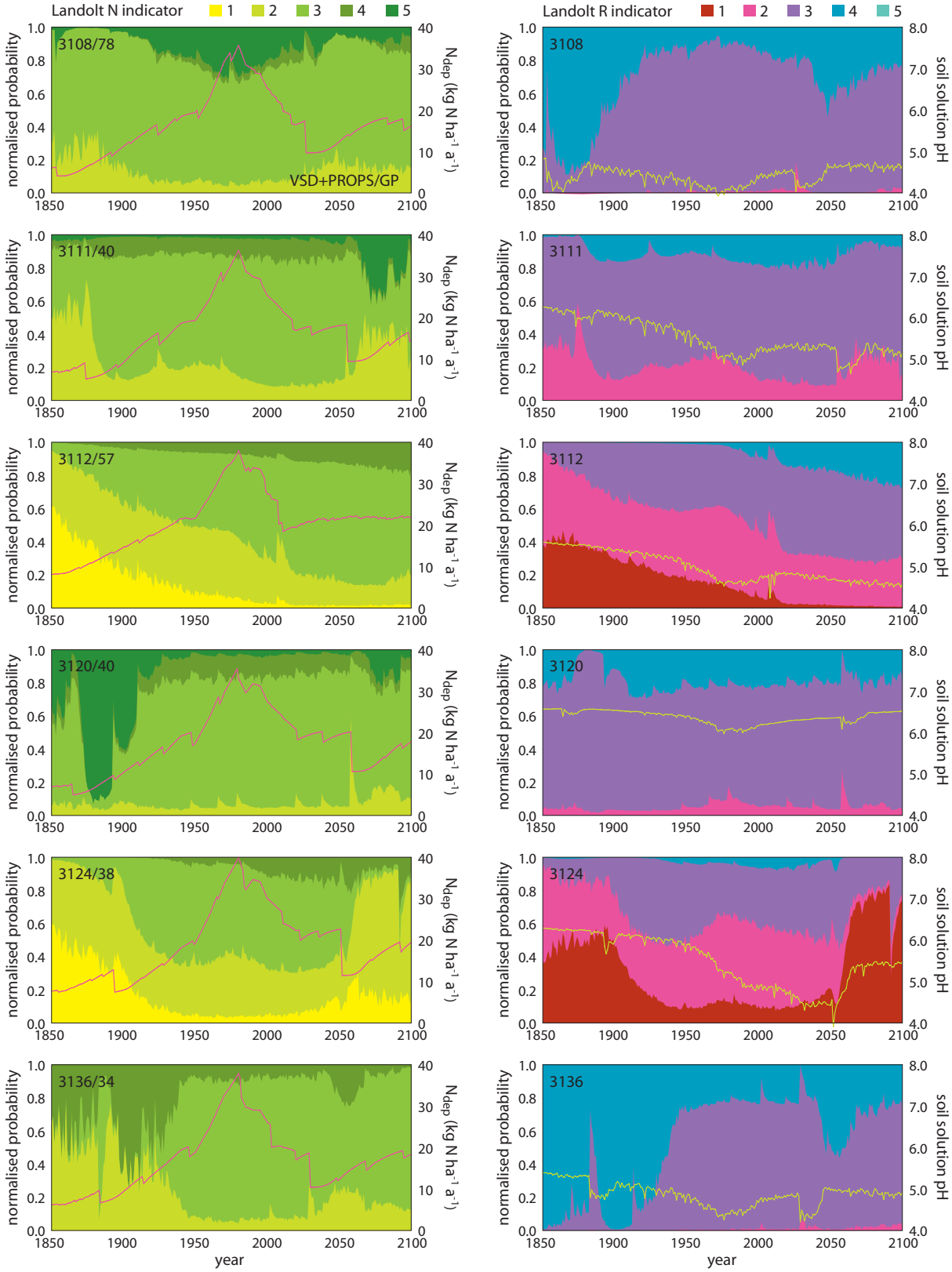
Landolt N indicator 1 2 3 4 5
Landolt R indicator 1 2 3 4 5
3108/78
VSD+PROPS/GP
3108
3111/40
3111
3112/57
3112
3120/40
3120
3124/38
3124
3136/34
3136
normalised probability
Ndep (kg N ha-1 a-1)
soil solution pH
year

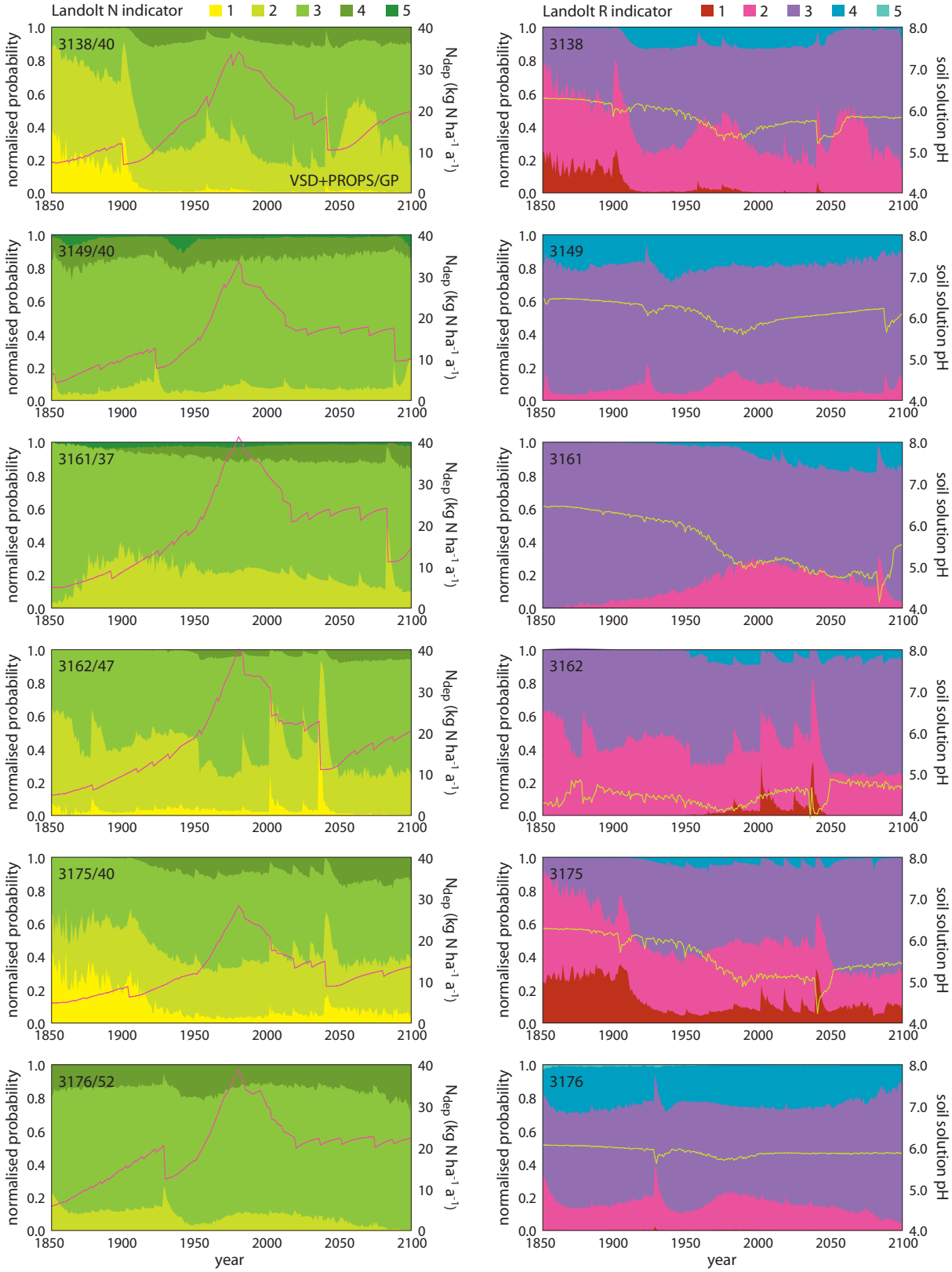
Landolt N indicator 1 2 3 4 5
Landolt R indicator 1 2 3 4 5
3138/40
VSD+PROPS/GP
3138
3149/40
3149
3161/37
3161
3162/47
3162
3175/40
3175
3176/52
3176
normalised probability
Ndep (kg N ha-1 a-1)
soil solution pH
year

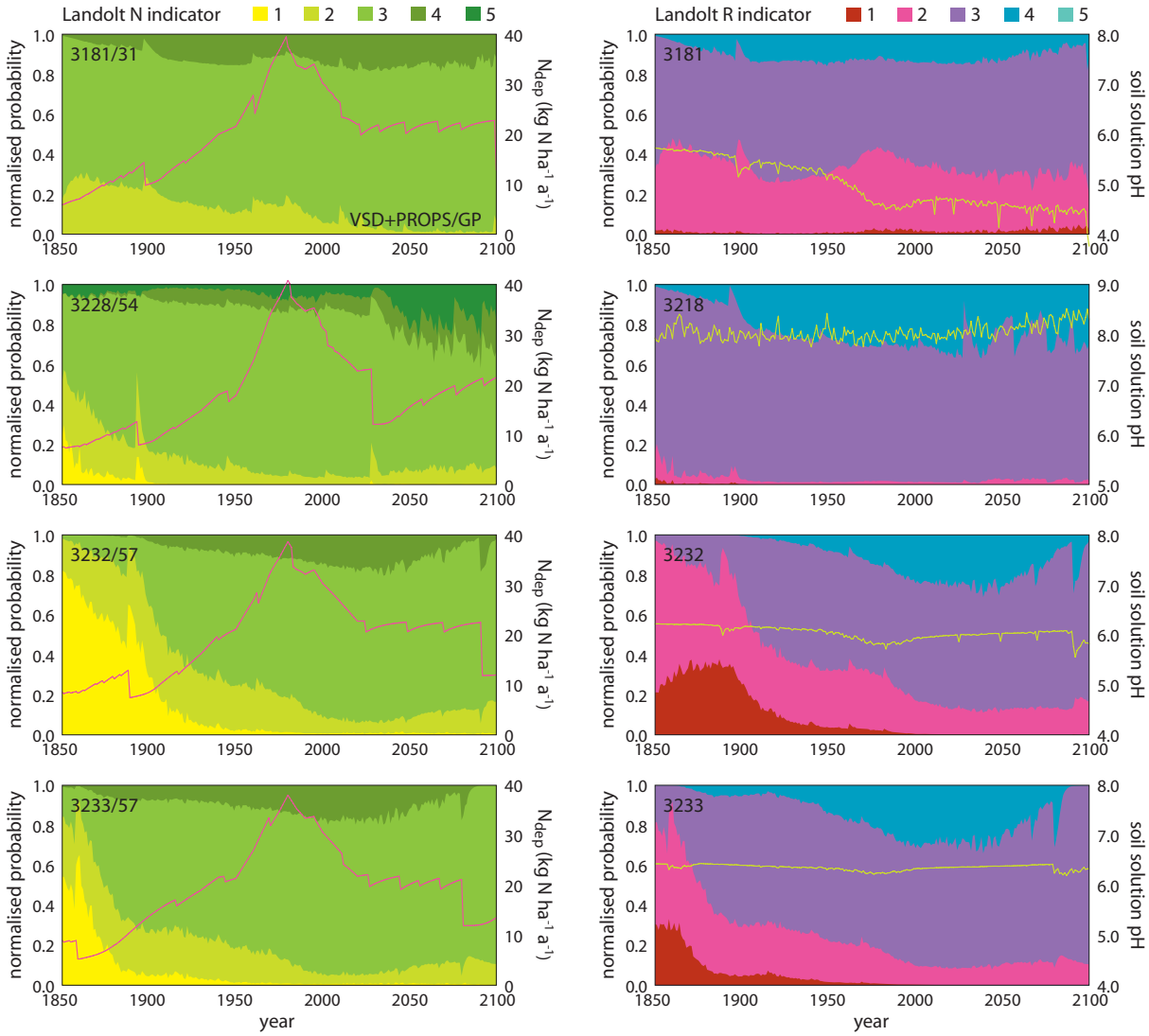
Landolt N indicator 1 2 3 4 5
Landolt R indicator 1 2 3 4 5
3181/31
VSD+PROPS/GP
3228/54
3232/57
3233/57
3181
3218
3232
3233
normalised probability
Ndep (kg N ha-1 a-1)
soil solution pH
year